博士論文

DOCTORAL DISSERTATION

Physical chemistry on evaporation removal of boron in molten silicon using reactive fluxes
（反応性フラックスを用いたシリコン中ホウ素の揮発除去に関する物理化学）

王　燁

(WANG Ye)

Table of Contents

CHAPTER ONE

INTRODUCTION

Since the industrial revolution, rapid development of human footsteps led to the boom of the global economy, but also caused serious environmental deterioration and exhausted the traditional energy. As the traditional energy sources coal, oil and gas, they are non-renewable resources; the irrefragable pollution of the environment is the biggest problem. Therefore, it is imperative to develop a kind of renewable and clean energy to change the energy structure, to adapt the demand of sustainable development. In various kinds of renewable energies, solar energy is undoubtedly the best choice, it is inexhaustible, unlimited, and almost won't bring serious pollution problems. In the field of solar energy application, photovoltaic (PV) technology is most widely used, so the research of production of the solar cells also became the focus of the world. Until 2013, silicon was the preferred base material due to its abundant reserve which makes up over 95% of the total PV market. But there is limited supply of the silicon which can satisfy the requirements for the use in solar cells, the main reason behind this is the technology used causes environmental pollution and its cost is still high. Although traditional preparation methods of monocrystalline silicon material can meet the requirements of solar cells, there are many restrictions on its application at a large scale, as these production methods were initially developed for the microelectronics industry. Hence, research and development of silicon materials with low cost and low environmental pollutions have become one of the hot research subjects in the world. The strategic significance to preempt completely independent property rights on development technology for silicon materials to be used in the field of solar energy cannot be emphasized greatly.

1.1 Research background

1.1.1 The world energy crisis

Energy is essential for economic and social development and improved quality of life in all countries [1]. The increase in economic growth of the developing countries in the last decades have caused rapid increase in energy consumption [2]. According to Kaygusuz and Bilgen, this trend is expected to increase in the near future [3]. Unsustainable consumption is a major cause of global environmental deterioration, including overexploitation of renewable resources and pollution caused by fossil fuels [4]. A strong relationship between economic depression in 2008 and energy exhaust was found by Mr. Li et al [5].

On the other hand, limitation of traditional energy reserves in the world forces us find other energy resources. According to an estimate by the geologists and economists, the traditional energy is facing a non-recyclable state. Table 1.1 shows the reserves and age limit of traditional energy resources [6, 7]. It tells that the limitation of reserves of traditional energies can only support human beings for around hundred years. Therefore, it is imperative that people need to develop a kind of renewable clean energy to change the energy structure, to adapt the demand of sustainable development.

Table 1.1 Reserves and age limit of traditional energy (until 2013)

	Oil	**Gas**	**Coal**	**Uranium**
Reserves	1.69 trillion barrels	186 trillion cubic meters	8.92 trillion tons	7.64 million tons
Age limit	53.3 years	54.8 years	113 years	120 years

British Petroleum (BP) reported that the world primary energy consumption grew by a below-average 2.3% in 2013, all fuels except oil, nuclear and renewables grew at below-average rates. Oil remains world's dominant fuel, but has lost market share for 14 years in a row. Hydroelectric and other renewables in power generation both reached record shares of global primary energy consumption (6.7% and 2.2%, respectively), as shown in Fig. 1.1. Although the renewable account for a lower status among all kinds of energy, the obvious increase can be found in Fig. 1.1.

Will the world have sufficient energy to fuel continued economic growth? Will that

energy be secure? And will it be sustainable? The Group Executive of BP, Mr. Bob Dudley said "yes." They project that global energy consumption will rise by 41% by 2035, with 95% of that growth coming from rapidly-growing emerging economies. New energy forms such as shale gas, tight oil, and renewables will account for a significant share of the growth in global supply. Energy efficiency promises to improve unabatedly, driven by globalization and competition [8].

In the forecast period, British Petroleum (BP) predicted that all fuels show growth from 1975 to 2035, with the fastest growth seen in renewables (6.4% annual average) obviously. Nuclear (1.9% annual average) and hydro-electric power (1.8% annual average) both grow more rapidly than total energy, as shown in Fig. 1.2 [9].

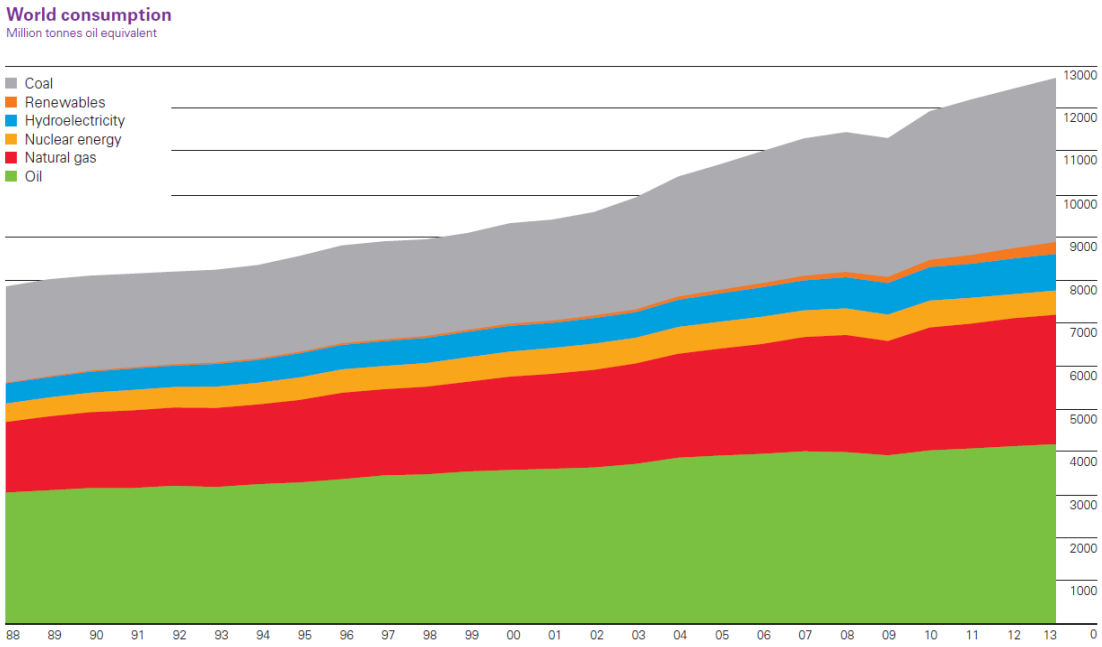

Figure 1.1. World consumption of various species of energy sources until 2013 [6]

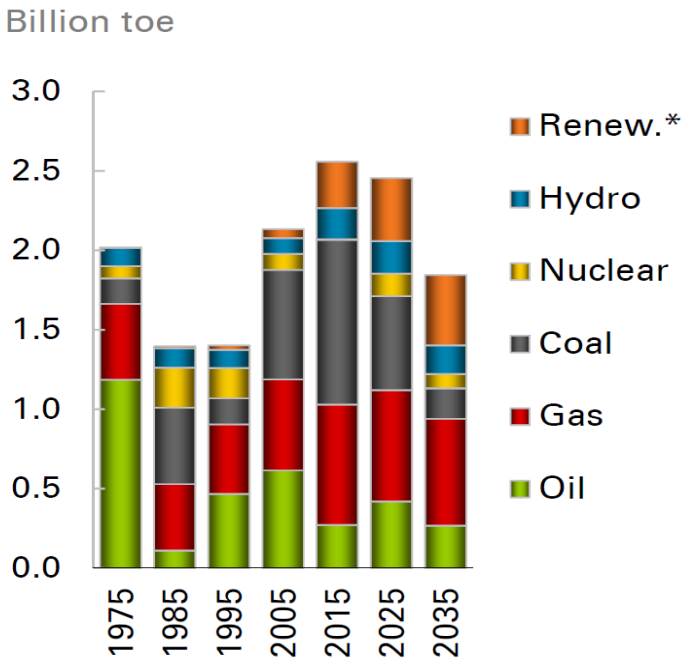

Figure 1.2. Tendency increments of energy sources until 2035 [9]

On the other hand, the traditional energy sources, such as coal, oil and gas, caused the irrefragable pollution problem. The issue is not new anymore. Wood and coal burning in factories and vehicle exhaust emissions have contributed to the air pollution [10]. For example, Shanghai and Beijing, two of the largest cities in China are concurrent with large increases in energy consumption. Particulate pollution, such as PM 2.5 (particle size smaller than 2.5 mm) and PM 10 have threatened people's health [11]. Furthermore, fuel combustion residues [12] and massive deforestation [13] have also caused water pollution along with water and soil loss.

In order to have a sustainable development of human beings and environmental protection, it is imperative that people need to develop a kind of renewable clean energy to change the energy structure, to adapt the demand of sustainable development.

1.1.2 The development of renewable energy

Global perceptions of renewable energy have shifted considerably since 2004 [14]. Over the last 10 years, continuing technology advances and rapid deployment of many renewable energy technologies have demonstrated that their potential can be achieved.

Renewable energy contains hydropower, Bio-power, geothermal power, solar PV, ethanol power, biodiesel and so on [15]. Table 1.2 shows the power of various renewable energy until 2013 [16].

Table 1.2 Renewable energy until 2013

Power	Unit	Start 2004	End 2012	End 2013
Renewable power capacity (total, not including hydro)	gigawatts (GW)	85	480	**560**
Renewable power capacity (total, including hydro)	GW	800	1440	**1560**
Hydropower capacity (total)	GW	715	960	**1000**
Bio-power capacity	GW	＜36	83	**88**
Geothermal power capacity	GW	8.9	11.5	**12**
Solar PV capacity (total)	GW	2.6	100	**139**
Concentrating solar thermal power (total)	GW	0.4	2.5	**3.4**
Wind power capacity (total)	GW	48	283	**318**
Solar hot water capacity (total)	GW	98	282	**326**
Ethanol production (annual)	billion liters	28.5	82.6	**87.2**
Biodiesel production (annual)	billion liters	2.4	23.6	**26.3**

From Table 1.2, we can find that the photovoltaics (PV) industry possess an important status in renewable power. Solar PV capacity (139 GW) accounts for 25% in the total of renewable power capacity (560 GW, not including hydro). Furthermore, Fig. 1.3 indicates that during the years 2009 through 2013, installed capacity as well as output of most renewable energy technologies grew at rapid rates, particularly in the power sector. Over this period, Solar PV experienced the fastest capacity growth rates of any energy technology. During 2013, Europe continued to see a significant loss of start-up companies (especially solar PV), resulting in widespread financial losses [17].

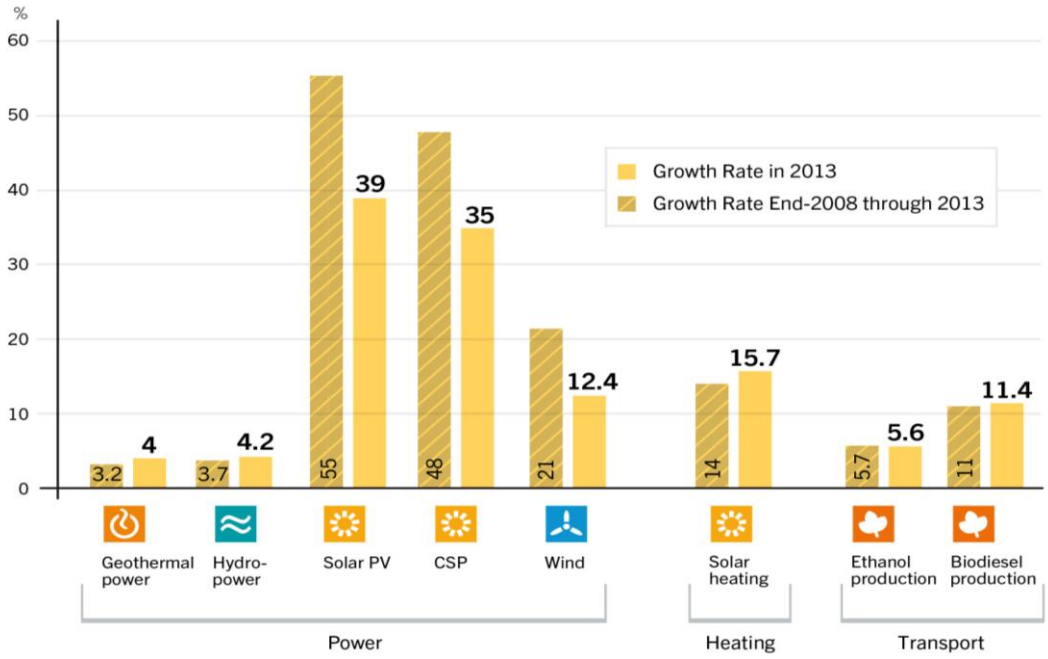

Figure 1.3. Average annual growth rates of renewable energy capacity and biofuels production, 2008-2013 [16]

From the above, rapid development of PV industry and increasing investment bespeaks the preparation technology and development of new materials of PV industry is an urgent affair.

1.1.3 PV industry and solar cells

Photovoltaics (PV) is a method of converting solar energy into direct current electricity using semiconducting materials that exhibit the photovoltaic effect. A photovoltaic system employs solar panels composed of a number of solar cells to supply usable solar power. Power generation from solar PV has long been seen as a clean sustainable [18] energy technology which draws upon the planet's most plentiful and widely distributed renewable energy source-the sun. Direct conversion of sunlight to electricity occurs without any moving parts or environmental emissions during operation. This is well proven, as photovoltaic systems have now been used for fifty years in specialized applications, and grid-connected PV systems have been in use for over twenty years [19].

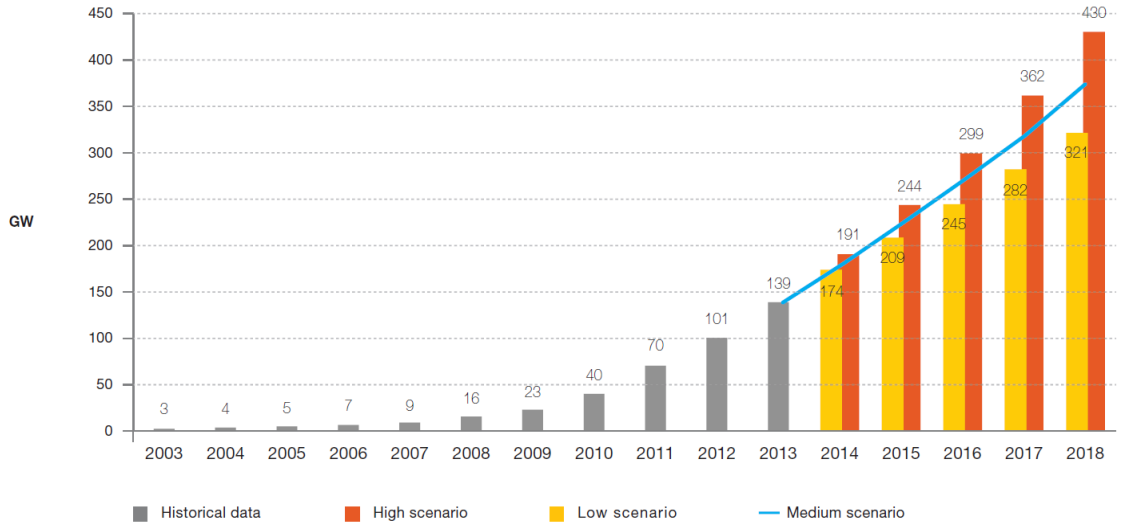

Figure 1.4. Global annual PV cumulative scenarios until 2018 [20]

European Photovoltaic Industry Association (EPIA) reported that the global annual PV cumulative increased rapidly from 3GW to the 139GW from 2003 to 2013, they also predicated the PV market will increase to the 430GW until 2018, as shown in Fig. 1.4 [20].

Thus, the increasing investment in PV industry needs the exploitation of preparation technology and development of solar cells.

A solar cell, or photovoltaic cell, is an electrical device that converts the energy of light directly into electricity by the photovoltaic effect [21]. It is a form of photoelectric cell, defined as a device whose electrical characteristics, such as current, voltage, or resistance, vary when exposed to light. Solar cells are the building blocks of photovoltaic modules, otherwise known as solar panels [22].

Solar cells mainly contain crystalline silicon, thin film and Multi-junction cells. The crystalline silicon are divided into monocrystalline silicon, polycrystalline silicon, ribbon silicon and mono-like-muti silicon (MLM). The thin film consists of cadmium telluride (CdTe), copper indium gallium selenide (CIGS), silicon thin film, gallium arsenide thin film (GaAs). Multi-junction cells [23] were originally developed for special applications such as satellites and space exploration, but are now used increasingly in terrestrial concentrated photovoltaics (CPV).

Crystalline silicon (c-Si) technology made up 90 percent of module production in 2013, compared to 89 percent in 2012. Roughly three-fourths of c-Si output was multicrystalline-based, which is a significant change from 2008, when production was

split almost evenly between multi and mono c-Si. Total thin film production declined for the second consecutive year in a row: 2013 production was estimated at 4.2 gigawatts, down from 2011's high of 4.7 gigawatts. Looking at thin film production more closely, CdTe (almost entirely First Solar) made up 39 percent of total thin film production in 2013, followed by CIGS (31%) and thin-film silicon (30 %). The global PV module production by technology in 2013 are shown in Fig. 1.5 [24].

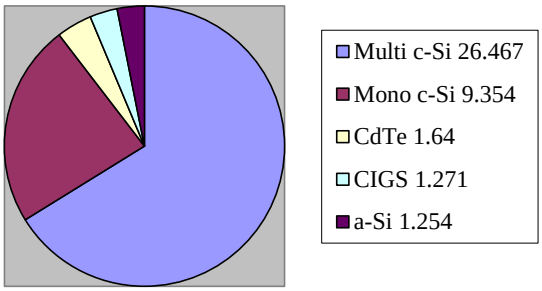

Figure 1.5. Global PV module production by technology, 2013 (MW) [24]

Solar cell efficiency may be broken down into reflectance efficiency, thermodynamic efficiency, charge carrier separation efficiency and conductive efficiency. The overall efficiency is the product of these individual metrics. The laboratory solar cell efficiency has been increased rapidly from around 10% to around 40% from 1992 to 2014 by improving the purity of Si. As shown in Fig. 1.6, the photoelectric conversion efficiency of different types of solar cells increased dramatically. In December 2014, a high concentration multi-junction solar cell achieved a new laboratory record with 46 percent efficiency in a French-German collaboration [25]. The record lab cell efficiency is 25 % for mono-crystalline and 20.4 % for multi-crystalline silicon wafer-based technology. The highest lab efficiency in thin film technology is 19.8 % for CIGS and 19.6 % for CdTe solar cells [26].

Among the species of solar cells, because the polycrystalline silicon accounts for 65%, and it also has relatively high efficiency. It is important to study its preparation methods urgently.

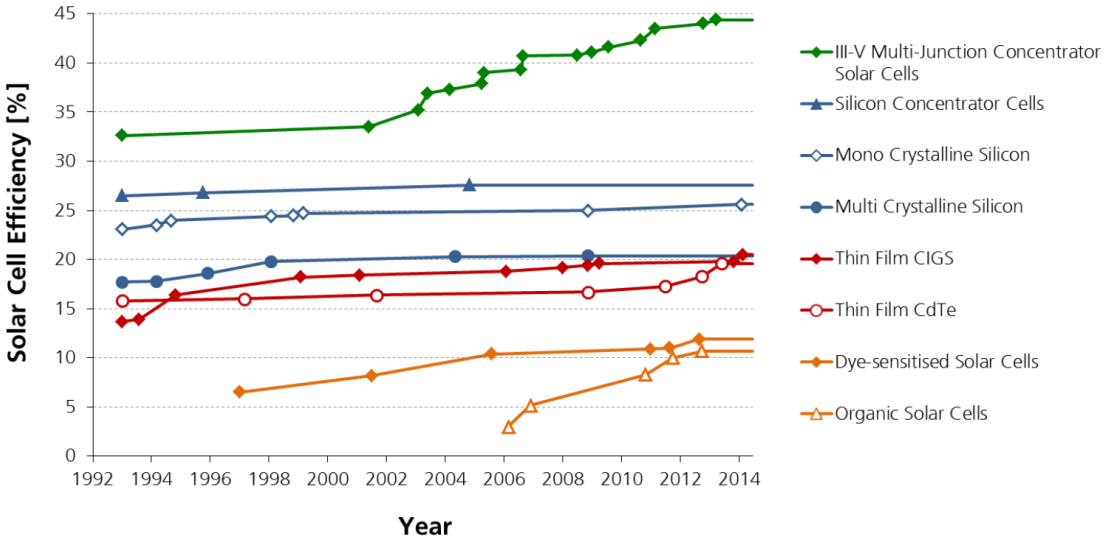

Figure 1.6. Development of laboratory solar cell efficiencies [26]

1.2 Preparation technology of solar grade silicon (SOG-Si)

As silicon is the main raw material of solar cells, the quantity of its production output determines the degree of industrialization. Purity requirements for silicon which is to be used in the solar cells define solar grade silicon (SOG-Si), which purity higher than 99.9999% (6N). The current supply of raw materials is mainly from two sources: one is the offcut of the electronic grade (EG: 9-12 N) silicon which is used in the semiconductor industry, and the other is SOG material obtained from the molten grade (MG: 4-5 N) silicon after the purification process. Two sources also correspond to two different purification processes, namely, the traditional production of EG silicon (chemical process) and metallurgical method (physical process).

1.2.1 Traditional production of SOG silicon

MG silicon is the raw material for SOG silicon. In the production method for MG silicon high purity quartz sand (SiO_2) is taken as raw material which undergoes a reduction reaction in the presence of coke in the electric arc furnace. The reaction equation is expressed as:

$$SiO_{2(s)} + 2C_{(s)} = Si_{(l)} + 2CO_{(g)} \quad (1\text{-}1)$$

Coarse silicon obtained in this way has a lot of metallic and non-metallic impurities, and conjunctions. Further purification is needed for its application in the solar cells industry.

Because most of the raw materials come from the offcut of EG silicon, Main production methods for EG silicon are separated into three methods: modified Siemens method, thermal decomposition of silane method and fluidized bed method.

a) Modified Siemens process

Modified Siemens process is also called trichlorosilane ($SiHCl_3$) reduction, which was invented by German Siemens Company in 1954. MG silicon and hydrogen chloride are used to produce an intermediate compound of $SiHCl_3$, the chemical reaction is

$$Si + 3HCl = SiHCl_3 + H_2 \quad (1\text{-}2)$$

After two crude distillation and rectification process, impurities of $SiHCl_3$ intermediate compounds can be reduced to 7~10N. Polysilicon thin rods are heated in the reaction chamber up to over 1100^{o}C, $SiHCl_3$ intermediate compounds and high-purity hydrogen are blown in and reduction reaction takes place, silicon rods are grown by chemical vapor deposition technology. The reactions are expressed as Eq. (1-3) and (1-4). Modified

Siemens polysilicon production process design is composed of the following steps: H_2 preparation and purification, HCl synthesis, $SiHCl_3$ synthesis, chlorosilane separation and purification, SiHCl reduction, reduction of dry exhaust gas, silicon core preparation and product finishing, waste gas and residue treatment, the specific process are shown in Fig. 1.7.

$$SiHCl_3 + H_2 = Si + 3HCl \quad (1\text{-}3)$$

$$2(SiHCl_3) = Si + 2HCl + SiCl_4 \quad (1\text{-}4)$$

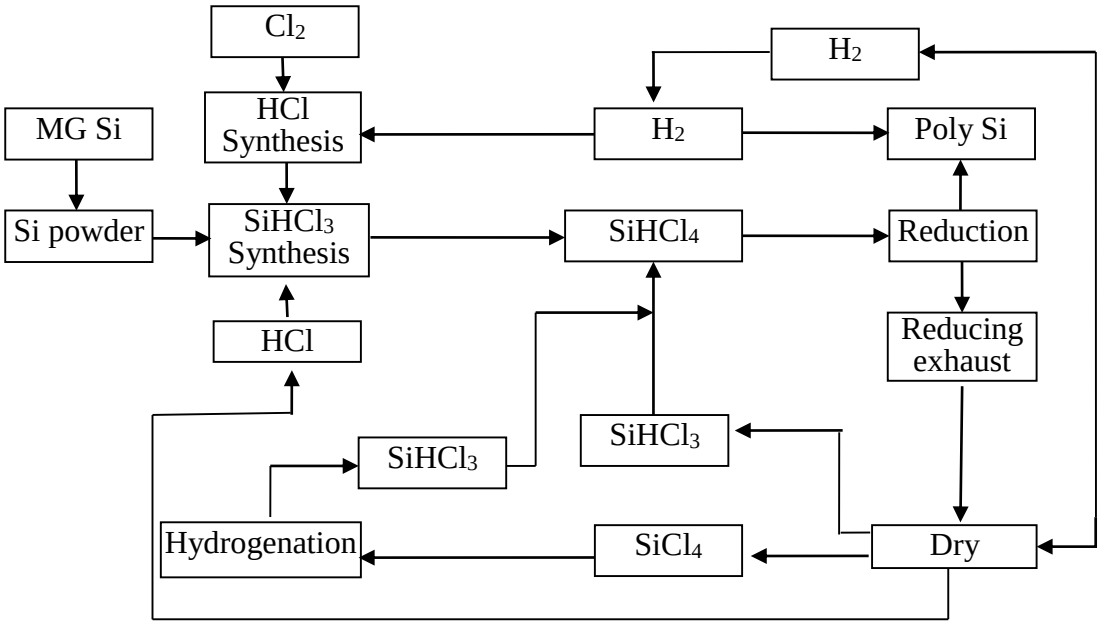

Figure 1.7. Improved Siemens polycrystalline production method process flow [27]

b) Thermal decomposition of silane method

There are several methods for preparing silane, in one of the methods, magnesium silicide and magnesium chloride in solvent ammonia are reacted at 0°C, which was invented by the Japanese Komatsu Electronics Company, and the specific reaction is expressed as Eq. (1-5).

$$Mg_2Si + 4NH_4Cl = 2MgCl_2 + 4NH_3 + SiH_4 \quad (1\text{-}5)$$

Another important technique was invented by Union Carbide Company, in which $SiCl_4$ and MG silicon are reacted and $SiHCl_3$ is generated, followed by disproportionation reaction of $SiHCl_3$ to generate SiH_2Cl_2. Finally, silane can be produced after disproportionation reaction of SiH_2Cl_2, the main reactions are:

$$3SiCl_4 + Si + 2H_2 = 4SiHCl_3 \quad (1\text{-}6)$$

$$2SiHCl_3 = SiH_2Cl_2 + SiCl_4 \quad (1\text{-}7)$$

$$3SiH_2Cl_2 = SiH_4 + 2SiHCl_3 \quad (1\text{-}8)$$

Using distillation techniques, high purity Si can be obtained from silane decomposition on a small polysilicon rod at over 850 ºC in the reaction chamber, the chemical reaction is [28]

$$SiH_3 = Si + 2H_2 \quad (1\text{-}9)$$

This method is more suitable for the production of inexpensive SOG polysilicon. The method currently is used in the production of granular polysilicon by Asimi Company (USA) and SGS Company (USA) [29].

c) Fluidized bed method

Fluidized bed technology was developed by Union Carbide Company. This method is based on silicon tetrachloride, hydrogen, hydrogen chloride and industrial silicon which are reacted in the fluidized bed (ebullated bed) under high temperature and high pressure. Then the generated $SiHCl_3$ disproportionates into SiH_2Cl_2 and generates silicon tetrachloride gas (same as Eq. 1-7). silicon tetrachloride gas is blown into the fluidized bed reactor which is filled of small particles of silicon powder and if we do the continuous thermal decomposition reaction (same as Eq. 1-8), granular polysilicon products will be generated finally [30, 31].

As shown in Fig. 1.8, Silane fluidized bed technology has low reaction temperature (575 ~ 6850), low power consumption (SiH_4 thermal decomposition of consumption is 10 kW ћ / kg, equivalent to 10% of Siemens method), high deposition efficiency (theoretically transformed rate can reach 100%), byproducts (H_2) are easy to handle, high yield and other significant advantages. In addition, the product is a granular polysilicon, which can be used in Czochralski Crystal Growth Furnace as continuous feed, reducing monocrystalline silicon cost and improve the yield. The only drawback is poor security. The product purity is not in high purity zone, but can meet the basic use of solar cell production. This method is more suitable for the production of inexpensive solar-grade polysilicon. Companies which are using this method are: REC (Norway), Wacker (Germany), Hemlock (USA) and MEMC Company (USA).

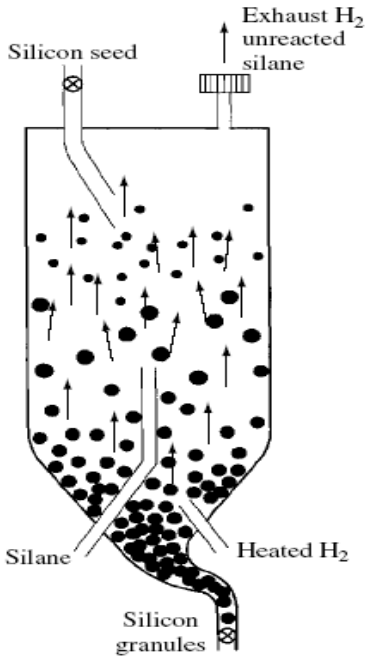

Figure 1.8. Schematic representation of a fluidized bed reactor [32]

1.2.2 Metallurgical production of SOG polysilicon

Although most of SOG silicon comes from the offcut of EG silicon using traditional production, the energy intensive, high cost and environmental pollution cannot be ignored. Therefore, another method called metallurgical method which has advantages such as high productivity, less cost, sustainable process has been applied. Table 1.3 shows the comparison of main indicators for the metallurgical and chemical methods.

Table 1.3 Comparison of main indicators for the metallurgical and chemical methods

Indicator	**Metallurgical method**	**Chemical method （Modified Siemens process）**
Purity	5-7 N	＞9 N
Photoelectric Conversion efficiency	16%	17%
Energy consumption (kW ħ/kg)	50-60	140-200
Cost (dollar /kg)	25-30	40
Contaminate	No toxic	toxic
Size	Large	Small

These are also the reasons why the metallurgy method was chosen to purify the MG silicon by our group. In order to meet the requirements of SOG silicon, many kinds of impurities, such as Fe, Al, Ca, Ti, P, B, C, Cr, Co, etc. in the MG silicon should be

removed step by step using metallurgical process. Because impurities in silicon will affect the properties of solar cells. After measuring the I-V data of solar cell, effects of various impurities on the performance of SOG silicon had been investigated by Davis *et al*. [33]. The conversion efficiencies of p- or n-type solar cells as a function of impurity concentrations are shown in Fig. 1.9.

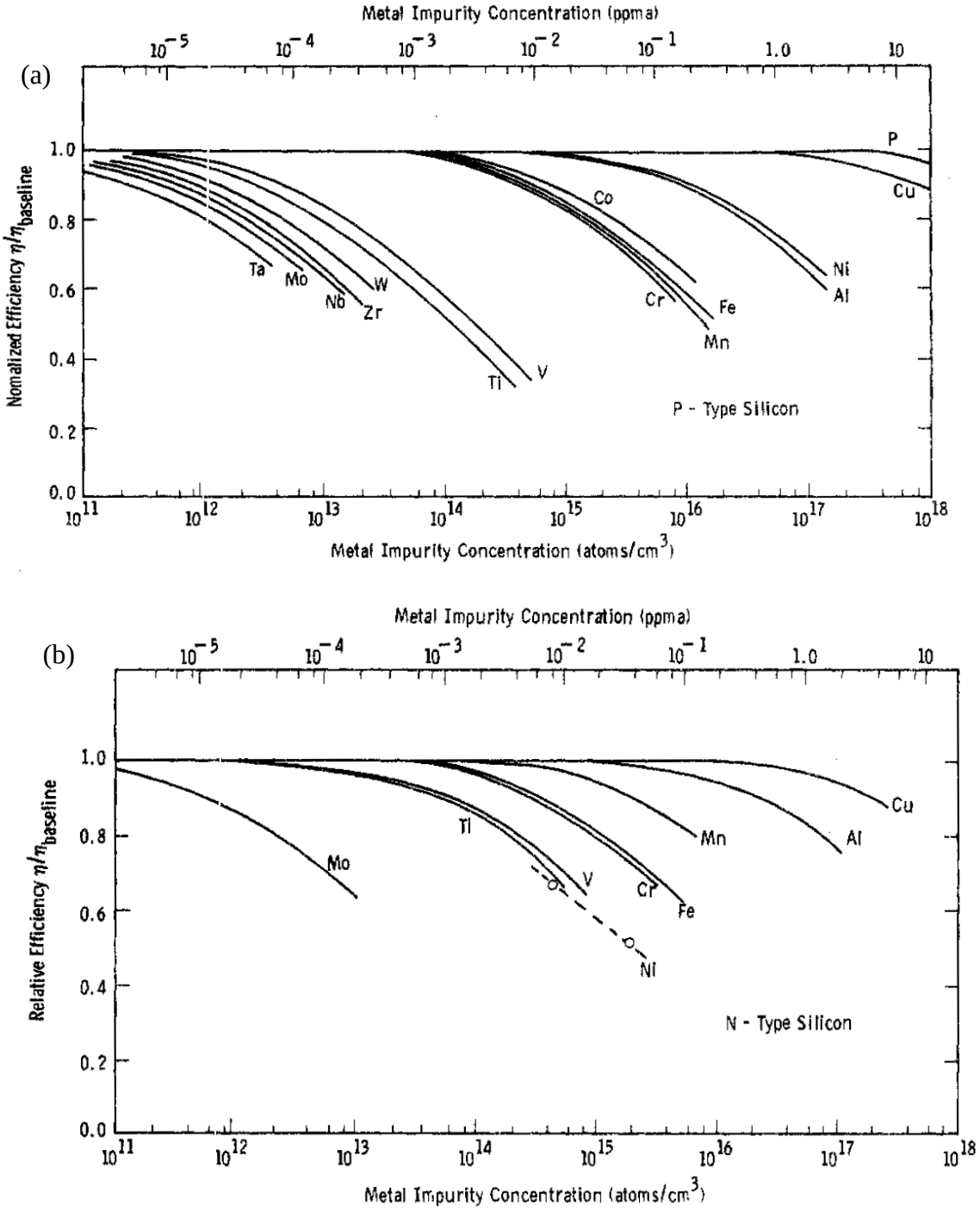

Figure 1.9. Solar-cell efficiencies versus impurity concentration for (a) 4-Ω cm p-base

devices and for (b) 1.5-Ω cm n-base devices [33].

Thus, the concentration of impurities must be controlled strictly. Generally, the required purity of SOG silicon is over 99.9999% (6N). The impurities are mainly divided into five groups: metals, C, O, P and B. Table 1.4 shows the contents of impurities in the MG silicon and requirement of SOG silicon.

Table 1.4 The contents of impurities in the MG silicon and SOG silicon

Impurities	MG silicon (ppmw)	Up-MG silicon (ppmw)	SOG silicon (ppmw)
B	40	<30	<0.3
P	20	<15	<0.1
O	3000	<2000	<5
C	600	<250	<5
Fe	2000	<150	<0.0003
Al	100~200	<50	<0.007
Cu	20~30	<5~10	<1.54
Ti	200	<5	<0.1
Cr	50	<15	<0.1

The typical metallurgical process for purification of MG-Si were applied by NEDO [34-37] and Elkem [38-40]. Fig. 1.10 shows the production process of Elkem, it was considered that the Elkem process was limited to the MG-Si raw materials with low B and P contents, and was not applicable for purification of MG-Si with high impurities.

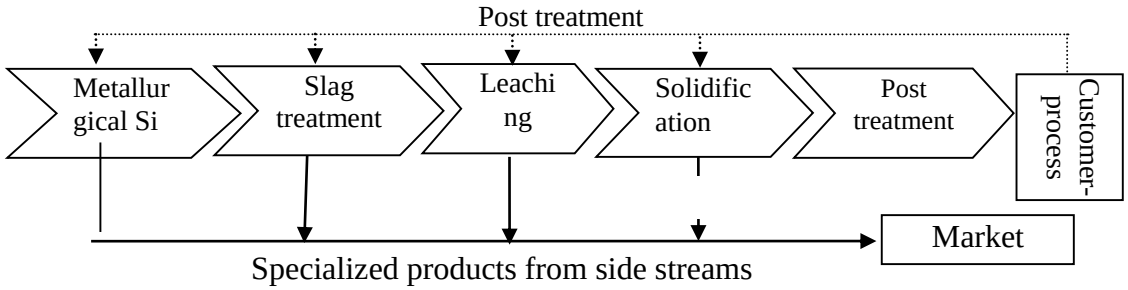

Figure 1.10. Flowchart of Elkem route for production of SOG-Si

The flowchart of metallurgical route for production of SOG-Si announced by Polysilicon Alliance of China is shown in Fig. 1.11. According to this method, the average efficiency reached 15% for polysilicon cells. But low purification (≤6N), light degradation and quality stability are the main problems which restrict the development of metallurgical production of SOG polysilicon.

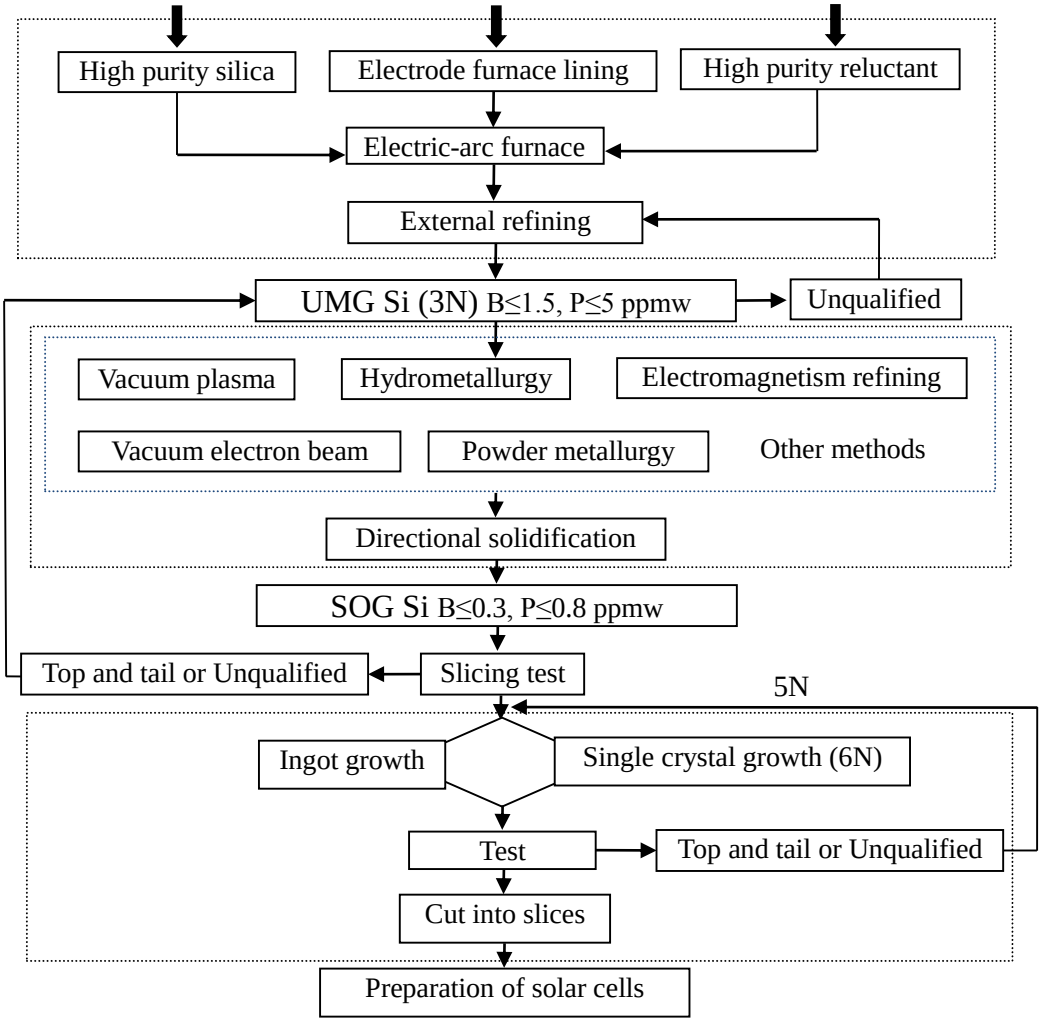

Figure 1.11. Flowchart of metallurgical route for production of SOG-Si

a) Removal process of metallic impurities

The major metallic impurities of MG silicon include Fe, Al, Ca, Ti, Ni, Cu, In, As, Sb, Bi, Sn, Li, Zn, Au, Co, Ta, etc. Most of metallic impurities have very low segregation coefficients with Si, as shown in Table 1.5. The segregation coefficient in thermodynamic equilibrium gives the relation between the concentration of impurity atoms in the growing crystal and that of the melt. It is usually much lower than 1 because impurity atoms "prefer" to stay in the melt. This can be seen from the liquidus and solidus lines in the respective phase diagrams. In order to utilize this obvious property, directional solidification was used to remove metallic impurities. The amount of impurities which are retained in the liquid phase can be calculated by Scheil's equation (1-10):

$$C_L = C_0 \cdot (f_L)^{k_0 - 1} \quad (1\text{-}10)$$

Where, C_0 and C_L are the initial and liquid concentration of impurities, f_L is mass fraction in the liquid phase and k_0 is the segregation coefficient, which is defined as the following Eq. (1-11):

$$k_0 = \frac{C_s}{C_l} \quad (1\text{-}11)$$

Here, C_s is the impurity concentrations in the solid phase.

Segregation coefficients (k_0) are shown in Table 1.5 [41]. In directional solidification process, head and tail of silicon ingot are cut off after the cooling down in vertical orientation. As these impurities are gathered in head and tail when the $k_0 < 1$ and $k_0 > 1$ respectively.

Table 1.5 Segregation coefficients of impurities in directional solidification process [41]

Element	k_0	**Element**	k_0
B	0.8	Sn	1.6×10^{-3}
P	0.35	Pd	5×10^{-5}
Al	2.8×10^{-3}	Au	3×10^{-5}
Ga	8×10^{-3}	Cu	5×10^{-6}
In	4×10^{-4}	Ag	1×10^{-5}
Ti	2×10^{-6}	Ni	3×10^{-5}
N	4×10^{-4}	Co	8×10^{-6}
As	0.3	Li	0.01
O	1.25	Mn	1×10^{-5}
C	0.05	S	1×10^{-5}

In the ideal state, concentration of impurities can be removed by directional solidification, as shown in Fig. 1.12. This method was found to be for the removal of metallic impurities except B and P. The directional solidification is supposed to be repeated twice for removal of Al, Fe and Ti to meet the requirement of SOG-Si.

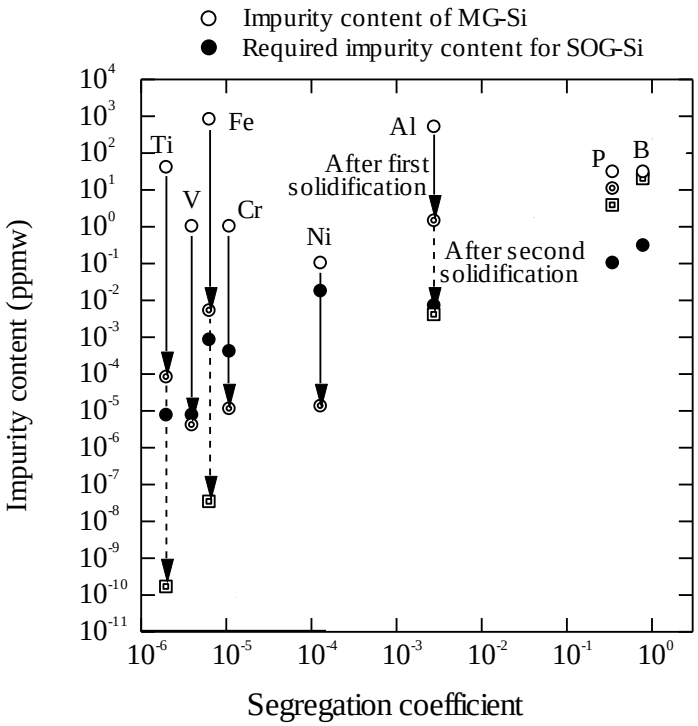

Figure 1.12 Removal of impurities by ideal directional solidification [42].

Besides directional solidification, hydrometallurgical method [43-48] is also a very effective method to remove metallic impurities [49], it refers to chemical treatment or an organic solvent extraction of solid silicon to remove impurities. Hydrometallurgical method, as the pretreatment step of metallurgical method, can not only effectively remove most of the Al, Fe and other metal impurities, reducing the initial concentration of impurities in the subsequent purification process, but also can improve the final product recovery.

b) Removal of carbon (C) from MG-Si

C is a tetravalent element, so without introducing electrical activity in the silicon defects, it will not affect the concentration of minority carrier. However, C can react with oxygen and vacancy existing in the crystal with stripes. When concentration of C exceed the solid solubility of C in the silicon, there will be a small C precipitation. These defects will reduce the breakdown voltage of silicon devices greatly, increase leakage current. Furthermore, SiC particles will be formed when concentration of C exceed the solid solubility, The SiC particles introduce dislocations which are detrimental to solar cell operation. Several researchers indicated that the solubility limit of C in molten Si is important for preventing the formation of SiC particles. The C solubility is summed up

as a relationship with temperature in Fig. 1.13 [50-54]. At 1693K (melting point of Si), the solubility of C in molten Si was identified as 10 ppmw.

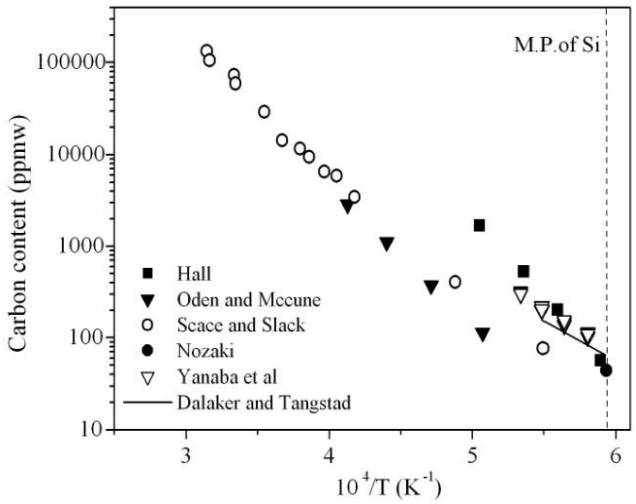

Figure 1.13. Solubility of C in molten Si

In order to remove C from MG-Si, filtration and oxidation method were applied by Sakaguchi *et al*. and they were successful in removing from 100 to 30-60 ppmw [55]. T. Ikeda *et al.* [56] reported that the concentration of C was decreased to 15 ppmw using electron beam melting (EBR) treatment under 10^{-2}Pa for 30 min. An attempt to remove C from molten Si by a plasma arc combined with conductive heating was reported by Søiland [57]. The non-transferred arc was run with equal quantities of H_2 and Ar, containing 2 vol% and 4 vol% O_2 in flow and with temperatures of 1823 K and 1753 K. Due to contamination from the atmosphere above the liquid surface, carbon level in the liquid silicon varies considerably. Reason for that might be the reaction between humidity contained in the furnace insulation and the graphite crucible, producing CO gas [58].

c) Removal of oxygen (O) from MG-Si

Because Si crystal growth is fast, thermal process time during the preparation of solar cells is short, the opportunity and quantity of defect formation and oxygen precipitation is very less. So the oxygen element has little impact on solar cells.

O in Si normally comes from the high-purity-fused quartz (SiO_2) crucible. The solubility of oxygen in molten Si has been investigated by some scholars [59, 60-63]. The solubility of O in molten Si is shown in Fig. 1.14. The value of O solubility in molten Si was estimated to be in the range of 20~40 ppmw, because it was hard to be determined precisely due to the formation of SiO vapor.

R. Einhaus *et al*. [64] indicated that the C concentration had been effectively reduced

from 90 ppmw to 20-25 ppmw using plasma treatment (section 1.2.3). Z.X. Zheng [65] introduced that as oxygen, hydrogen and water vapor are blown into the silicon fluid, the invention leads the hydrogen and the oxygen to be reacted in the silicon fluid, so as to generate local high temperature and remove the O element in the silicon fluid along with the emission of the gas, thereby providing a method which has simple operation step and low production cost for reducing the content of oxygen and carbon in the silicon metal.

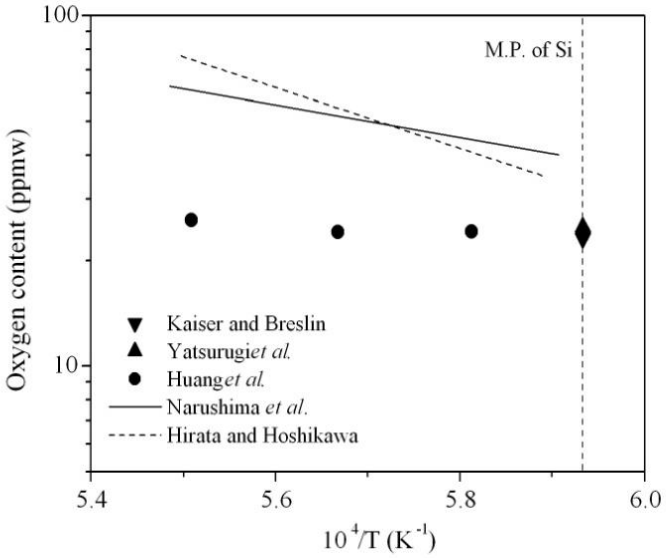

Figure 1.14. Solubility of oxygen in molten Si.

d) Removal process of phosphorus (P)

P cannot effectively be removed by directional solidification method due to its high segregation coefficient (k_0 = 0.35). The most effective techniques are electron beam (EB) treatment and vacuum treatment. Vacuum distillation technique for the purification of molten metals and alloys has been developed mainly in the last century. difference in the vapor pressures of liquid silicon and volatile impurities is the basic principle of vacuum refining [66]. The criterion for refining of an element from liquid silicon through vacuum refining is expressed in Eq. (1-12):

$$\frac{p_{\mathrm{i}}}{p_{\mathrm{Si}}} > \frac{x_{\mathrm{i}}}{x_{\mathrm{Si}}} \tag{1-12}$$

Where p_i and p_{Si} represent the partial pressure of the impurity and silicon, respectively. x_i and x_{si} are their molar fractions in the molten Si.

By equilibrating a molten Si-P alloy in a controlled phosphorus partial pressure

(P_{P2}=0.00118-0.493 Pa) in the temperature range of 1723-1848 K, the Gibbs energy change of phosphorus dissolution into molten silicon shown in Eq. (1-13) was determined by analyzing the equilibrium P concentration in Si.

$$\frac{1}{2}P_{2(g)} = \underline{P}\ (mass\ \text{pct, in Si}) \tag{1-13}$$

It was confirmed that equilibrium was attained for each experiment and Henry's law is valid up to 0.1 mass%P. The Gibb energy change for Eq. (1-13) was determined as Eq. (1-14) [42].

$$\Delta G^0 = -139,000(\pm 2,000) + 43.4(\pm 10.1T)\ (J/mol) \tag{1-14}$$

Fig. 1.15 [67] shows the relationship between equilibrium partial pressure of P, P_2 and phosphorous content of silicon at 1823K. From the experimental results, at the condition that P is lower than 50 ppm, P gas was found to be dominant as the equilibrating P vapor species rather than P_2 gas.

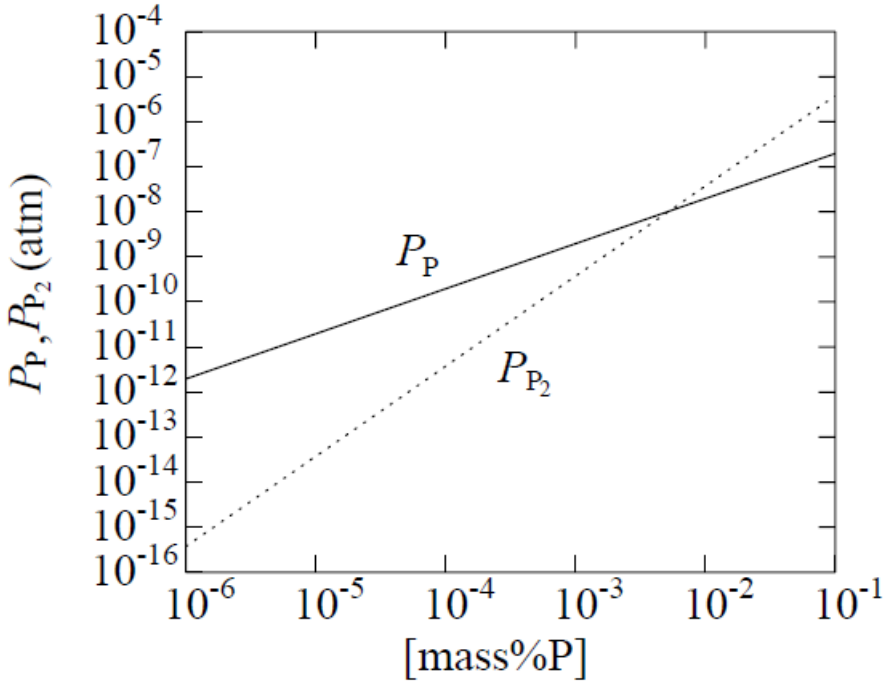

Figure 1.15. Relationship between equilibrium partial pressure of P, P_2 and phosphorous content of silicon at 1823K.

Many researchers did lots of work about P removal. Maeda *et al.* [56] declared that Al, C, P and Ca were removed 75%, 90%, 93% and 89% from Si, respectively using EB treatment under 10^{-2} Pa for 30 min. The content of P in MG-Si decreased from 32 ppmw to around 6 ppmw after 1 hour using vacuum treatment by Suzuki *et al.* [68]. After pilot-

scale experiment, Zheng *et al.* [69-71] reported that the concentration of P decreased from 15 ppmw to 0.08 ppmw. Shuang Shi [72] introduced that the content of P was decreased from 33.2×10^{-4} wt.% to 0.07×10^{-4} wt.% after 1920 s using electron beam method at a power of 21 kW, which achieves the target for solar-grade silicon of less than 0.1×10^{-4} wt.%.

Research about vacuum method still continues, the key issue is to determine the theoretical support such as reaction control conditions, the reaction order and how to improve the removal rate and lower production costs. In addition, how to improve loading capacity for realize industrialization also needs to be resolved as soon as possible.

e) Removal process of boron (B)

B is one of the principal impurities to affect the properties of solar cells. If the content of B is more than 0.3 ppmw, the lifetime of minority carrier and the photoelectric conversion efficiency will be decreased. In addition, B is the most difficult impurity to be removed due to the high segregation coefficient (k_0=0.8) and low saturated vapor pressure (6.78×10^{-7} Pa, 1823 K). Thus, the conventional directional solidification and vacuum melting methods cannot effectively remove it.

How to remove B? Nowadays, high-temperature plasma, gas blowing, low-temperature with Si-based solvent, slag refining are main methods for B removal. The details will be discussed in next section.

1.2.3 Boron removal treatments from MG silicon using metallurgical method

a) high-temperature plasma treatment

The plasma treatment [68] using thermal plasma combined with liquid silicon, can increase the dynamics of impurity separation ability, to achieve the purpose of B removal. In the plasma treatment, gaseous boron oxides such as BO, B_2O, B_2O_3, etc. are expected to form at temperatures higher than 2300 K. In these boron oxides, BO has a relatively high vapor pressure. Ar-H_2O [73], Ar-CO_2 [68], Ar-H_2-H_2O [74], Ar-H_2-O_2 [75] and Ar-He-H_2O [76] were chosen as plasma gas to oxide and hydrogenate the B. the schematic diagram of the plasma process is shown in Fig. 1.16 [77].

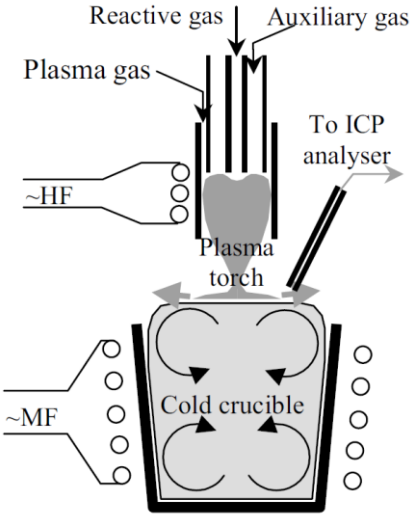

Figure 1.16 Schematic diagram of the plasma process [77]

b) Gas blowing treatment

The gas blowing method can be defined as the process in which oxidizing gas such as O_2+H_2O or O_2 are blown into liquid Si and B contained in Si is oxidized, generating a B-contained gas, such as BHO gas, which is vented out.

Kondo Jiro, *et al*. [78] applied a process in which reaction gases (Ar, H_2, H_2O and O_2) were blown to the bottom of the liquid Si to oxidize B, B content decreased from 25 ppmw to 5 ppmw. A gaseous mixture of steam and Ar (or Ar-H_2) was used to blow high purity SiO_2 powder by Sharp Corporation [79], B, C, and non-metallic elements, Fe, Ca, Al metal elements were removed from the molten Si, and B content could be reduced to 1.2 ppmw.

At high temperature (T > 1685K), beside the oxidation of B in molten Si forming gases, such as BO, B_2O_3, B_2O, BO_2, B_2O_2, hydroxide gases, including $B_3H_3O_6$, BHO_2, BH_3O_3, BHO, BH_2O_2, $B_2H_4O_4$ can also be formed under humid atmosphere (Ar-H_2O-O_2). Their equilibrium partial pressures are 10^5 to 10^{10} times than oxidizing gases and can be easily vapored.

c) Low-temperature with Si-based solvent treatment

Low-temperature with Si-based solvent treatment is based on the limitation of boron' solubility in Si-based solvent, such as Si-Al [80], Si-Cu [81], Si-Sn [82], Si-Al-Sn [83] at low-temperature (below Si melting point), B can be removed during a solidification refining process.

According to Aluminum Company of America and Union Carbide Corporation's patent,

Cu, Cu-Al or Al solvent can be used to predicate MG-Si [84, 85]. It was effective to remove the metallic impurities, but the removal of B and P were not revealed. From 2003, the thermodynamics on SOG-Si refining with Si-Al melt at low temperature has been intensively investigated by Yoshikawa and Morita [80, 86-90]. A novel concept of low-temperature solidification refining of Si with Si-based solvent has been proposed. In particular, the possibility of the removal of elements such as P and B, which cannot be effectively removed by conventional directional solidification method was clarified as shown in Fig. 1.17. The B content was decreased from 56 ppmw to 0.88 ppmw using Al-Si alloy treatment [87].

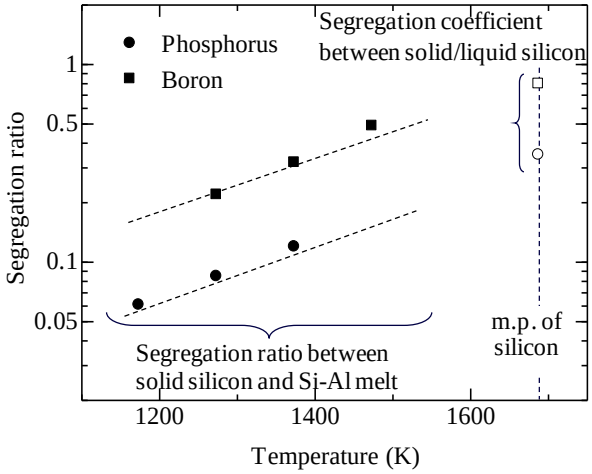

Figure 1.17. Temperature dependence of segregation ratios of phosphorus and boron between solid silicon and Si-Al melt [89].

d) Slag refining treatment

In slag refining method the oxidation reactions are utilized between impurities in molten Si and slag, during the process, oxidized impurities are transferred from molten Si to the slag, the impurities in silicon melt float to the surface or sink to the bottom of the silicon melt, after solidification Si ingot and slag are separated.

In 1990, Suzuki *et al*. [68] reported that B can be removed from molten Si using oxidized slag such as $CaO\text{-}SiO_2$, $CaO\text{-}CaF_2\text{-}SiO_2$, $CaO\text{-}MgO\text{-}SiO_2$ ($\text{-}CaF_2$), and $CaO\text{-}BaO\text{-}SiO_2$ ($\text{-}CaF_2$) due to the partition ratio of B between Si and various slags at 1723 to 1823 K under CO or Ar atmosphere. The principle of B removal using slag refining is shown in Eq. (1-15). B is oxidized to $BO_{1.5}$, which is transferred from molten Si to the slag due to the partition ratio between molten Si and slag, as shown in Fig. 1.18.

$$B_{(l)} + \frac{3}{4}SiO_{2(l)} = BO_{1.5(l)} + \frac{3}{4}Si_{(l)} \quad (1\text{-}15)$$

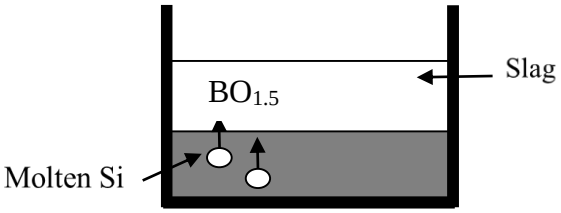

Figure 1.18 Schematic diagram of B removal by slag refining

The effectiveness of a slag to extract impurities is determined by thermodynamics and the kinetics of the system. The thermodynamics determines the potential of a slag to remove impurities and can be evaluated by the partition ratio given by Eq. (1-16)

$$L_B = (mass\%B)/[mass\%B] \quad (1\text{-}16)$$

Where L_B is the partition ratio of B between molten Si and slag, (mass%B) is the weight concentration of B in the slag, $[mass\%B]$ is the weight concentration of B in the molten Si. The partition ratio should be as high as possible to minimize the amount of slag needed for refining, and thus the cost. Unfortunately, typical values of the L_B range are between 1 and 2. L. A. V. Teixeira *et.al*. reported that the highest value of L_B is around 5.5, as shown in Fig. 1.19 [91]. It means that large amounts of slag are needed to refine Si.

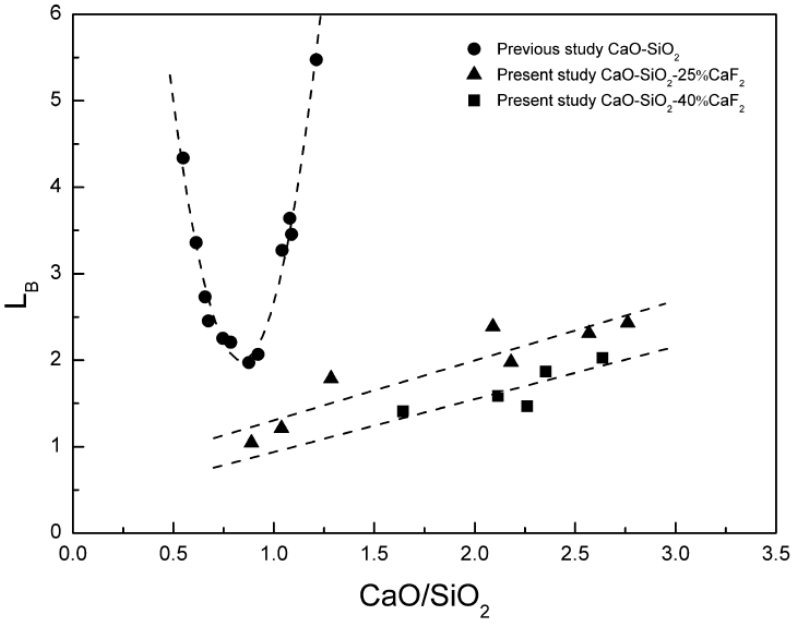

Figure 1.19. Boron partition ratio between the slag and the silicon phase for silicate

slags as a function of the final basicity of the slag equilibrated at 1823K [91]

Recently, various slags were tried to refine MG-Si by many researchers. $CaO-SiO_2-Al_2O_3$, $CaO-SiO_2-MgO$ and $CaO-SiO_2-Na_2O$ have been investigated [92], which are commonly employed in the steelmaking industry. Khattak and Ravi [93] described that boron in MG-Si was reduced from 18 ppmw to 1 ppmw using a calcium silicate slag in an arc furnace. Johnston and Barati [94], Cai *et al*. [95] and Luo *et al*. [96] studied the effects of $Al_2O_3-CaO-MgO-SiO_2$, $Al_2O_3-BaO-SiO_2$, $CaO-SiO_2-CaF_2$ and $CaO-SiO_2-Al_2O_3$ slag basicity on boron removal. Wu J., *et al*. [97] reported that a little obvious advantage to boron removal was found using $CaO-Li_2O-SiO_2$, the B concentration in MG-Si could be reduced from 18 ppmw to 1.3 ppmw with the mass ratio of slag to MG-Si for 4:1.

Although slag refining treatment has obvious advantages such as low cost, Low equipment requirements and large scale, the limitation of B removal need us to find new methods to comprehensively utilize the four treatments.

1.3 Comprehensive utilization for Boron removal process

Nowadays, researchers have begun to remove B using two or more removal methods, such as plasma and gas blowing, slag and gas blowing, Si-based solvent and slag. It can be predicted that these kind of ideas have good prospects in B removal.

1.3.1 Boron removal from Si-Sn alloy and CaO-SiO_2-CaF_2 slag

Ma, *et al*. [82] introduced that B can be removed from Si-Sn alloy and CaO-SiO_2-24mol%CaF_2 slag at 1673K. A remarkable increase in the activity coefficient of B by the addition of Sn to Si from the equilibrium relation between the Si-Sn melt and SiB_6 or B solid solution was found [98]. Thus, by applying the slag treatment to Si-Sn melt, higher partition ratio of B can be expected according to Eq. (1-17):

$$L_B^{'} = \frac{x_{BO1.5}}{x_B} = \frac{K \cdot (\gamma_B)}{(\gamma_{BO_{1.5}})} \cdot \left(\frac{a_{SiO_2}}{a_{Si}} \right)^{3/4} \quad (1\text{-}17)$$

Where K is the equilibrium coefficient of Eq. (1-15).

The schematic diagram of experimental setup is shown in Fig. 1.20. 3g of pre-melted Si-Sn alloys added with 90~900 ppmw B were charged in a graphite crucible with the mixture of about 9g of SiO_2-CaO-24mol%CaF_2 slag (CaO/SiO_2 =0.32~4.35). The crucible was then kept at 1673 K under the Ar gas for 18 hours for preliminary experiments. Since the vapor pressure of pure Sn is as high as 12 Pa at 1673 K, the crucible was sealed with a lid. After equilibrium, the graphite crucible was quickly withdrawn from the furnace and quenched in a water bath. The slags were mechanically separated from alloys. The surfaces of slag and alloy were cleaned for chemical analysis [99].

The partition ratio of B is plotted against the CaO/SiO_2 ratio in Fig. 1.21, together with the reported data where molten Si was equilibrated with CaO-SiO_2-(20 or 33 mol%) CaF_2 slag at 1823 K [91] for comparison. The partition ratio of B between slag and Si-Sn melt was increased with the increase in CaO/SiO_2 ratio and was over 5 times higher than that for slag/Si equilibration [82].

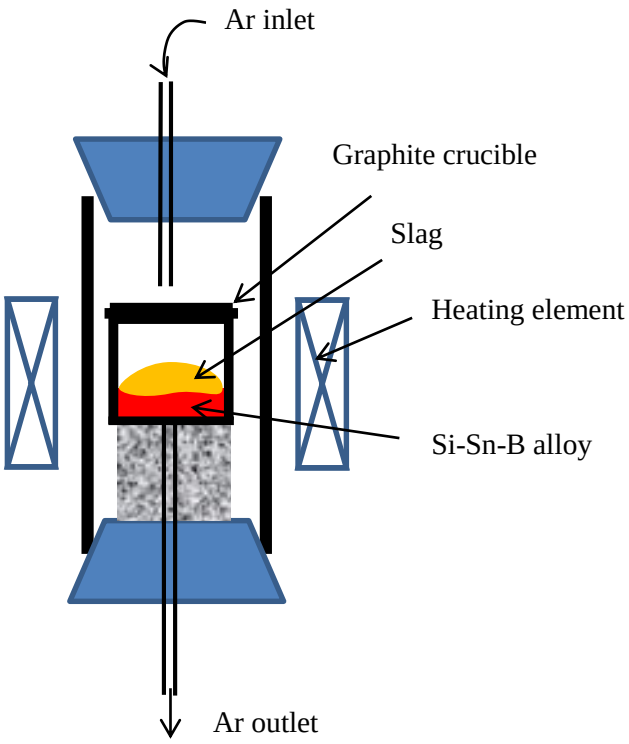

Figure 1.20. The experimental setup for equilibration experiment [99]

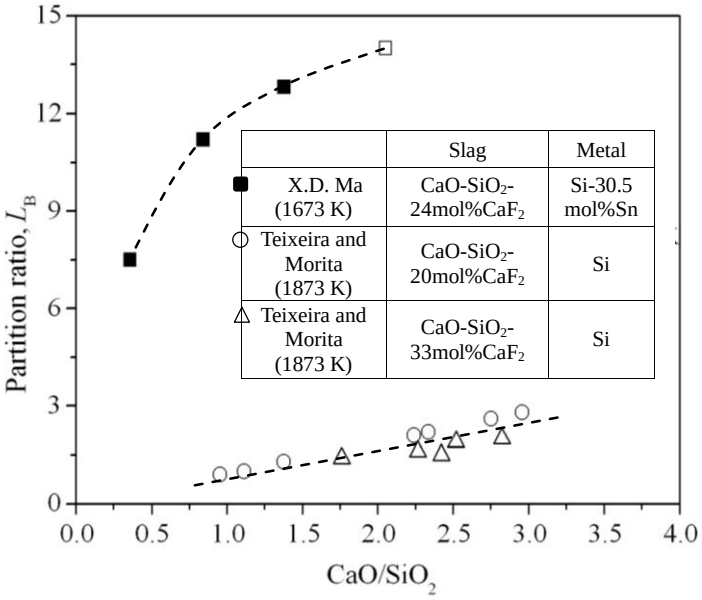

Figure 1.21. Relationship between partition ratio of B and CaO/SiO_2 ratio [82]

(□: Initial ratio of CaO/SiO_2. The alloy with slag during experiment.)

The total process for Si refining by using Si-Sn solvent is, (1) alloying MG-Si with Sn to form the Si-Sn melt, (2) slag treatment, (3) solidification of Si from Si-Sn melt, and (4) collection of the refined Si crystals by acid leaching.

1.3.2 Evaporation of boron in hydrogen atmosphere

Bjerke Helene, *et al*. [100] introduced that B can be removed and evaporated using Al_2O_3-MgO-SiO_2 slag or CaO-SiO_2-TiO_2 slag with hydrogen atmosphere at 1823K. When boron enters the slag phase it will be oxidized. However, evaporation of boron oxides is thermodynamically unfavorable. Boron hydrides such as HBO, BHO_2 and $B_3H_3O_3$ are previously reported to have higher vapor pressures than the boron oxides, a hydrogen atmosphere may therefore improve the vaporization of boron from the slag [101]. For HBO the reaction can be written as:

$$B_2O_3 + 2H_{2(g)} = 2HBO_{(g)} + H_2O_{(g)} \quad (1\text{-}18)$$

If B can be evaporated from the slag as HBO gas, less slag will be needed in the refining and a higher refining rate will be obtained. In turn the cost of the process will be reduced as well as the waste slag after refining. B can be evaporated from the CaO-SiO_2 slag when refined in an atmosphere containing 50% hydrogen, but the evaporation rate is low.

B evaporation was investigated in the temperature range 1723-1823K, the refining time was 0-6 hours and the slag/silicon mass ratio was varied between 0.25 and 1.5. Fig. 1.22 illustrates the increased refining effect by using hydrogen for this particular system. It is shown that the refining efficiency compared to conventional slag refining is increased by 51%, when the amount of slag is a quarter of silicon amount. If the amount of slag is 1.5 times the amount of silicon the refining efficiency is increased by 34% with the use of hydrogen. [100]

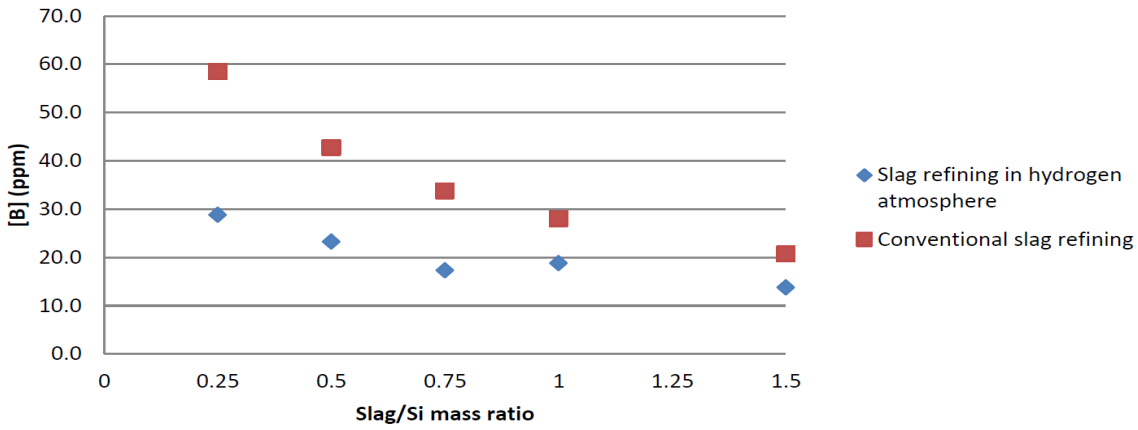

Figure 1.22. The amount of boron in silicon after 3 hours refining for conventional slag refining and slag refining in hydrogen atmosphere, respectively.

1.3.3 Evaporation of boron in chlorine atmosphere

Nishimoto *et al*. [102] in our group investigated B removal by 55wt%CaO-45wt%SiO_2 slag in Cl_2 atmosphere. Some experiments on chlorination of B in Si and that of borate in slag using Cl_2 gas were also carried out. Experimental results showed that the slag refining process with chlorination can be proposed as a promising method for the B removal from molten Si [103].

In the experiments, slag with a composition of 55 wt% CaO and 45 wt% SiO_2 was melted together with silicon containing approximately 300 mass ppmw boron. The melting took place in a graphite crucible at 1823K in a resistance furnace. Cl_2 gas was introduced into the furnace (P_{Cl2}=0.25 atm, 400 ml/min STP). After the reaction, the atmosphere was purged with Ar gas, and the sample was solidified by decreasing the temperature to 1573 K.

Fig. 1.23 shows the result of the experiment in which Cl_2 gas was blown onto the mixture of silicon and slag. The B content of the slag and silicon decreased 20% and 10% in the Cl_2 gas stream, respectively, which brought about the decrease in partition ratio of B from 2.2 to 2.0, probably due to the slower mass transfer of B in slag phase. Considering that B in molten silicon was only removed by chlorination when slag exists, the chlorinated species of B is considered to be boron oxy-chloride, BO_xCl_y. Further investigation on specifying the species would be helpful in optimizing the slag treatment with chlorination.

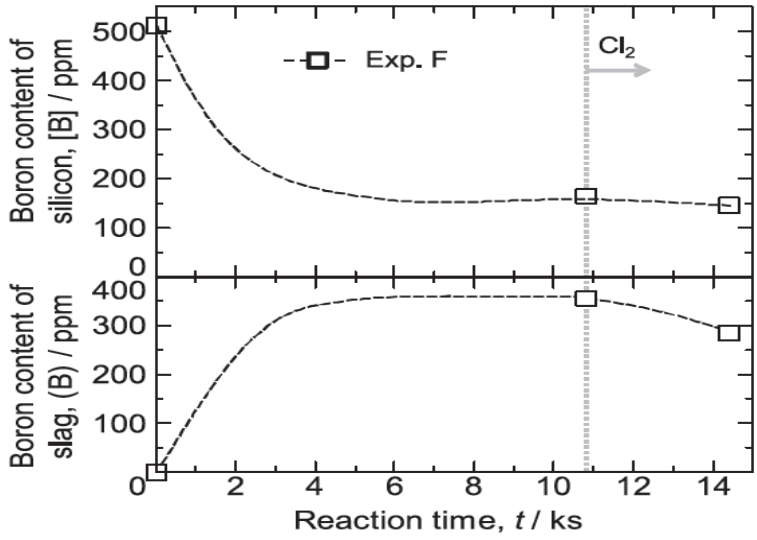

Figure 1.23. Changes in B content of silicon and slag during the Ar-Cl_2 gas blowing [103]

1.4 Innovation and objectives of this study

1.4.1 Innovation of this study

The availability of abundant and low-cost solar grade silicon (SOG-Si) feedstock is essential for the widespread use of solar cells. The potential for cost reduction in chemical processes is limited by the low productivity of Si. An alternative cost-effective, energy-efficient process to produce solar grade silicon (SOG-Si) is the metallurgical process, which is considered to be sustainable and offers benefits in productivity and process cost.

B removal by slag treatment has been studied mainly for $CaO\text{-}SiO_2$ slag. The partition ratio (L_B), is not high enough for B removal by a single slag treatment. In order to improve B removal efficiency in slag refining, evaporation of B in hydrogen and chlorine atmosphere with various slags were investigated by Helene Bjerke *et al.* and Nishimoto *et al.*, respectively. It was found that if only Cl_2 gas blown into the molten Si, the B did not decrease, but if Cl_2 gas together with $CaO\text{-}SiO_2$ slag were supplied, B content decreased which presumably is due to B oxy-chloride gas formation. Although such removal by gaseous evaporation during slag treatment is considered to be a possible refining technique, the reaction mechanism has not been clarified yet. In addition, considerable Si loss occurs during the reaction with Cl_2 gas.

Thus, the innovation of this study is that instead Cl_2 gas, high purity $CaCl_2$ was selected as another candidate material for the Si refining with $CaO\text{-}SiO_2$ slag by considering the following advantages.

1) B is expected to be removed by slag and oxy-chloride gas formation.
2) $CaCl_2$ can reduce the melting point and viscosity of slag.
3) Compared with Cl_2 gas, $CaCl_2$ is more safe and environmental friendly.

1.4.2 Objectives and works of this study

In this study, physical chemistry on MG-Si refining using $CaO\text{-}SiO_2\text{-}CaCl_2$ slag was investigated with the objective of developing a new B removal process for meeting the requirement of SOG-Si production (B<0.3 ppmw).

This dissertation contains 7 chapters, and the first chapter is introduction.

In chapter 2, in order to determine the possibility of B evaporation from $CaO\text{-}SiO_2\text{-}CaCl_2$ slag system, thermodynamics of the reaction was investigated and the estimated relationships between the partial pressures of BOCl, BCl_x, $SiCl_x$, and $CaCl_2$ and the mole

fraction of CaO in the $CaO\text{-}CaCl_2$ slag were also studied.

In chapter 3, to identify the property of $CaO\text{-}SiO_2\text{-}CaCl_2$ slag, the density and mole volume of $CaO\text{-}SiO_2\text{-}CaCl_2$ slag at 1723K were investigated by an improved Archimedian method. The solidus, liquidus and binary phase diagram of $SiO_2\text{-}CaCl_2$ were investigated by TG-DTA method. Furthermore, the liquidus and phases of $CaO\text{-}SiO_2\text{-}CaCl_2$ ternary slag were also investigated at 1723K.

In chapter 4, for the sake of quantifying the transfer rate of B from molten Si to the $CaO\text{-}SiO_2\text{-}CaCl_2$ slag, reaction mechanism of B removal from molten Si to molten slag and that of evaporation from slag to gas phase was clarified. Hence, assuming a diffusion model of B transfer from Si to molten slag and its evaporation as a gas phase, the diffusion coefficient of B in the slag was investigated based on the tube-molten pool method at 1723K. Furthermore, the mass transfer coefficients of B in the slag were also measured and calculated according to Fick's law.

In chapter 5, after confirming the possibility of evaporating B oxychloride species through the reaction of $BO_{1.5}$ with $CaCl_2$, B removal processes from MG-Si using $CaO\text{-}CaCl_2$, $SiO_2\text{-}CaCl_2$ and $CaO\text{-}SiO_2\text{-}CaCl_2$ slag systems were carried out at 1723K in the resistance furnace at laboratory scale. Having confirmed that a $CaO\text{-}SiO_2\text{-}CaCl_2$ slag system offers the best potential to achieve good B-removal, it was explored further to ascertain whether this performance held true at various scales in an industrial environment. Therefore, various scales of Si/slag refining were carried out with the times of 1, 1.5 and 2 hours at 1723K using induction furnace and vacuum furnace.

Chapter 6 summarizes the important findings in this research.

Reference

[1] S. Bilgen, Acta Physico-Chimica Sinica, 2009. 25(8): p. 1645-1649.

[2] S. Bilgen, Renew Sust Energ Rev, 2014. 38: p. 890-902.

[3] K. Kaygusuz and S. Bilgen, Energ Sources, Part B, 2008. 3(4): p. 396-410.

[4] K. Rennings, B. Brohmann, J. Nentwich, J. Schleich, T. Traber and R. Wüstenhagen, Springer-Verlag, 2013.

[5] F.Y. Li, Z.Y. Song and W.D. Liu, Energy Policy, 2014. 64: p. 193-202.

[6] British Petroleum. Statistical review of world energy June 2014. 2014.

[7] Nuclear Energy Agency. 2014: The Stationery Office.

[8] BP Energy Outlook. 2014, BP, London: UK. p. 4.

[9] BP Energy Outlook. 2014, BP, London: UK. p. 12.

[10] S. Bilgen, K. Kaygusuz and A. Sari, Energy Sources, Part A, 2008. 30: p. 325-333.

[11] X.H. Yao, C.K. Chan, M. Fang, S. Cadle, T. Chan, P. Mulawa, K.B. He and B.M. Ye, Atmospheric Environment, 2002. 36(26): p. 4223-4234.

[12] M.D. Bermejo, Á. Martín, J.P.S. Queiroz, P. Cabeza, F. Mato and M.J. Cocero, Editors. 2014, Springer. p. 401-426.

[13] F. Bran, I. Ioan, C.V. Rădulescu and I.M. Ghidiu-Bita, Inter. J. of Acad. Res. in Enviro. and Geo., 2014. 1(1): p. 45-51.

[14] G. Boyle. 2004: Oxford university press.

[15] N. Armaroli and V. Balzani, Wiley-VCH, Weinheim, 2011.

[16] REN21. 2014: France. p. 15.

[17] V. Vladislav. Renewable Energy World 2013 ; Available from: http://www.renewableenergyworld.com/rea/news/article/2013/08/azerbaijan-aims-to-boost-output-of-renewable-energy?cmpid=WNL-Friday-August2-2013.

[18] J.M. Pearce, Futures, 2002. 34(7): p. 663-674.

[19] M. Bazilian, I. Onyeji, M. Liebreich, I. MacGill, J. Chase, J. Shah, D. Gielen, D. Arent, D. Landfear and S. Zhengrong, Renew Energy, 2013. 53: p. 329-338.

[20] EPIA, in *Global Market Outlook for Photovoltaics 2014-2018*. 2014. p. 42.

[21] M.A. Green. Solar cells: operating principles, technology, and system applications. 1982.

[22] Wikipedia. Feb, 2015 ; Available from: http://en.wikipedia.org/wiki/Solar_cell.

[23] ISE. Fraunhofer, Fraunhofer ISE, 2013.

[24] Global Competitive Intelligence Tracker. Mar 25, 2014, GTM Research.

[25] B. Paul. 2014 ; Available from: http://www.electronics-eetimes.com/en/french-german-collaborators-claim-solar-cell-efficiency-world-record.html?cmp_id=7&news_id=222923159.

[26] ISE Fraunhofer, Fraunhofer ISE, 2014: p. 25.

[27] T. Yang, Guizhou Chemical Industry, 2009. 34(3): p. 7-11.

[28] M.S. Gordon, D.R. Gano, J.S. Binkley and M.J. Frisch, J Am Chem SOC, 1986. 108(9): p. 2191-2195.

[29] P. Qu, M. Qu and J. Zhou, Solar Energy 2008. 7: p. 8.

[30] Y. Poong and S. Yongmok. 1990, Google Patents.

[31] S.M. Lord. 2004, Google Patents.

[32] A. Luque and S. Hegedus. 2011: John Wiley & Sons.

[33] J.R. Davis, A. Rohatgi, R.H. Hopkins, P.D. Blais, P. Rai-Choudhury, J.R. McCormick and HC. Mollenkopf, Ieee T Electron Dev, 1980. 27(4): p. 677-687.

[34] R.F. Clark, M.G. Mauk, R.B. Hall and A.M. Barnett. 2003, Google Patents.

[35] Y. Kato, K. Hanazawa, H. Baba, N. Nakamura, N. Yuge, Y. Sakaguchi, S. Hiwasa and F. Aratani, ISIJ Int, 2000. 86(11): p. 717-724.

[36] K. Hanazawa, M. Abe, H. Baba, N. Nakamura, N. Yuge, Y. Sakaguchi, Y. Kato and F. Aratani. 2001, Google Patents.

[37] N. Yuge, M. Abe, K. Hanazawa, H. Baba, N. Nakamura, Y. Kato, Y. Sakaguchi, S. Hiwasa and F. Aratani, Prog Photovoltaics, 2001. 9(3): p. 203-209.

[38] K. Peter, R. Kopecek, T. Pemau, E. Enebakk, K. Friestad, R. Tronstad and C. Dethloff. in Photovoltaic Specialists Conference. 2005. : IEEE.

[39] K. Peter, R. Kopecek, A. Soiland and E. Enebakk. in *This conference*. 2008.

[40] M. Kaes, G. Hahn, K. Peter and E. Enebakk. in *Photovoltaic Energy Conversion*. 2006. : IEEE.

[41] RH. Hopkins and A. Rohatgi, J Cryst Growth, 1986. 75(1): p. 67-79.

[42] K. Morita and T. Miki, Intermetallics, 2003. 11(11): p. 1111-1117.

[43] TL. Chu and S.S. Chu, J. Electrochem. Soc. , 1983. 130(2): p. 455-457.

[44] X.M. Li, Y. M. Dang, W. F. Li, J. X. Zhao and Y. R. Cui, AMR, 2013. 813: p. 7-10.

[45] K.Q. Xie, Y. Mai, W.H. Ma, K.X. Wei, J.H. Zhou and L. Zhang, Metallurgist, 2013.

57(7-8): p. 633-638.

[46] IC. Santos, AP. Goncalves, C.S. Santos, M. Almeida, MH. Afonso and M.J. Cruz, Hydrometallurgy, 1990. 23(2): p. 237-246.

[47] JM. Juneja and TK. Mukherjee, Hydrometallurgy, 1986. 16(1): p. 69-75.

[48] SK. Sahu and E. Asselin, Hydrometallurgy, 2012. 121: p. 120-125.

[49] X.D. Ma, J. Zhang, T.M. Wang and T.J. Li, Rare metals, 2009. 28(3): p. 221-225.

[50] RN. Hall, J Appl Phys, 1958. 29(6): p. 914-917.

[51] LL. Oden and RA. McCune, MMTA, 1987. 18(12): p. 2005-2014.

[52] H. Dalaker and M. Tangstad, Mater Trans, 2009. 50(5): p. 1152-1156.

[53] K. Yanaba, M. Akasaka, M. Takeuchi, M. Watanabe, T. Narushima and Y. Iguchi, Materials Transactions, JIM, 1997. 38(11): p. 990-994.

[54] RI. Scace and GA. Slack, J Chem Phys, 1959. 30(6): p. 1551-1555.

[55] K. Sakaguchi and M. Maeda, ISIJ Int, 1987. 73: p. S1440.

[56] T. Ikeda and M. Maeda, ISIJ Int, 1992. 32(5): p. 635-642.

[57] A.K. Søiland, NTNU, 2005.

[58] A. Ciftja, in *Refining and Recycling of Silicon: A Review*. 2008, NTNU.

[59] Y. Yatsurugi, N. Akiyama, Y. Endo and T. Nozaki, J Electrochem Soc, 1973. 120(7): p. 975-979.

[60] W. Kaiser and J. Breslin, J Appl Phys, 1958. 29(9): p. 1292-1294.

[61] H. Hirata and K. Hoshikawa, J Cryst Growth, 1990. 106(4): p. 657-664.

[62] X.M. Huang, K. Terashima, H. Sasaki, E. Tokizaki and S. Kimura, JJAP, 1993. 32(9R): p. 3671.

[63] T. Narushima, K. Matsuzawa, Y. Mukai and Y. Iguchi, Mater T JIM, 1994. 35(8): p. 522-528.

[64] R. Einhaus, J. Kraiem, F. Cocco, Y. Caratini, D. Bernou, D. Sarti, G. Rey, R. Monna, C. Trassy and J. Degoulange, Proc. of the 21st Euro. PVSEC, 2006: p. 6-9.

[65] Z.X. Zheng, L. Nanan City Sanjing Silicon Products Co., Editor. 2009: China.

[66] J. Safarian and M. Tangstad, MMTB, 2012. 43(6): p. 1427-1445.

[67] T. Miki, K. Morita and N. Sano, MMTB, 1996. 27(6): p. 937-941.

[68] K. Suzuki, K. Sakaguchi, T. Nakagiri and N. Sano, J Jpn I Met 1990. 54(2): p. 161-167.

[69] S. S. Zheng, W.H. Chen, J. Cai, J.T. Li, C. Chen and X.T. Luo, MMTB, 2010. 41(6):

p. 1268-1273.

[70] S.S. Zheng, T.A. Engh, M. Tangstad and X.T. Luo, Sep Purif Technol, 2011. 82: p. 128-137.

[71] S.S. Zheng, Jafar J. Safarian, S. SEOK, S. KIM, M. Tangstad and X.T. Luo, Trans. Nonferrous Met. Soc. China, 2011. 21(3): p. 697-702.

[72] S. Shi, W. Dong, X. Peng, D. Jiang and Y. Tan, Appl Surf Sci, 2013. 266: p. 344-349.

[73] K. Suzuki, T. Kumagai and N. Sano, ISIJ int, 1992. 32(5): p. 630-634.

[74] H. C. Theuerer, J Met, 1956. 6: p. 1316.

[75] J. Amouroux, F. Slootman, N. Madigou, T. Rogen and D.Morvan, 1987. 3: p. 1868.

[76] H.Baba, N. Yuge, Y. Sakaguchi, F. Aratani and Y. Habu Dordrecht, Proc. l0th E.C. Photovoltaic Solar Energy Conf., 1991: p. 286.

[77] Y. Delannoy, C. lemany, F.Y. Li, P. Proulx and C. Trassy, Sol Energ Mat Sol C, 2002. 72(1): p. 69-75.

[78] J. Kondo and K. Okazawa. 2011, Google Patents.

[79] Sharp Co., The method of refining silicon and the refined silicon, 2005. 200580023743.X.

[80] T. Yoshikawa and K. Morita, J Electrochem Soc, 2003. 150(8): p. G465-G468.

[81] A.M. Mitrašinović and T.A. Utigard, Silicon, 2009. 1(4): p. 239-248.

[82] X.D. Ma, T. Yoshikawa and K. Morita, MMTB, 2013. 44(3): p. 528-533.

[83] Y.Q. Li, Y. Tan, J.Y. Li, Q. Xu and Y. Liu, J Alloy Compd, 2014. 583: p. 85-90.

[84] P.S. Kotval and H.B. Strock. 1980, Google Patents.

[85] R.K. Dawless. 1989, Google Patents.

[86] T. Yoshikawa and K. Morita, Sci Technol Adv Mat, 2003. 4(6): p. 531-537.

[87] T. Yoshikawa and K. Morita, ISIJ int, 2005. 45(7): p. 967-971.

[88] T. Yoshikawa, K. Arimura and K. Morita, MMTB, 2005. 36(6): p. 837-842.

[89] T. Yoshikawa and K. Morita, J Cryst Growth, 2009. 311(3): p. 776-779.

[90] K. Morita and T. Yoshikawa, Trans. Nonferrous Met. Soc. China, 2011. 21(3): p. 685-690.

[91] L.A.V. Teixeira and K. Morita, ISIJ int, 2009. 49(6): p. 783-787.

[92] T. Watanabe, H. Fukuyama, K. Nagata and M. Susa, MMTB, 2000. 31(6): p. 1273-1281.

[93] CP. Khattak and KV. Ravi, Silicon Processing for Photvoltaics. I, 1985.

[94] MD. Johnston and M. Barati, J Non Cryst Solids, 2011. 357(3): p. 970-975.

[95] J. Cai, J.T. Li, W.H. Chen, C. Chen and X.T. Luo, Trans. Nonferrous Met. Soc. China 2011. 21(6): p. 1402-1406.

[96] N. Liu D. Luo, Y. Lu, G. Zhang, T. Li, Nonferrous Met. Soc. China 2011: p. 1178-1184.

[97] J.J. Wu, W.H. Ma, B.J. Jia, B. Yang, D.C. Liu and Y.N. Dai, J Non-Cryst Solids, 2012. 358(23): p. 3079-3083.

[98] X.D. Ma, T. Yoshikawa and K. Morita, J Alloy Compd, 2012. 529: p. 12-16.

[99] X.D. Ma, doctoral dissertation, The Univsersity of Tokyo, 2012.

[100] B. Helene, doctoral dissertation, NTNU, 2012.

[101] J.J. Wu, B. Yang, Y.N. Dai and K. Morita, Trans. Nonferrous Met. Soc. China, 2009. 19(2): p. 463-467.

[102] H. Nishimoto and K. Morita, High Temp Mat PR, 2011: p. 701-708.

[103] H. Nishimoto, Y. Kang, T. Yoshikawa and K. Morita, High Temp Mat PR, 2012.

CHAPTER TWO

THERMODYNAMIC EVALUATION OF BORON EVAPORATION REMOVAL WITH $CACL_2$-CONTAINING SLAG

2.1 Introduction

As mentioned in Chapter 1, B is one of the most difficult impurities to be removed when preparing SOG Si. Because of the high segregation coefficient (k_0=0.8) in Si, leaching and directional solidification is not suitable for removal of B. Furthermore, the vapor pressure of elemental boron is not high enough to be removed by vaporization (6.78×10^{-7} Pa, 1823 K). One solution is to remove boron by plasma refining, but this method requires a large initial investment for the plasma equipment and operation. Slag refining has shown to be a proper method for B removal, but the limitation of partition ratio of B between molten Si and slag ($L_B \approx 2$) restrict the improvement of this method. For these reasons, in order to break through the limitation, two ways of improving the method are discussed;

(a) Optimization of the slag composition:

CaO-SiO_2 slag are usually used as the slag agent, the total reaction relating to B removal by slag treatment can be represented in Eq. (2-1).

$$\mathrm{B}_{(l)} + \frac{3}{4}\mathrm{SiO}_{2(l)} = \mathrm{BO}_{1.5(l)} + \frac{3}{4}\mathrm{Si}_{(l)} \tag{2-1}$$

$$K_1 = \frac{(a_{\mathrm{BO}_{1.5}})(a_{\mathrm{Si}})^{3/4}}{a_{\mathrm{B}}(a_{\mathrm{SiO}_2})^{3/4}} = \frac{(\gamma_{\mathrm{BO}_{1.5}} X_{\mathrm{BO}_{1.5}})}{(\gamma_{\mathrm{B}} X_{\mathrm{B}})} \cdot \left(\frac{a_{\mathrm{Si}}}{a_{\mathrm{SiO}_2}}\right)^{3/4} \tag{2-2}$$

$$L_{\mathrm{B}}^{'} = \frac{X_{\mathrm{BO}_{1.5}}}{X_{\mathrm{B}}} = \frac{K_1 \cdot (a_{\mathrm{SiO}_2})^{3/4}(\gamma_{\mathrm{B}})}{(\gamma_{\mathrm{BO}_{1.5}})(a_{\mathrm{Si}})^{3/4}} \tag{2-3}$$

Here, the *l* and *g* in parenthesis denote the liquid and gas standard states, and K_1 is the equilibrium constant of Eq. (2-1). a_i and γ_i represent the activity and activity coefficient of component *i* respectively. $L_{\mathrm{B}}^{'}$ is the partition ratio in molar basis [1].

According to Eq. (2-3), because the content of B is less than 10^{-5} ppmw, the activity of Si can be regard as 1. K_1 is a constant which can be determined by changing the Gibbs energy, which is shown in Eq. (2-4) and Eq. (2-5)

$$\Delta G = \Delta G^0 + RT\ln K_1 \quad (2\text{-}4)$$

Here ΔG^0 represents the standard Gibbs energy for the reaction, R is the gas constant, T is the temperature measured in Kelvin. For a system in equilibrium $\Delta G=0$ and the equilibrium constant K_1 can be expressed as

$$K_1 = \exp(\frac{-\Delta G^0}{RT}) \quad (2\text{-}5)$$

Activity coefficients of $BO_{1.5}$ and B are also constants. The value of $L_B^{'}$ can be increased when increasing the activity of SiO_2. In fact, the acidity - alkalinity of slag will turn to acid when increase the activity of SiO_2, it is bad for $BO_{1.5}$ transfer from molten Si to the slag. Many experiments showed that the CaO can increase the basicity of slag which is good for $BO_{1.5}$ transfer from molten Si to the slag. So an appropriate ratio between CaO and SiO_2 is important. The slag composition will affect the above mentioned properties such as viscosity, density, interfacial tensions and diffusivities. When it comes to the structure of the slag, the slag composition is usually divided into basic oxides, acid oxides and amphoteric oxides. The ratio between the basic and acid oxides will hence explain the above mentioned properties. The basic oxides donate oxygen. They have network breaking properties since they can bind themselves to oxides and therefore break up bonds between other oxides; this is illustrated in Fig. 2.1.

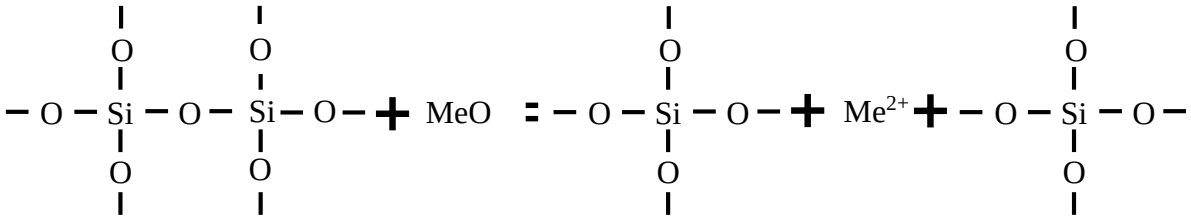

Figure 2.1 Addition of a network breaking oxide, MeO, to a silicate network [2]

As the slag becomes more basic the network breaking leads to a decrease in the viscosity. For the basic oxide CaO, oxygen ions are provided by Eq. (2-6):

$$CaO = Ca^{2+} + O^{2-} \quad (2\text{-}6)$$

The acidic oxides are oxygen acceptors and will therefore form chemical bonds with other oxides and thereby increase the viscosity of the slag. An acid oxide such as SiO_2 is characterized by Eq. (2-7):

$$SiO_2 + 2O^{2-} = SiO_4^{4-} \quad (2\text{-}7)$$

The last group, amphoteric oxides, act as a basic or acidic oxide depending on the other oxides present; Al_2O_3 is an example of an amphoteric oxide. The basicity is defined as the sum of the basic oxides divided by the acidic oxides:

$$Basicity = \frac{\sum(\%Basic\ oxides)}{\sum(\%Acidic\ oxides)} \quad (2\text{-}8)$$

For the $CaO\text{-}SiO_2$ slag system, the basicity is the mass ratio CaO/SiO_2.

Control of the slag chemistry is important to optimize the extraction effect of the impurities from molten Si. The impurities are absorbed into the slag as oxidized species and the reactivity of different elements with oxygen is therefore important. Si will be oxidized to SiO_2 when O_2 is present. To avoid high losses of Si into the slag phase it usually contains SiO_2 as one of the components [3].

By changing the components and/or the composition of the slag more B can possibly be extracted by the slag.

(b). Evaporation of B from the slag:

Slag refining as a method for B removal can be improved by chloridizing $BO_{1.5}$ from the slag through an evaporation process. Oxidized B is transported through the slag phase, transferred through the boundary layer and evaporated at the interphase between slag and gas. As long as boron is removed from the slag through evaporation, more boron will be transported from silicon to slag since the reactive fluxes evaporated completely [4].

The $CaCl_2$-containig slag was selected as a candidate slag for B removal from MG-Si. The concept of a new process for the removal of B from molten Si is schematically shown in Fig. 2.2. When oxidizing slag is added onto the molten Si, [B] in molten Si is oxidized and transferred to the slag as $BO_{1.5}$, as shown in Eq. (2-9):

$$B_{(l)} + \frac{3}{4}O_{2(g)} = BO_{1.5(l)} \quad (2\text{-}9)$$

ΔG^0 = -664.7 + 0.13T kJ/mol [5]

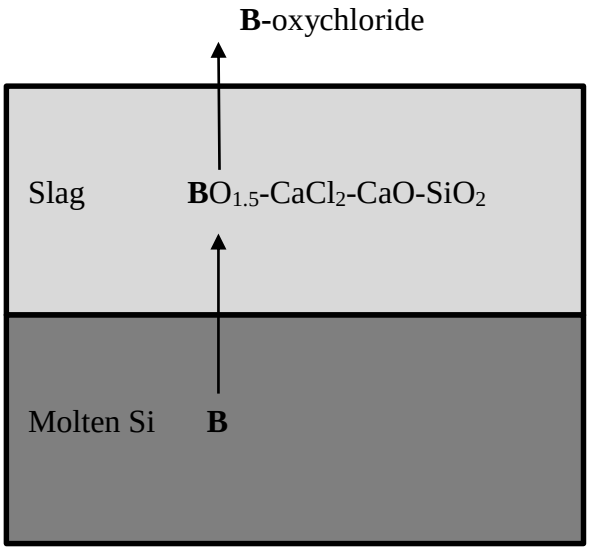

Figure 2.2. Mechanism of the proposed B removal method

Then, $BO_{1.5}$ in molten slag is chlorinated by $CaCl_2$ according to the principle of selective chlorination, B-oxychloride gas will be generated and evaporated.

In order to consider the possible generated gas species, various reactions between B, Si and slag were taken into account.

2.2 Gibbs energy reactions of B and Si with $CaCl_2$-containing slag

In the process of slag refining using $CaCl_2$-containing slag, oxychloride reactions might happen in both molten Si and B impurity. The standard Gibbs energy (ΔG^0) of each reaction was calculated with the help of HSC Chemistry 6.0 software [6], as shown in Table 2.1:

Table 2.1 Possible reactions and standard Gibbs energy

	Reaction equation	**Standard Gibbs energy of reaction**
1	$B_{(l)}+CaO+0.5CaCl_{2(l)}=BOCl_{(g)}+1.5Ca$	$\Delta G^0 = -92.5 + 0.01T$ kJ/mol
2	$B_{(l)}+0.5CaCl_{2(l)}=BCl_{(g)}+0.5Ca$	$\Delta G^0 = 480.84 - 0.10T$ kJ/mol
3	$B_{(l)}+CaCl_{2(l)}=BCl_{2(g)}+Ca$	$\Delta G^0 = 629.10 - 0.074T$ kJ/mol
4	$B_{(l)}+1.5CaCl_{2(l)}=BCl_{3(g)}+1.5Ca$	$\Delta G^0 = 691.65 - 0.019T$ kJ/mol
5	$Si_{(l)}+0.5CaCl_{2(l)}=SiCl_{(g)}+0.5Ca$	$\Delta G^0 = 522.69 - 0.097T$ kJ/mol
6	$Si_{(l)}+CaCl_{2(l)}=SiCl_{2(g)}+Ca$	$\Delta G^0 = 533.43 - 0.056T$ kJ/mol
7	$Si_{(l)}+1.5CaCl_{2(l)}=SiCl_{3(g)}+1.5Ca$	$\Delta G^0 = 697.3 - 0.020T$ kJ/mol
8	$Si_{(l)}+2CaCl_{2(l)}=SiCl_{4(g)}+2Ca$	$\Delta G^0 = 799.7 + 0.054T$ kJ/mol
9	$CaCl_{2(l)}=CaCl_{2(g)}$	$\Delta G^0 = 277.12 - 0.066T$ kJ/mol

From Table 2.1, temperature dependence of standard Gibbs energy of various reactions between B and Si with $CaCl_2$ are shown in Fig. 2.3. We can find that in standard state, the easiest reaction is generation of $CaCl_2$ gas, the BOCl gas also has a possibility to be generated.

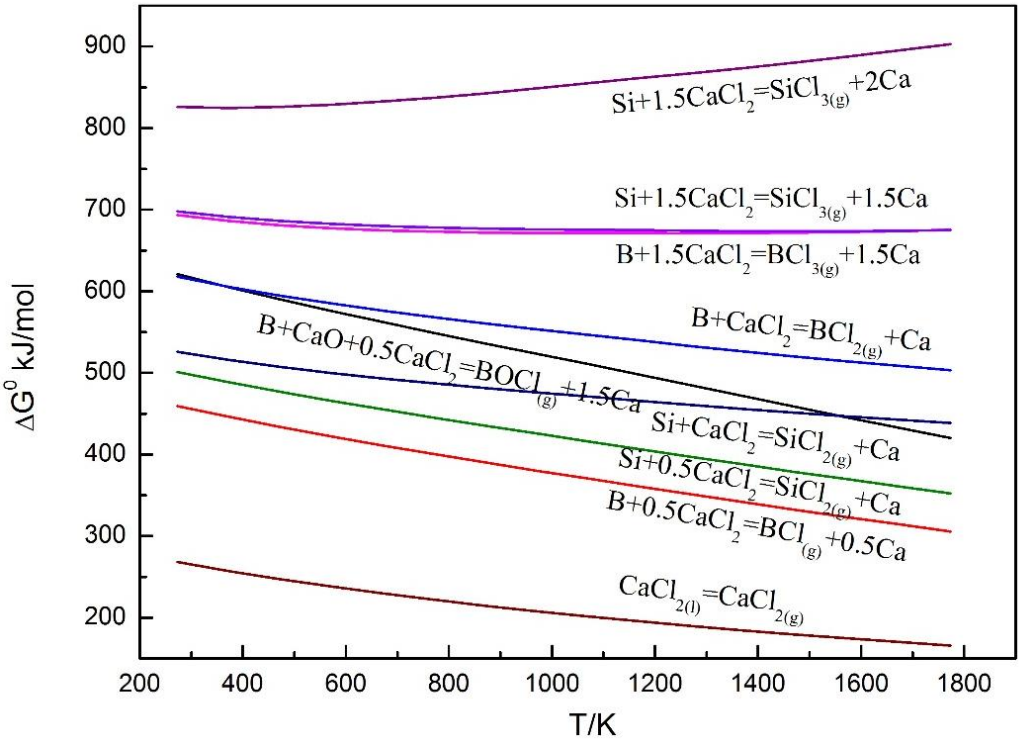

Figure 2.3 Temperature dependence of standard Gibbs energy of reactions change for various reactions between B and Si with $CaCl_2$

2.3 Vapor pressure of chloride gases

In a mixture of gases, each gas has a partial pressure which is the hypothetical pressure of that gas if it alone occupied the volume of the mixture at the same temperature. The partial pressure of a gas is a measure of thermodynamic activity of the gas's molecules. Gases dissolve, diffuse, and react according to their partial pressures, and not according to their concentrations in gas mixtures or liquids [7]. Therefore, the partial pressure of various reactions between B and Si with $CaCl_2$ should be calculated.

According to the mechanism of proposed B removal method as shown in Fig. 2.2, after Eq. (2-10) happens, $BO_{1.5}$ will react with $CaCl_2$ and generate BOCl gas, which can be represented as

$$BO_{1.5(l)} + 0.5CaCl_{2(l)} = BOCl_{(g)} + 0.5CaO_{(s)} \quad (2\text{-}10)$$

$$\Delta G^0 = 572.2 - 0.13T \text{ kJ/mol.}$$

The overall reaction associated with B removal by slag treatment can be represented by combining Eq. (2-9) and Eq. (2-10) as follows:

$$B_{(l)} + 0.75O_2 + 0.5CaCl_{2(l)} = BOCl_{(g)} + 0.5CaO_{(s)} \quad (2\text{-}11)$$

$$\Delta G^0 = -92.5 + 0.01T \text{ kJ/mol.}$$

Assuming that CaO-$CaCl_2$ slag coexists with molten Si and that the oxygen partial pressure at the slag-Si interface is controlled by CaO in the slag and Ca in Si, B is expected to evaporate as BOCl as follows:

$$B_{(l)} + CaO_{(s)} + 0.5CaCl_{2(l)} = BOCl_{(g)} + 1.5Ca_{(l)} \quad (2\text{-}12)$$

$$\Delta G^0 = 1204.4 - 0.31T \text{ kJ/mol}$$

The equilibrium constant $K_{(1)}$ of Eq. (2-13) can be expressed as:

$$K_{(1)} = \frac{(P_{BOCl})^2 \cdot (X_{Ca}\gamma_{Ca})^3}{(X_B\gamma_B)^2 (a_{CaO})^2 (a_{CaCl_2})^2} \quad (2\text{-}13)$$

Thus, the partial pressure of BOCl can be given as

$$P_{BOCl} = \frac{K_{(1)} \cdot (x_B\gamma_B)(a_{CaO})(a_{CaCl_2})^{1/2}}{(x_{Ca}\gamma_{Ca})^{3/2}} \quad (2\text{-}14)$$

Because the mole fraction of CaO is very low, the solution can be regarded as dilute solution, so the partial pressure of $CaCl_2$ can be calculated by Raoult's law. In addition to B chlorides (BCl, BCl_2, BCl_3), $CaCl_2$ and Si chlorides (SiCl, $SiCl_2$, $SiCl_3$, and $SiCl_4$) might also be generated during the reaction. Thus, the partial pressure equations of Cl-

contained gases which were showed in Table 2.1 can be deduced in Table 2.2.

Table 2.2 Partial pressures equations of Cl-contained gases

	Reaction equation	Standard Gibbs energy
1	$B_{(l)}+CaO+0.5CaCl_{2(l)}=BOCl_{(g)}+1.5Ca$	$P_{BOCl}=\frac{K_{(1)}\cdot(x_B\gamma_B)(a_{CaO})(a_{CaCl_2})^{1/2}}{(x_{Ca}\gamma_{Ca})^{3/2}}$
2	$B_{(l)}+0.5CaCl_{2(l)}=BCl_{(g)}+0.5Ca$	$P_{BCl}=\frac{K_{(2)}\cdot(x_B\gamma_B)(a_{CaCl_2})^{1/2}}{(x_{Ca}\gamma_{Ca})^{1/2}}$
3	$B_{(l)}+CaCl_{2(l)}=BCl_{2(g)}+Ca$	$P_{BCl_2}=\frac{K_{(3)}\cdot(x_B\gamma_B)(a_{CaCl_2})}{(x_{Ca}\gamma_{Ca})}$
4	$B_{(l)}+1.5CaCl_{2(l)}=BCl_{3(g)}+1.5Ca$	$P_{BCl_3}=\frac{K_{(4)}\cdot(x_B\gamma_B)(a_{CaCl_2})^{3/2}}{(x_{Ca}\gamma_{Ca})^{3/2}}$
5	$Si_{(l)}+0.5CaCl_{2(l)}=SiCl_{(g)}+0.5Ca$	$P_{SiCl}=\frac{K_{(5)}\cdot(x_{Si}\gamma_{Si})(a_{CaCl_2})^{1/2}}{(x_{Ca}\gamma_{Ca})^{1/2}}$
6	$Si_{(l)}+CaCl_{2(l)}=SiCl_{2(g)}+Ca$	$P_{SiCl_2}=\frac{K_{(6)}\cdot(x_{Si}\gamma_{Si})(a_{CaCl_2})}{(x_{Ca}\gamma_{Ca})}$
7	$Si_{(l)}+1.5CaCl_{2(l)}=SiCl_{3(g)}+1.5Ca$	$P_{SiCl_3}=\frac{K_{(7)}\cdot(x_{Si}\gamma_{Si})(a_{CaCl_2})^{3/2}}{(x_{Ca}\gamma_{Ca})^{3/2}}$
8	$Si_{(l)}+2CaCl_{2(l)}=SiCl_{4(g)}+2Ca$	$P_{SiCl_4}=\frac{K_{(8)}\cdot(x_{Si}\gamma_{Si})(a_{CaCl_2})^{2}}{(x_{Ca}\gamma_{Ca})^{2}}$
9	$CaCl_{2(l)}=CaCl_{2(g)}$	$P_{CaCl_2}=P^{*}_{CaCl_2}\cdot x_{CaCl_2}$

The concentrations of Ca (C_{Ca}) and B (C_B) in Si were assumed to be 200 and 50 ppmw, respectively. The activity of CaO in CaO-$CaCl_2$ slag system was taken from the work by Tago and Morita [8], as shown in Fig. 2.4 and Table 2.3.

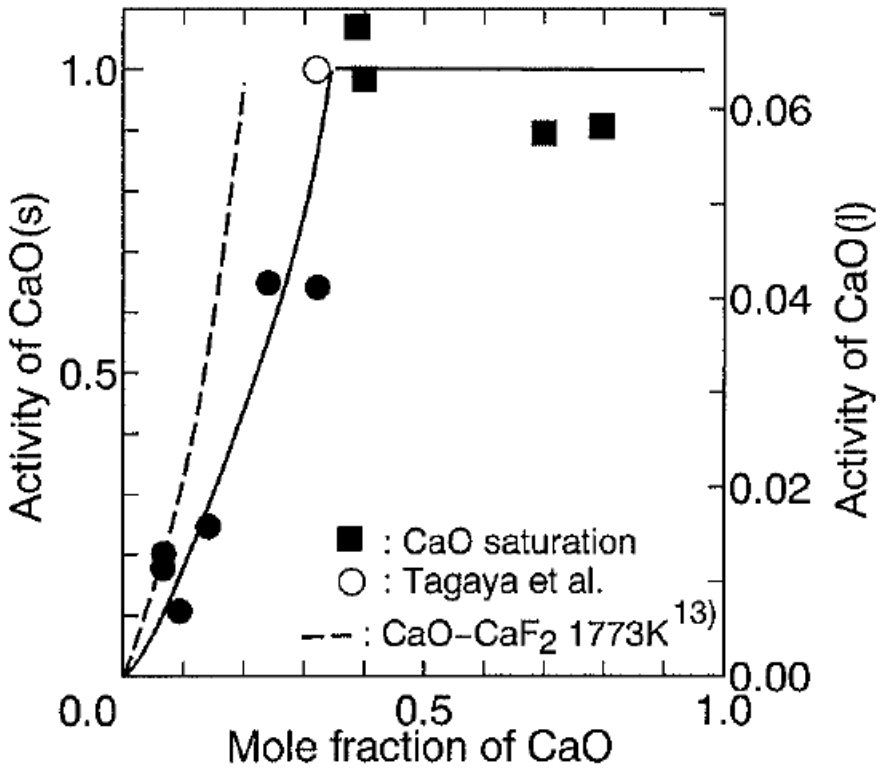

Figure 2.4. The activity of CaO in CaO-$CaCl_2$ system at 1673K [8]

According to Fig. 2.4, a one - to - one correspondence between various mole fraction of CaO (x_{CaO}) and activity of CaO (a_{CaO}) in CaO-$CaCl_2$ system. The activity of $CaCl_2$ was estimated using Gibbs-Duhem equation, as shown in Eq. (2-15):

$$x_{CaO} d\ln a_{CaO} + x_{CaCl_2} d\ln a_{CaCl_2} = 0 \qquad \text{(T, P = constant)} \qquad (2\text{-}15)$$

Table 2.3 shows the calculation results of activity of $CaCl_2$ from Fig. 2.4 using Gibbs-Duhem function. Fig. 2.5 shows the integration results between x_{CaO} / x_{CaCl2} and $-\ln a_{CaO}$.

Table 2.3 Calculation of activity of $CaCl_2$ from Fig. 2.4 using Gibbs-Duhem function

x_{CaO}	x_{CaCl2}	x_{CaO} / x_{CaCl2}	a_{CaO}	$-\ln a_{CaO}$	Unit square of Fig. 2.5	-ln (a_{CaCl2})	a_{CaCl2}
0	1	0	0	0	0	0	**1**
0.050	0.950	0.053	0.071	2.645	0.071	0.005	**0.995**
0.100	0.900	0.111	0.170	1.772	0.087	0.159	**0.853**
0.150	0.850	0.176	0.312	1.165	0.070	0.229	**0.795**
0.200	0.800	0.250	0.434	0.835	0.080	0.309	**0.734**
0.250	0.750	0.333	0.571	0.560	0.111	0.421	**0.657**
0.300	0.700	0.429	0.765	0.268	0.133	0.553	**0.575**
0.360	0.640	0.563	1.000	0.000	0.000		**0**

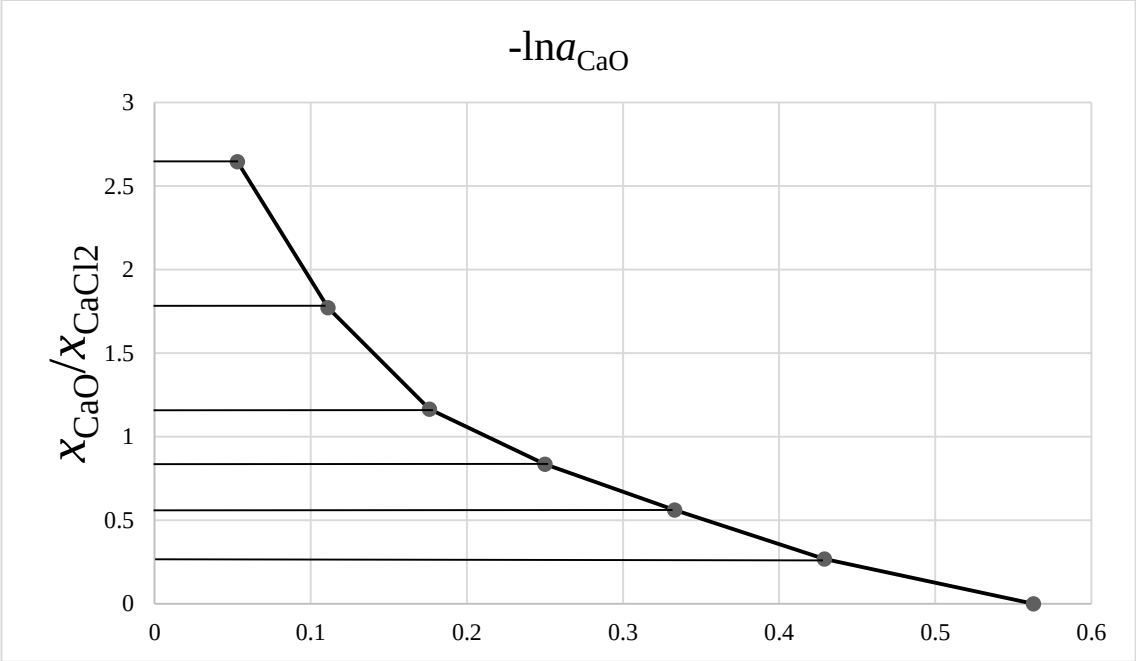

Figure 2.5. Integration results between x_{CaO} / x_{CaCl2} and -lna_{CaO}

Previously reported data ([9, 10]) were used to determine the activity coefficients of Ca (γ_{Ca}=0.00117, T=1723K) and B (γ_B=3.88, T=1723K) in molten Si. The equilibrium constant K can also be calculated from Eq. (2-5), as shown in Table 2.4.

Table 2.4. The equilibrium constants of reaction equations (K) from Table 2.2

Reaction equation	**Equilibrium constant (K)**	**Reaction equation**	**Equilibrium constant (K)**
1	2.04×10^{-12}	5	6.77×10^{-10}
2	6.93×10^{-9}	6	8.25×10^{-11}
3	3.48×10^{-13}	7	2.89×10^{-16}
4	1.16×10^{-16}	8	1.96×10^{-21}
9	8.16×10^{-6}		

The estimated relationships between the partial pressures of BOCl, BCl_x, $SiCl_x$, and $CaCl_2$ and the mole fraction of CaO in the CaO-$CaCl_2$ slag are shown in Fig. 2.6. It shows that the partial pressures (P_i) of BCl_x and $SiCl_x$ decrease when the mole fraction (x_i) of CaO increases, whereas P_{BOCl} increases when x_{CaO} increases. Therefore, the P_{BOCl} can be increased by increasing x_{CaO}. Furthermore, because the ratio of P_{BOCl} and P_{SiCl2} (1/500) is larger than that of x_B and x_{Si} (1/8000), the removal of B by the generation of BOCl gas is

theoretically possible. However, it would be difficult to suppress the evaporation of $CaCl_2$ during the experiments owing to the high partial pressure of $CaCl_2$.

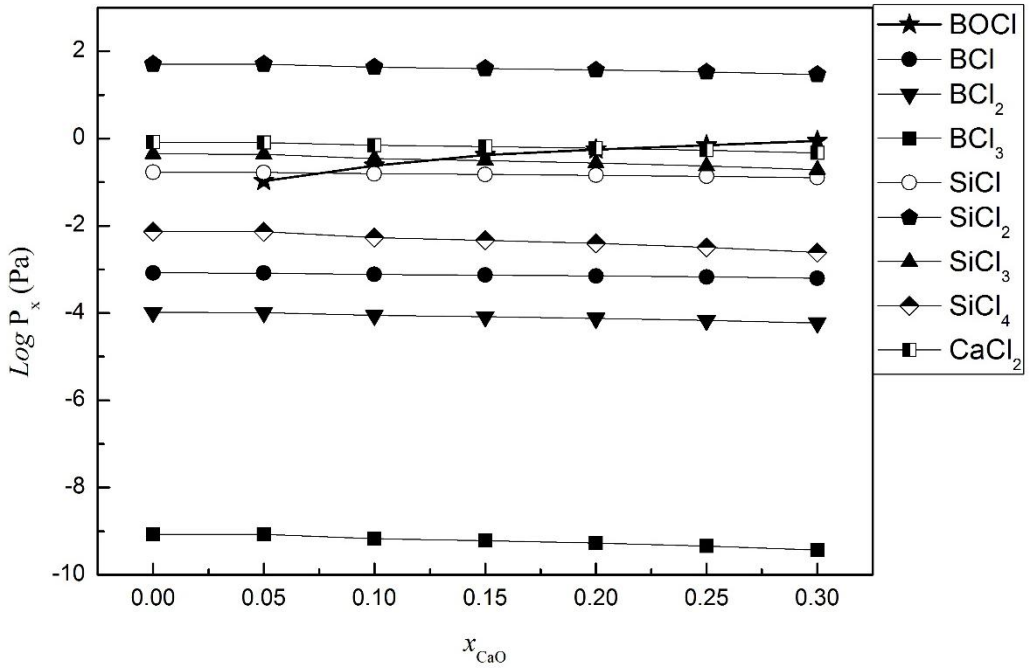

Figure 2.6. The estimated relationship between partial pressure of BOCl, BCl_x, $SiCl_x$, $CaCl_2$ and mole fraction of CaO at 1723K

2.4 Experiment for confirmation of B evaporation

After thermodynamic evaluation demonstrates that the BOCl gas should be generated at 1723K theoretically, confirming experiments of B evaporation were carried out. In order to confirm the generation of B-containing gas species along with $CaCl_2$, Powders of $BO_{1.5}$ and $CaCl_2$ (mole ratio = 1:1) were mixed very well, heated in a graphite crucible at 1273, 1473, and 1723 K for 6 h under an Ar gas atmosphere. Simultaneously, NaOH solution was used to absorb the evaporated gases and B concentration (c_B) in the NaOH and the precipitant attached on the wall of tube were measured by ICP-AES.

2.4.1 Experimental chemicals

The chemicals used in the experiments are shown in Table 2.5

Table 2.5 Species and types of chemicals

Name	Chemical formula	Producer	Purity
Boron oxide	B_2O_3	Wako pure Chemical industries, Ltd.	99.5%
Calcium chloride	$CaCl_2$	Wako pure Chemical industries, Ltd.	95.0%

2.4.2 Experimental Setup

In order to confirm the evaporation of B with the help of $CaCl_2$, preliminary experiments using B_2O_3 and $CaCl_2$ were carried out for 6 hours at 1273 K, 1473 K, and 1723 K. NaOH solution was used as B absorbent. The procedure and setup are shown in Fig. 2.7.

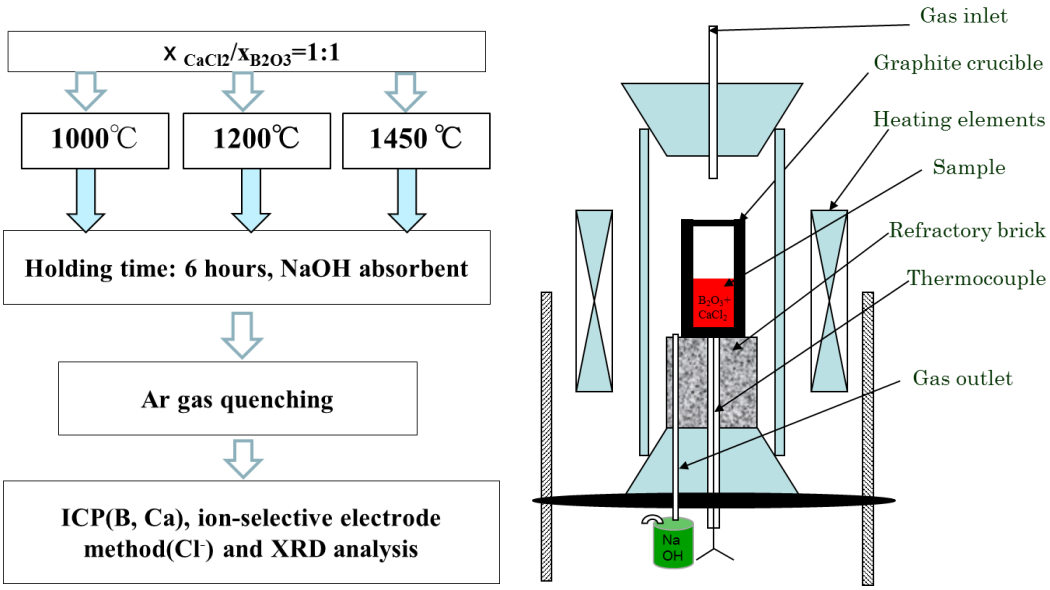

Figure 2.7. The experimental apparatus of confirmation experiments.

2.4.3 Sample analysis

B contents in NaOH solution

1) The 50ml NaOH solution was filtered into a 50 ml volumetric flask (Teflon) using a Teflon funnel and a filtered paper.
2) The concentrations of B was analyzed by Seiko SPS7700 Inductive Coupled Plasma Atomic Emission Spectroscope instrument. The standard solutions of B was prepared in the range of 0.1~4 ppm, respectively. The acid matrix of standard solutions and blank were adjusted to be the same as the sample solutions. The wavelength of B was selected to be 249.773 nm.

2.4.4 Results and discussion

The mole fractions (x_i) and c_B in NaOH solution after the experiment to confirm the evaporation of B are shown in Table 2.6. It is found that some amount of B generated during the reaction between $BO_{1.5}$ and $CaCl_2$ was captured in the 100 mL NaOH solution. A decrease in $x_{BO1.5}$ and x_{CaCl2} along with an increase in x_{CaO} suggests that Eq. (2-10) might have occurred. These results demonstrate that B can be evaporated as a gaseous species. Moreover, the content of B in NaOH solution increases, as Ar gas flow rate increases from 0.05 L/min to 0.2 L/min.

Table 2.6. Mole fractions (x_i) of slag and c_B in NaOH solution

T/K	$x_{BO1.5}$	x_{CaCl2}	x_{CaO}	$c_{B\ in\ NaOH}$ (ppmw)	Ar flow rate (L/minute)

1273	0.16	0.12	0.72	22.03	0.1
1473	0.20	0.17	0.63	37.62	0.2
1723	0.24	0.17	0.59	16.80	0.05

The product species after reaction between B_2O_3 and $CaCl_2$ were analyzed by XRD. The XRD patterns are shown in Fig. 2.8.

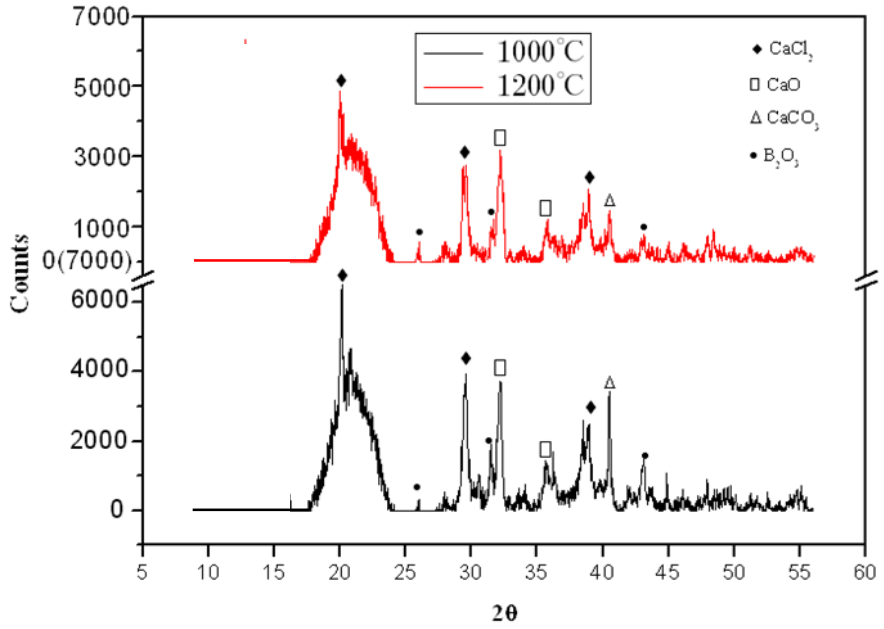

Figure 2.8. XRD patterns of products of after reaction between B_2O_3 and $CaCl_2$

In Table 2.6, Concentration of B in NaOH solution gives the amount of the evaporated B in the form of B-contained gas species (BOCl, BCl_x). From Fig. 2.8, It can be seen that B_2O_3, CaO, B_2O_3 were generated and the reaction (2-10) might be occurred possibility. Fig. 2.9 shows the precipitant attached on the alumina ceramic tube after 6 hours. Most of the precipitant is CaCl2, and the content of B (15 ppmw) were also found in the precipitant using ICP-AES, which also demonstrated that B-contained gas species (BOCl, BCl_x) might be generated and evaporated possibility.

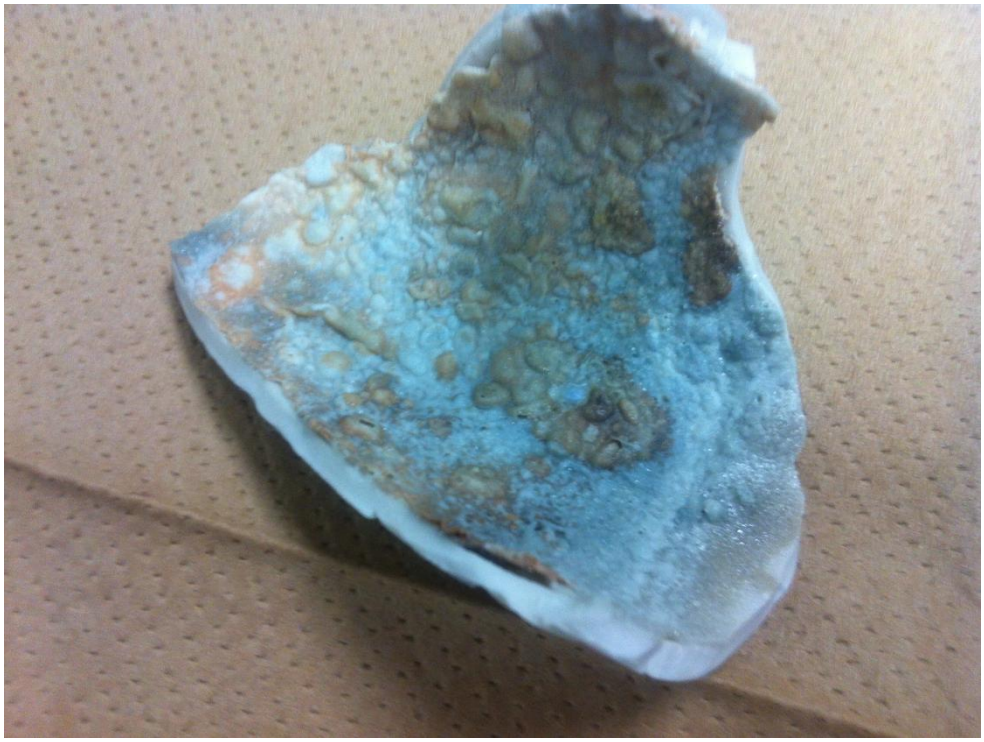

Figure 2.9. Precipitant attached on the alumina ceramic tube

2.5 Summary

A new process for the removal of B in molten Si has been proposed, this method is based on the principle of oxidized chlorination and evaporation. On the basis of standard Gibbs energy and equilibrium constant of oxychloride reactions, partial pressures of B chlorides (BCl, BCl_2 and BCl_3), $CaCl_2$ and Si chlorides (SiCl, $SiCl_2$, $SiCl_3$ and $SiCl_4$) are calculated. It demonstrates that the BOCl gas should be generated at 1723K theoretically. Finally, evaporation of B-containing gas species was confirmed according to the confirming experiments using refining $BO_{1.5}$ and $CaCl_2$ powder at 1723K.

Reference

[1] X.D. Ma, T. Yoshikawa and K. Morita, MMTB, 2013. 44(3): p. 528-533.

[2] S.E. Olsen, S. Olsen, M. Tangstad and T. Lindstad, Production of manganese ferroalloys. 2007: Tapir Academic Press.

[3] M. Tangstad, J. Safarian, and K. Tang, Compendium: New solar grade silicon production processes. 2010:p.65-91.

[4] B. Helene, doctoral dissertation, NTNU, 2012.

[5] Landolt, JANAF 98, Binnewies 02. 1998, HSC Chemistry sofrware.

[6] A. Roine, HSC 6.0 Chemistry. Chemical Reactions and Equilibrium Software with Extensive Thermochemical Database and Flowsheet Simulation, 2006.

[7] D.R. Gaskell, Introduction to the Thermodynamics of Materials. 2008: CRC Press.

[8] Y. Tago, Y. Endo, K. Morita, F. Tsukihashi and N. Sano, ISIJ Int, 1995. 35(2): p. 127-131.

[9] T. Miki, doctoral dissertation, The University of Tokyo, 1999.

[10] T. Yoshikawa, doctoral dissertation, The University of Tokyo, 2005.

CHAPTER THREE

PHYSICOCHEMICAL PROPERTIES OF CAO-SiO_2-$CaCl_2$ SLAG SYSTEM

3.1 Introduction

In the metallurgical treatments, slag method [1] was used to remove boron, as boron is difficult to be removed due to high segregation coefficient (L_B=0.8) and low partial pressure [2]. It was proved that the molten slag based on CaO-SiO_2 binary system is an efficient agent for boron removal from molten MG-Si. The slag systems including CaO-SiO_2 [3], CaO-SiO_2-CaF_2 [4], CaO-SiO_2-Al_2O_3 [5], CaO-SiO_2-MgO, CaO-Li_2O-SiO_2 [6] and CaO-SiO_2-Na_2O [5, 7, 8] have been investigated. However, all of slag systems have limiting boron removal efficiency.

In Chapter two, according to the thermodynamic analysis and confirm experiments, the CaO-SiO_2-$CaCl_2$ slag has been confirmed in more effective for the B removal. However, the density, phase diagrams of SiO_2-$CaCl_2$ and CaO-SiO_2-$CaCl_2$ have not reported yet. These are essential fundamental data for B removal experiments and dynamic analysis. Thus, in order to determine the density of CaO-SiO_2-$CaCl_2$ slag, SiO_2-$CaCl_2$ phase diagram and liquidus area of CaO-SiO_2-$CaCl_2$ slag at experimental temperature (1723K), high temperature quenching experiments followed by the an improved Archimedean method [9], thermo gravimetric [10] and differential thermal analysis (TG-DTA), XRD phase determination and morphological observation were carried out.

3.2 Density and mole volume of $CaO-SiO_2-CaCl_2$ slag

3.2.1 Research principle

The Archimedean method of determining the density of a liquid slag is based on the buoyancy of a bob dipped in the liquid. The difficult point of Archimedean method is how to avoid the effect of surface tension tends to add to the weight of the bob [11]. In order to minimize the influence of surface tension, a two-sphere method [12] has been used, as shown in Fig. 3.1. In this, when only the lower bob is dipped into the molten slag, the weight W_1 measured by the balance is given by:

$$W_1 = W_0 + V_1\rho_l + \pi d\gamma\cos\theta \tag{3-1}$$

Where W_0 is the weight of the whole probe measured above the liquid surface; V_1 is the volume of the lower bob, including the submerged part of the string; ρ_l is the density of the liquid; d is the diameter of the string; γ is the surface tension of the liquid; and θ is the contact angle between the liquid and the string. When both bobs are dipped into the liquid, then the weight W_2 is given by:

$$W_2 = W_0 + (V_1 + V_2)V_1\rho_l + \pi d\gamma\cos\theta \tag{3-2}$$

Where V_2 is the volume of the upper bob, which includes the submerged portion of the string.

By subtracting Eq. (3-1) from Eq. (3-2), the surface tension term is cancelled and the density ρ_l can be obtained as:

$$\rho_l = (W_1 - W_2)/V_2 \tag{3-3}$$

In this instance, the parameter V_2 can be determined by an Archimedean volume measurement at room temperature using a liquid for which an accurate density is known, provided that the thermal expansion coefficient of the bob material is taken into account.

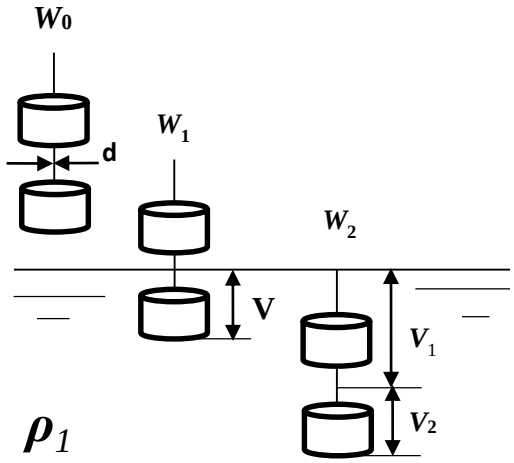

$$W_1 = W_0 - V_1\rho_l + \pi d\gamma\cos\theta$$

$$W_2 = W_0 - (V_1+V_2)\rho_l + \pi d\gamma\cos\theta$$

$$W_1 - W_2 = V_2\rho_l$$

Figure 3.1. Concept of the double-bob method

3.2.2 Experimental procedure

To apply the method described in section 3.2.1 to the measurement of slag density, the bob material needs to meet certain key requirements. Graphite was therefore selected, as compared with SiC, Si_3N_4 and metal materials, it is far more nonreactive, nonwettable and easier to prepare [13] . All experiments were carried out using a high speed heating furnace (RMF-1, Hirochiku Co., Ltd.), which had a cylindrical chamber measuring 40 mm in O.D., 220 mm in I.D., and 78 mm in length. The heating element was a Kanthal Super ($MoSi_2$) with an Al_2O_3 refractory material. The maximum temperature was controlled at 1473 ±2 K using a proportional integral differential (PID) controller with a Pt-6% Rh/Pt-30% Rh thermocouple. A Pt crucible was used to hold the slag, which was kept under an Ar atmosphere during testing. An electronic balance (Shimadzu-UX8205) was used to measure any change in the weight of the bob. An illustration of the furnace, showing its various components and dimensions, is given in Fig. 3.2.

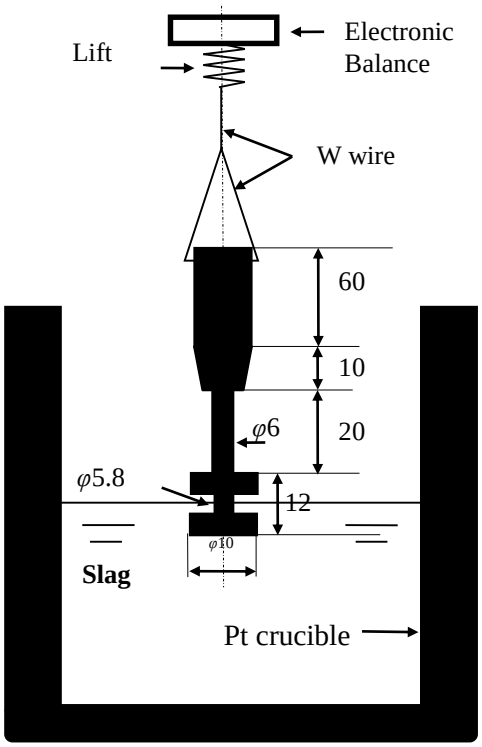

Figure 3.2 Schematic diagram of experimental set-up (mm)

The mole fraction of the slag used was x_{CaO}/ x_{SiO2} / x_{CaCl2} = 0.47 / 0.23 / 0.3 [14], giving a total sample mass of 15 grams. After experimentation, the concentration of Ca was measured by ICP-AES, and the SiO_2 and Cl^- concentrations were measured using a gravimetric [15] and ion-selective electrode method [13], respectively. The weight of the bob was measured at temperature intervals of 1073 K (800 ℃), 1173 K (900 ℃), 1273 K (1000 ℃) and 1373 K (1100 ℃). Owing to the fact that the furnace was limited to 1473 K (1200 ℃), but the weight loss of the graphite bob increases above 1373 K, the density of slag at 1723 K (1450 ℃) was extrapolated by linear prediction.

3.2.3 Results and discussion

During measurement of the molten slag height, the bob was first lowered to the bottom of the crucible, with subsequent lifting of the bob causing the balance reading to change accordingly. The height at which the balance reading ceased to change was considered to represent the top of the molten slag. With the height of the molten slag estimated, the bob was lowered by 6 mm to find the balance reading equating to W_1, and then by a further 6 mm again to find W_2. The difference in the weight of the bob in argon and inside the slag gave the weight loss as a result of the buoyant force applied by the molten slag bath. The volume of the slag being displaced by the bob was considered equal to the volume of the

bob immersed multiplied by a factor containing the volumetric expansion ratio for the linear expansion of graphite (α_T) [16] at any given temperature T (K): $\alpha_{273}=2.67\times10^{-5}$/T, $\alpha_{1073}=2.90\times10^{-5}$/T, $\alpha_{1173}=2.91\times10^{-5}$/T, $\alpha_{1273}=2.92\times10^{-5}$/T, $\alpha_{1373}=2.93\times10^{-5}$/T [17] and $V_2=0.367\text{cm}^3$. Thus, according to Eq. (3-3), the density at any temperature can be expressed as follows [18]:

$$\rho_T = (W_1 - W_2)/V_2\left(1+3\alpha_T\Delta T\right) \tag{3-4}$$

Table 3.1. Density of slag with different compositions and temperature

	x_{CaO}:x_{CaCl2}:x_{SiO2} (x_{CaCl2}/x_{SiO2}=2/1)	No.	T (K)	ΔW (g)	α (T)	V (cm^3)	ρ (g/cm^3)
Ⅰ	Initial: 0.1 : 0.6 : 0.3	1	1073	0.81	2.90×10^{-5}	0.367	**2.06**
		2	1173	0.81	2.91×10^{-5}	0.367	**2.05**
	Final: 0.18:0.51:0.31	3	1273	0.80	2.92×10^{-5}	0.367	**2.00**
Ⅱ	Initial: 0.3:0.47:0.23	4	1173	0.89	2.91×10^{-5}	0.367	**2.25**
		5	1273	0.89	2.92×10^{-5}	0.367	**2.23**
	Final: 0.36:0.40:0.24	6	1373	0.87	2.93×10^{-5}	0.367	**2.16**
Ⅲ	Initial: 0.4 : 0.4:0.2	7	1173	1.04	2.91×10^{-5}	0.367	**2.63**
		8	1273	1.03	2.92×10^{-5}	0.367	**2.58**
	Final: 0.44:0.33:0.23	9	1373	1.03	2.93×10^{-5}	0.367	**2.56**

Based on the calculated results given in Table 3.1, the relationship between CaO-$CaCl_2$-SiO_2 slag density and temperature for different slag compositions is shown in Fig. 3.3. From this, the linear fitted relationship between density and temperature is found as:

$$\rho_{\text{Slag I}} = 2.39\text{-}3\times10^{-4}\text{T};\ \rho_{\text{Slag II}} = 2.79\text{-}4.5\times10^{-4}\text{T};\ \rho_{\text{Slag III}} = 3.04\text{-}3.5\times10^{-4}\text{T} \tag{3-5}$$

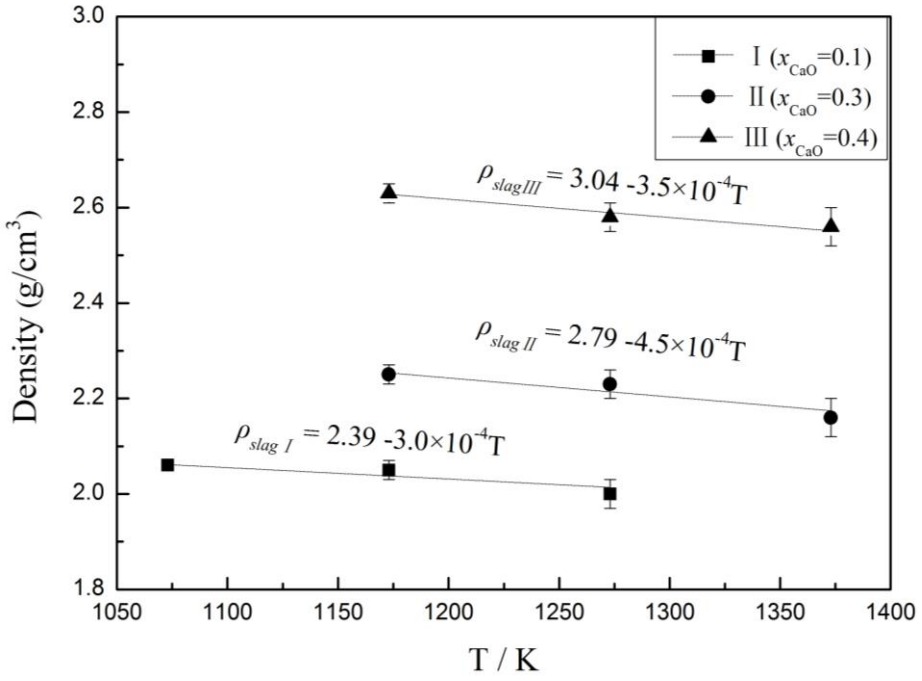

Figure 3.3. Temperature dependence of slag density

The first thing of note in Fig. 3.3 is that as the mole fraction of CaO increases from 0.1 (Slag I) to 0.4 (Slag III), the density of the slag increases from 2.00 to 2.63 g/cm^3, which is due to the density of CaO (3.35 g/cm^3) being greater than that of $CaCl_2$ (2.15 g/cm^3) and SiO_2 (2.65 g/cm^3). Secondly, the density of all the slags decreased slightly when the temperature increased, as this causes both the thermal motion of molecules and the volume to increase. Thirdly, using a linear fitting of the points between 1073 and 1373 K, the density of Slag I (2.43 g/cm^3), Slag II (2.01 g/cm^3) and Slag II (1.87 g/cm^3) at 1723 K was determined. Thus, if Slag II is used to remove boron from silicon at 1723 K, its density would be 2.01 g/cm^3.

The molar volume (V_m) of a molten slag can be calculated from its molar mass and density by the following equation:

$$V_m = M/\rho \tag{3-6}$$

Where V_m and M are the molar volume and molar mass of the slag, respectively. By inserting the values for M and ρ for the three slags into Eq. (3-6), their molar volume can be expressed as follows:

$$V_{m\mathrm{I}} = 88.6/\left(2.39-3\times10^{-4}T\right)$$

$$V_{m\mathrm{II}} = 78.0/\left(2.79-4.5\times10^{-4}T\right)$$

$$V_{m\mathrm{III}} = 72.4 \Big/ \left(3.04 - 3.5\times10^{-4}T\right) \tag{3-7}$$

The temperature dependence of the molar volume of the slags is shown in Fig. 3.4, which clearly shows an increase in molar volume with increasing temperature.

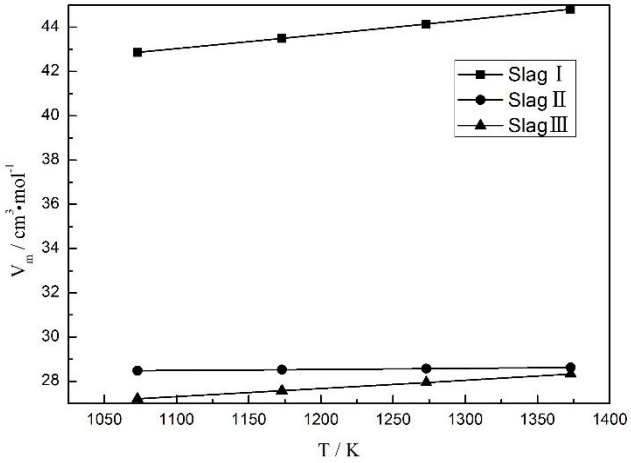

Figure 3.4. Temperature dependence of molar volume for different slags

3.3 Phase diagram of SiO_2-$CaCl_2$ slag

3.3.1 Experimental procedure

Reagent grade calcium carbonate ($CaCO_3$, ≥ 99.5 wt.% in purity, Wako, Japan), silicon dioxide (SiO_2, Cica-Reagent, Kanto Chem. Co., Inc. Japan) were used for preparing the starting materials. CaO was prepared by heating $CaCO_3$ for 12 hours ($CaCO_3 \rightarrow CaO + CO_2$) at 1273K. Appropriate proportions of starting materials were carefully weighed, mixed and stored in a desiccator in batches of 3 g.

Firstly, various compositions of CaO-SiO_2 high purity powders were mixed and then sealed of graphite crucible (23.5 mm inner diameter, 30 mm outer diameter, and 60 mm length). Secondly, the sample was premelted using the vertical SiC resistance furnace equipped with a mullite tube (60 mm outer diameter, 53 mm inner diameter, and 1000 mm length) at 1723 K for 5 mins followed by argon gas quenching. The temperature was controlled at 1723K ±2 K using PID controller. Thirdly, the premelted slag was crushed into pieces, 20 mg of slag was put into the Pt crucible (4.9 mm inner diameter, 5.1 mm outer diameter, and 2.6 mm length) with Pt cover, the solidus and liquidus temperature were measured using TG-DTA. Photos of Experimental apparatus are shown in Fig. 3.5.

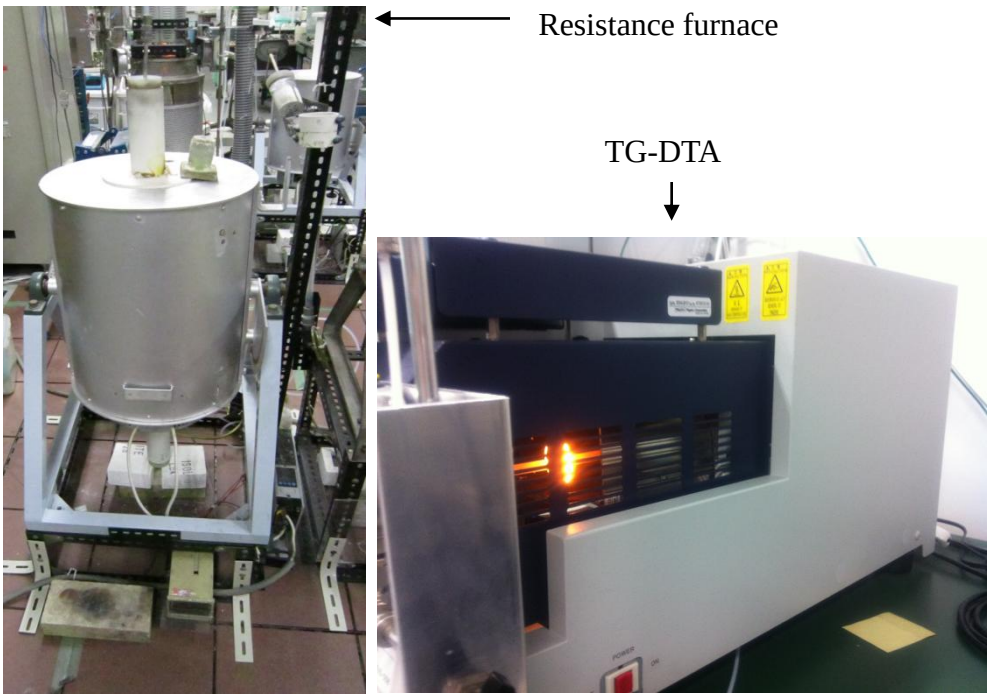

Figure 3.5 Photos of Experimental apparatus

During the TG-DTA process, all of the thermograms were obtained using Thermo plus

EVO Π series TG-DTA (Rigaku Company) is shown in Fig. 3.6. The maximum temperature of it is 1723K. The pelletized 20 mg samples were placed in open platinum pans which fit into the rings of balance. The pans were formed from 0.05 mm thick Pt sheet. Calcined alumina was employed as the reference material. Moreover, because the DTA curve and solidus and liquidus did not change very much when various heating rate of 5K min^{-1}, 10K min^{-1}, 15K min^{-1} and 20K min^{-1} were carried out, A normal constant heating rate of 10K min^{-1} [19] was employed for all samples with Ar gas blowing (50 ml/min). Data were obtained only during the heating cycle as severe supercooling occurred during the cooling cycle.

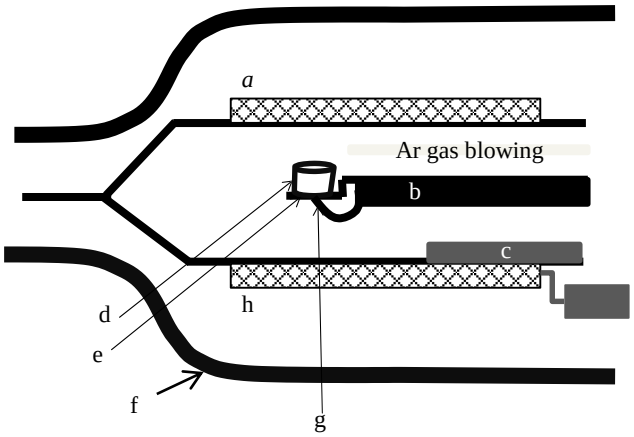

Figure 3.6 The set-up of TG-DTA measurement

(a: heating resistor; b: heating resistor; c: thermo element; d: Pt crucible; e: pan of sample holder; f: Al_2O_3 tube chamber; g: DTA thermo element; h: heating resistor).

3.3.2 TG-DTA analysis

In TG-DTA, the material under study and an inert reference are made to undergo identical thermal cycles, while recording the temperature difference between sample and reference. Many physical and chemical phenomena can be distinguished by the exothermic (positive curve) and endothermic (negative curve) curves. A positive curve in DTA represents the absorption, change of crystal structure, crystallization, oxidation, chemisorption and the negative curve represents desorption, melting, vaporization, sublimation, reduction [20]. The solidus and liquidus temperature can be obtained from the onset and ending of last curve.

The TG-DTA diagrams of four CaO-SiO_2-$CaCl_2$ samples with 10%, 30%, 50%, 70% mole compositions of $CaCl_2$ are shown in Fig. 3.7. It shows the change of heat flow with as increase in temperature. Last peak of each curve represents the melting process, solidus

point is denoted by the onset of the peak and liquidus point lies at the end of the peak.

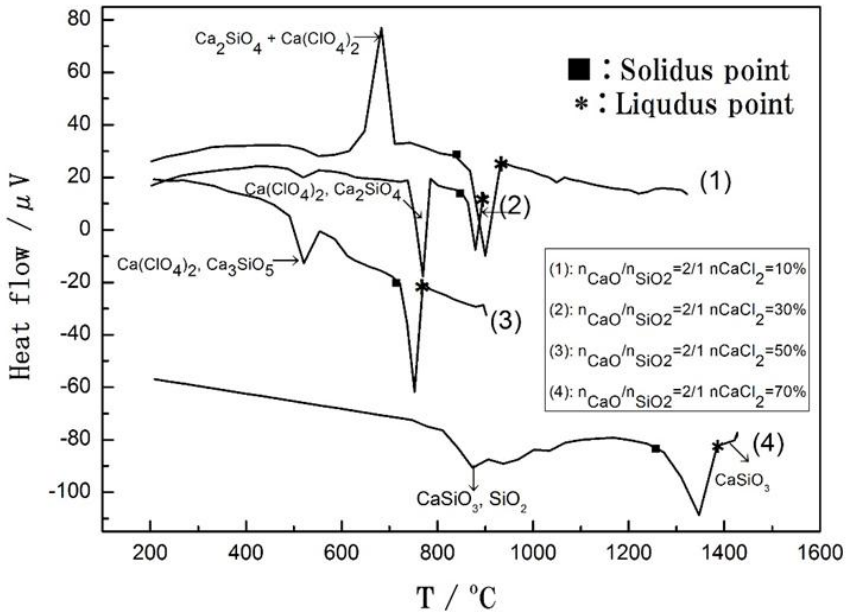

Figure 3.7. Typical TG-DTA diagrams

3.3.3 Results and discussion

Various mole compositions of SiO_2-$CaCl_2$ slags were heated by TG-DTA equipment. Results of all the SiO_2-$CaCl_2$ mixtures and solidus temperature and liquidus temperature are listed in Table 3.2 and the resulting phase diagram is shown in Fig. 3.8.

Table 3.2. DTA results for $CaCl_2$-SiO_2 binary system

$CaCl_2$:SiO_2 mole ratio	**Solidus, K**	**Liquidus, K**	**$CaCl_2$:SiO_2 mole ratio**	**Solidus, K**	**Liquidus, K**
100:0		1055	50:50	1049	1050
95:05	1026	1054	45:55	1046	1058
90:10	1023	1053	40:60	1047	1066
85:15	1013	1038	35:65	1044	1071
80:20	1018	1047	30:70	1053	1074
75:25	1020	1023	25:75	1281	1295
70:30	1022	1034	20:80	1712	1730
65:35	1019	1058	15:85	>1723	>1723
60:40	1021	1048	10:90	>1723	>1723
55:45	1017	1067	0:100	-	1943

Heating rate: 10 K/min. Mass lost: 1%-3%

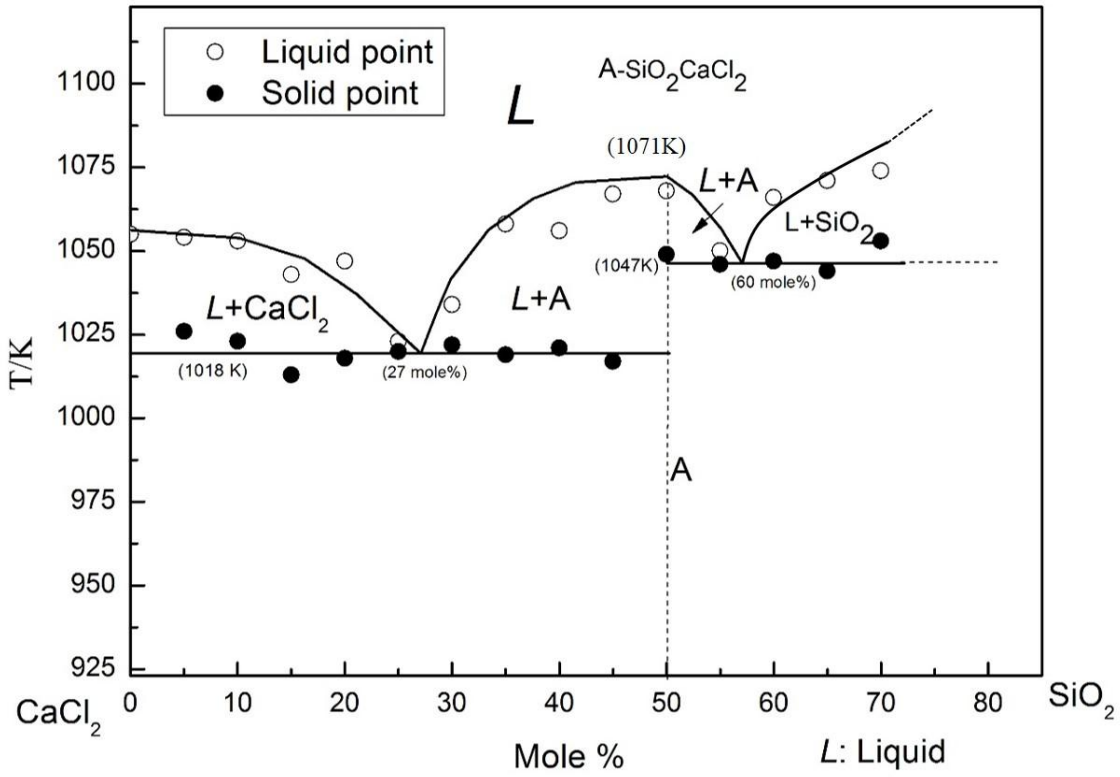

Figure 3.8. $CaCl_2$-SiO_2 phase diagram

Fig. 3.8 shows that with the addition of the SiO_2, the liquidus decreases firstly from the melting point of $CaCl_2$ (1055K) until the eutectic points (1018K), and increases to the congruent melting point (1071K) when the mole fraction of SiO_2 is 50%, then the liquidus decreases again to another eutectic points (1047K) and increases again until to the melting point of SiO_2 (1943K). The SiO_2-$CaCl_2$ phase diagram includes a compound of SiO_2·$CaCl_2$ which melts congruently at 1071K, when the mole fraction of SiO_2 is 50%. It also indicates that between 0 % and 50 mol% of SiO_2, an eutectic reaction takes place at 1018K, the eutectic point is 27 mole % of SiO_2, the liquid-solid phase denotes the liquid-$CaCl_2$ and liquid-SiO_2·$CaCl_2$. From 50 mol% to the around 70 mol% of SiO_2， another eutectic reaction occurs at 1047K, the eutectic point is 60 mol% SiO_2, the liquid-solid mixed phase represents the liquid-SiO_2·$CaCl_2$ and liquid-SiO_2.

Compared with SiO_2-CaF_2 phase diagram [21], as shown in Fig. 3.9, on the one hand, the liquidus in the both of SiO_2-CaF_2 and SiO_2-$CaCl_2$ phase diagrams have the similar tendency which decreases from the melting point of $CaCl_2$ or CaF_2 and increases to the melting point of SiO_2 with the addition of SiO_2. It was also found that both of them have two eutectic reactions and two eutectic points when the weight percent of CaF_2 are 53%

and 77%. On the other hand, SiO_2-CaF_2 phase diagram contains a two liquid coexist area between 57% to 77%, but in SiO_2-$CaCl_2$ experiment, it was found that the slag is homogeneous when the mole fraction of SiO_2 lies between 40% to 60%, as shown in Figure 3.10.

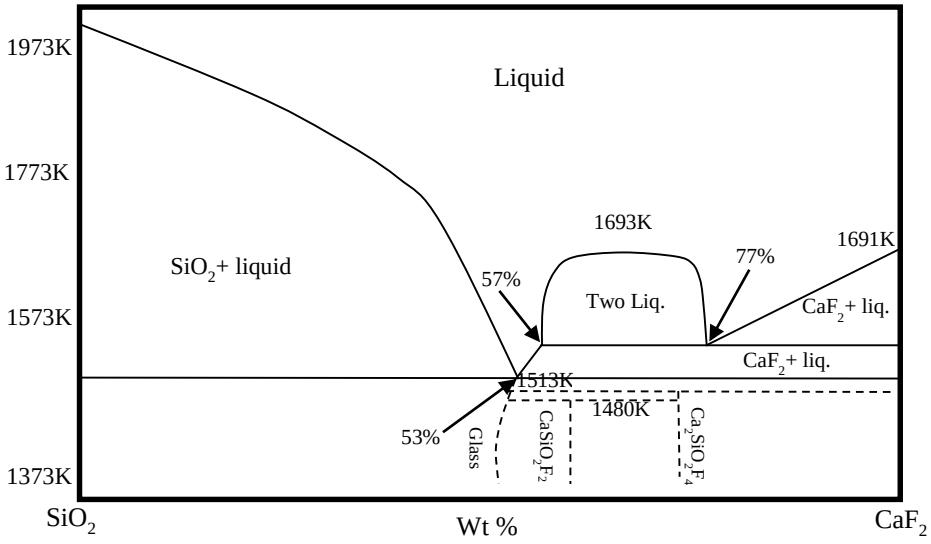

Figure 3.9. Phase diagram of SiO_2-CaF_2 [21]

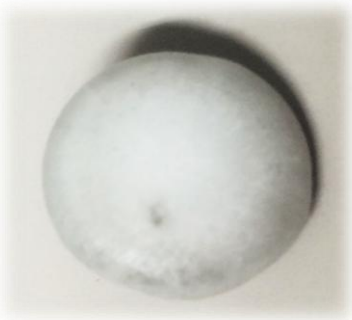

Figure 3.10. Slag sample of 50mol% SiO_2-50mol% $CaCl_2$ after quenching

Compared with and $CaCl_2$-KCl phase diagram [22], as shown in Fig. 3.11, both of $CaCl_2$-KCl and SiO_2-$CaCl_2$ phase diagrams have two eutectic reactions and two eutectic points. Moreover, both of them have an intermediate compound and a congruent melting point when the mole fraction of $CaCl_2$ is 50%.

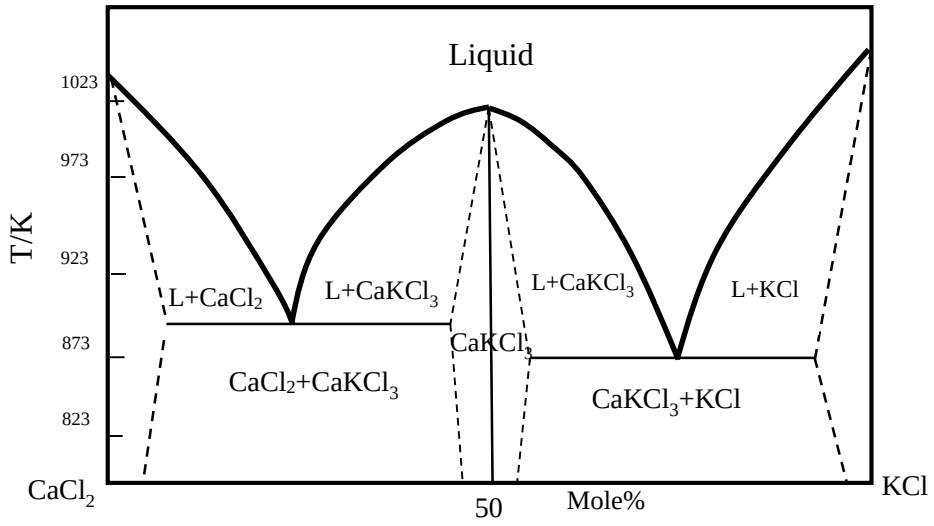

Figure 3.11. Phase diagram of $CaCl_2$-KCl

Compared with the $CaCl_2$-CaF_2 phase diagram [23], as shown in Fig. 3.12, both of the $CaCl_2$-KCl and SiO_2-$CaCl_2$ phase diagrams have an intermediate compound (SiO_2CaCl_2 and CaFCl).

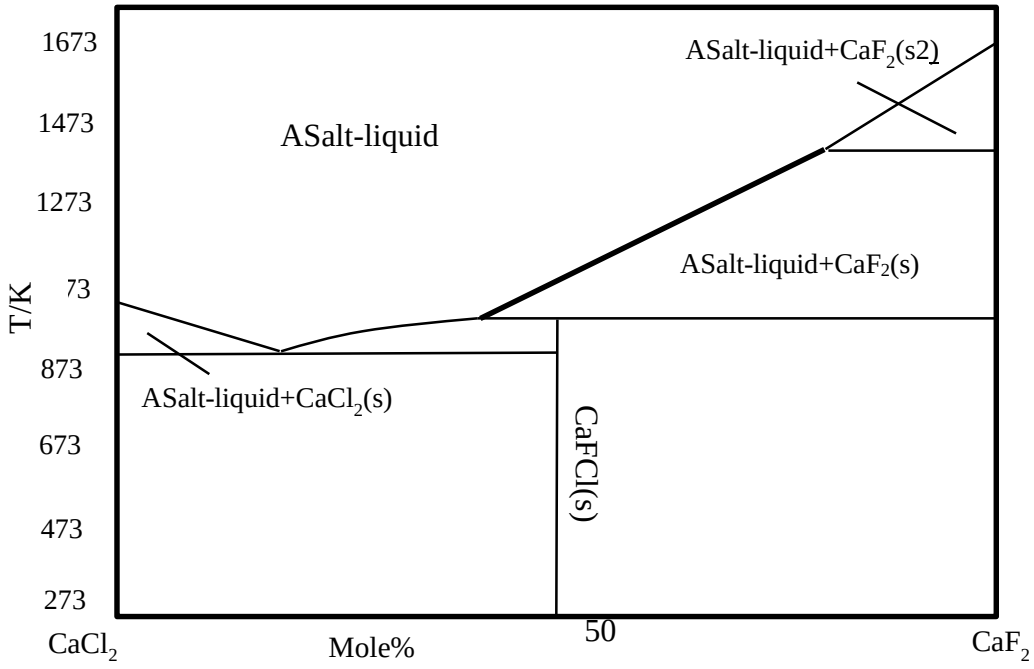

Figure 3.12. Phase diagram of $CaCl_2$-CaF_2

3.4 Liquidus of $CaO-SiO_2-CaCl_2$ slag

3.4.1 Experimental procedure

Firstly, reagent grade calcium chloride ($CaCl_2$, ≥ 95 wt% in purity, Wako, Japan), CaO (as mentioned before) and SiO_2 (as mentioned before) were used for preparing the starting materials. Secondly, various compositions of the slag (total weight =3 g) were mixed properly and sealed in the graphite crucible. Thirdly, the sealed slag was premelted at 1723K for 10 min using SiC resistance furnace and then quenched with Ar gas blowing (50 ml/min), as shown in Fig. 3.13. Fourthly, it was distinguished if the slag melted fully or partially by morphological observation, and then 20 mg of melted slag was put into the Pt crucible (4.9 mm inner diameter, 5.1 mm outer diameter, and 5 mm length). Finally, when the composition of samples are in the $CaCl_2$-rich region (sample number: 80-85), the evaporation rate of $CaCl_2$ is fast. Thus, in order to keep the composition of samples maintain stable during the heating process, the Pt crucible sealed by spot welding (mass lost: 3-5%) was used in the TG-DTA. The end of Pt crucible was sealed by spot welding, folded and welded again, as shown in Fig. 3.14. The solidus and liquidus points were measured using the same TG-DTA method as mentioned before.

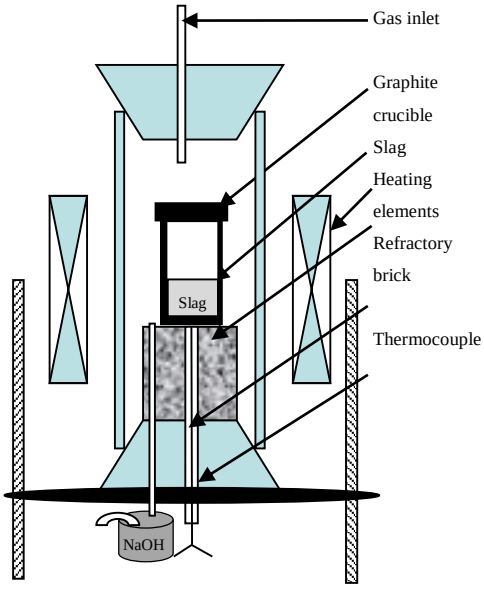

Figure 3.13. Experiment set up of resistance furnace

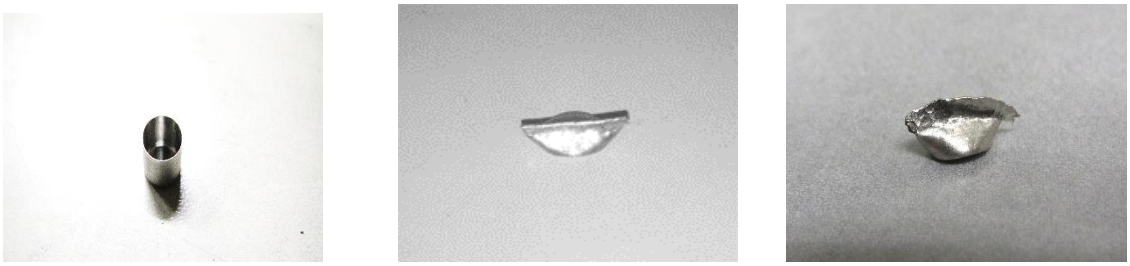

Figure 3.14. Samples in the sealed Pt crucible by spot welding

3.4.2 Results and discussion

a) Morphology of the samples

According to the phase diagrams of $CaO\text{-}SiO_2$ [24], $CaO\text{-}CaCl_2$ [25] and $SiO_2\text{-}CaCl_2$ which we detected, a ternary $CaO\text{-}SiO_2\text{-}CaCl_2$ slag system was further discussed. In this study, it can be distinguished whether sample was melted or not according to the sample morphology. As shown in Fig. 3.15, the powder sample shows it was not melted, the glass phase shows it was melted or partially melted slag. The results are shown in Table 3.3.

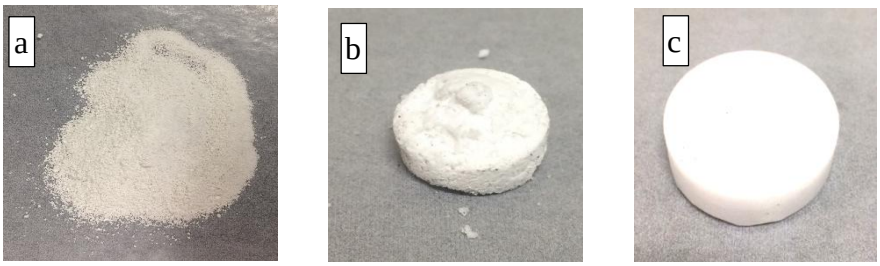

Figure 3.15. Morphology of sample-a) powder, b) partially melted, c) melted

Table 3.3. Results of different compositions of slag (mol %)

No.	CaO	SiO_2	$CaCl_2$	State	No.	CaO	SiO_2	$CaCl_2$	State
1	0.95	0	0.05	Not melted	2	0.925	0	0.075	Not melted
3	0.9	0	0.1	Not melted	4	0.8	0	0.2	Not melted
5	0.6	0	0.4	Partially melted	6	0.55	0	0.45	Partially melted
7	0.45	0	0.55	Melted	8	0.3	0	0.7	Melted
9	0.2	0	0.8	Melted	10	0	0.2	0.8	Melted
11	0	0.25	0.75	Melted	12	0	0.3	0.7	Melted
13	0	0.65	0.35	Melted	14	0	0.75	0.25	Melted
15	0	0.8	0.2	Partially melted	16	0	0.9	0.1	Not melted
17	0.05	0.05	0.9	Melted	18	0.5	0.05	0.45	Melted
19	0.6	0.05	0.35	Partially melted	20	0.85	0.05	0.1	Not melted
21	0.125	0.075	0.8	Melted	22	0.2	0.1	0.7	Melted
23	0.35	0.1	0.55	Melted	24	0.55	0.1	0.35	Melted
25	0.6	0.1	0.3	Partially melted	26	0.7	0.1	0.2	Not melted

27	0.05	0.15	0.8	Melted	28	0.15	0.15	0.7	Melted
29	0.55	0.15	0.3	Melted	30	0.6	0.15	0.25	Melted
31	0.65	0.15	0.2	Not melted	32	0.7	0.15	0.15	Partially melted
33	0.325	0.175	0.5	Melted	34	0.1	0.2	0.7	Melted
35	0.2	0.2	0.6	Melted	36	0.4	0.2	0.4	Melted
37	0.55	0.2	0.25	Melted	38	0.6	0.2	0.2	Melted
39	0.65	0.2	0.15	Partially melted	40	0.25	0.25	0.5	Melted
41	0.45	0.25	0.3	Melted	42	0.5	0.25	0.25	Melted
43	0.65	0.25	0.1	Not melted	44	0.2	0.3	0.5	Melted
45	0.55	0.3	0.15	Melted	46	0.5	0.3	0.2	Melted
47	0.625	0.3	0.075	Not melted	48	0.65	0.3	0.05	Partially melted
49	0.625	0.325	0.05	Partially melted	50	0.3	0.35	0.35	Melted
51	0.35	0.35	0.3	Melted	52	0.55	0.35	0.1	Melted
53	0.575	0.35	0.075	Melted	54	0.35	0.4	0.25	Melted
55	0.1	0.45	0.45	Melted	56	0.55	0.45	0.1	Melted
57	0.5	0.45	0.05	Partially melted	58	0.25	0.5	0.25	Melted
59	0.4	0.5	0.1	Melted	60	0.525	0.425	0.05	Melted
61	0.425	0.55	0.025	Partially melted	62	0.15	0.6	0.25	Melted
63	0.2	0.6	0.2	Melted	64	0.25	0.6	0.15	Partially melted
65	0.3	0.6	0.1	Partially melted	66	0.375	0.6	0.025	Partially melted
67	0.15	0.65	0.2	Partially melted	68	0.2	0.65	0.15	Partially melted
69	0.05	0.7	0.25	Partially melted	70	0.1	0.7	0.2	Partially melted
71	0.2	0.7	0.1	Partially melted	72	0.075	0.85	0.075	Partially melted

b) Determination of liquidus area of SiO_2-CaO-$CaCl_2$ slag system at 1723K

The solidus and liquidus temperature of the $CaCl_2$-rich region of the SiO_2-CaO-$CaCl_2$ slag system could be measured by TG-DTA after sealing the Pt crucible. The results of the solidus temperature and liquidus temperature of the SiO_2-CaO-$CaCl_2$ slag are shown in Table 3.3 and Table 3.5

Table 3.5 Solidus and liquidus points of SiO_2-CaO-$CaCl_2$ slag (T/K, mole fraction)

No.	**CaO**	**SiO_2**	**$CaCl_2$**	**Solidus**	**Liquidus**	**No.**	**CaO**	**SiO_2**	**$CaCl_2$**	**Solidus**	**Liquidus**
73	0.575	0.35	0.075	1092	1595	74	0.525	0.425	0.05	1093	1611
75	0.425	0.55	0.025	1091	1735	76	0.375	0.6	0.025	1094	1734
77	0.25	0.6	0.15	1094	1733	78	0.15	0.65	0.2	1093	1733
79	0.2	0.65	0.15	1090	1734	80	0.05	0.7	0.25	1092	1733
81	0.1	0.7	0.2	1093	1733	82	0.50	0.05	0.45	1051	1466
83	0.55	0.05	0.40	1053	1730	84	0.55	0.15	0.30	1321	1673

85	0.60	0.15	0.25	1247	>1743	86	0.625	0.20	0.175	1265	>1743
87	0.65	0.05	0.30	1233	>1743						

According to Table 3.3 and Table 3.5, the liquidus of ternary slag was drawn in Fig. 3.16. The white points represent the not melted and partially melted slag, the black points represent the melted slag. In addition to the liquidus temperature of various compositions of slag as shown in Table 3.5, the liquidus curve of CaO-SiO_2-$CaCl_2$ slag at 1723K are shown in Fig. 3.16. In the SiO_2-riched region, it contains a ternary eutectic involving the compounds SiO_2, CaO·SiO_2 and $CaCl_2$·SiO_2 in equilibrium at 1093K, the liquidus points are over 1723K, which is beyond the capability of the instrument. There are six kinds of species which are CaO·SiO_2 (CS), 3CaO·2SiO_2 (C_3S_2), Ca_2O_4Si, 3CaO·SiO_2 (C_3S), CaO and CaO·$CaCl_2$ in the six parts of liquidus curve.

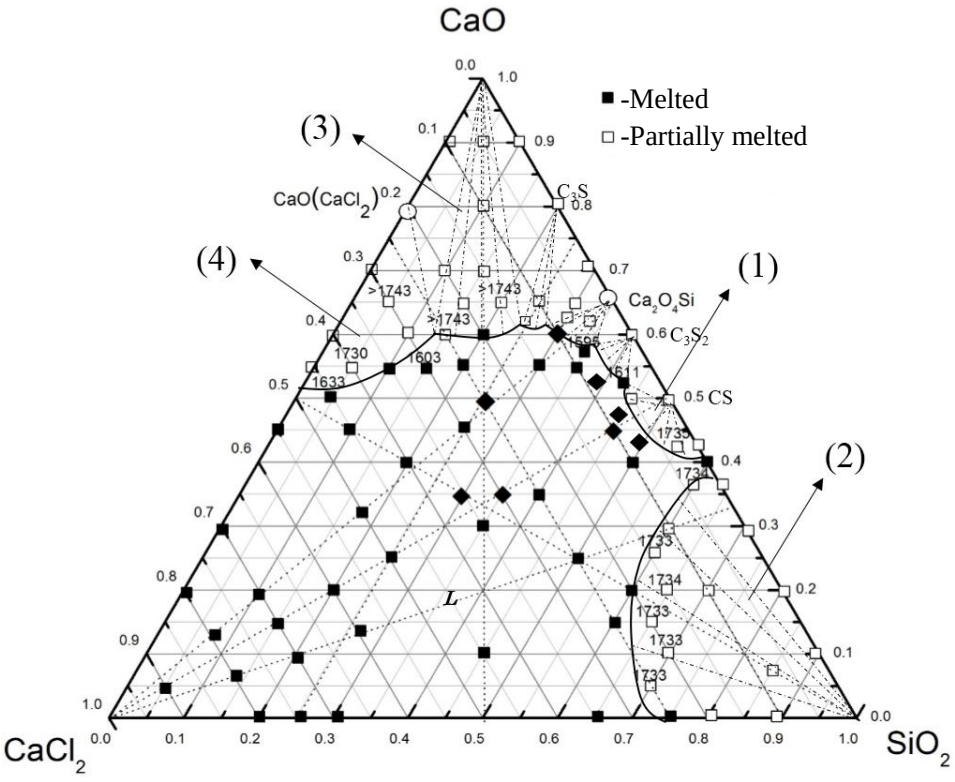

Figure 3.16. Liquidus of CaO-SiO_2-$CaCl_2$ slag at 1723K

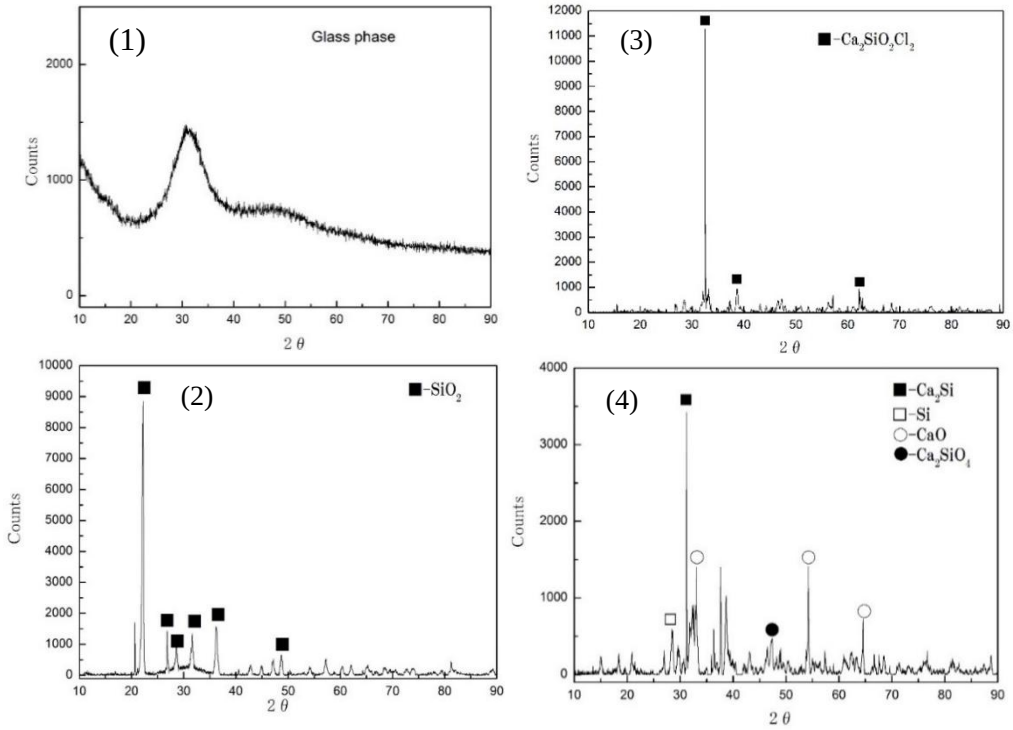

Figure 3.17. XRD patteren of samples

According to the results of XRD measurement, main phases of different compositions of CaO-SiO_2-$CaCl_2$ slag are also shown in Fig. 3.17. In the region (1), the main phase is glass phase, which is in accordance with the CaO-SiO_2 binary phase diagram. In region (2), XRD indicates the SiO_2 phase, it lies in SiO_2-rich region. In region (3), $Ca_2SiO_2Cl_2$ exists as the main phase. Ca_2Si, Si, CaO and Ca_2SiO_4 are coexisting in region (4).

Compared with the melting point ternary phase diagram of CaO-SiO_2-CaF_2 [22] as shown in Fig. 3.18, both of the CaO-SiO_2-$CaCl_2$ diagram and the CaO-SiO_2-CaF_2 diagram have the large area of high melting point (over 1723K) in the SiO_2-rich area and CaO-rich area. With the increase of $CaCl_2$ or CaF_2, both of them tends to have a large liquidus area.

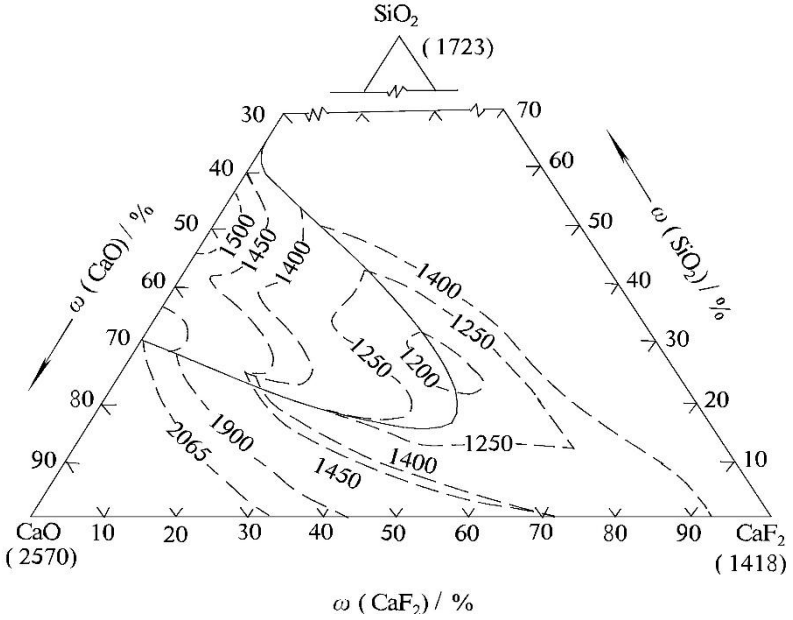

Figure 3.18. The melting point ternary phase diagram of $CaO\text{-}SiO_2\text{-}CaF_2$ (^oC) [26]

3.5 Summary

1) The density of a CaO-SiO_2-$CaCl_2$ slag decreases slightly with increasing temperature, but increases with increasing mole fraction of CaO increases.
2) The molar volume of CaO-SiO_2-$CaCl_2$ slags increases with temperature.
3) Two eutectics in the SiO_2-$CaCl_2$ binary system were located at 27 mole% SiO_2 (m.p. 1018K) and 60 mole% SiO_2 (m.p.1047K), and intermediate compound $SiO_2 \cdot CaCl_2$ melting congruently at (m.p. 1071 K) was found.
4) The low activation energy value of vaporization shows that the evaporation could occur easily. The negative values of interaction coefficients such as $\varepsilon_{CaCl_2}^{CaCl_2}$, $\varepsilon_{CaCl_2}^{CaO}$, $\varepsilon_{CaCl_2}^{SiO_2}$ show that the CaO and SiO_2 can decrease the activity of $CaCl_2$.
5) Liquidus of CaO-SiO_2-$CaCl_2$ ternary system at 1723K was detected as shown in Fig. 3.16. It was found that the ternary eutectic involving the compounds SiO_2, $CaO \cdot SiO_2$ and $CaCl_2 \cdot SiO_2$ is in equilibrium at 1093K in the SiO_2-rich region.

Reference

[1] K. Morita and T. Yoshikawa, Trans. Nonferrous Met. Soc. China, 2011. 21(3): p. 685-690.

[2] F. A. Trumbore, Bell System Technical Journal, 1960. 39(1): p. 205-233.

[3] L.A.V. Teixeira and K. Morita, ISIJ int, 2009. 49(6): p. 783-787.

[4] J. Cai, J.T. Li, W.H. Chen, C. Chen and X.T. Luo, Trans. Nonferrous Met. Soc. China 2011. 21(6): p. 1402-1406.

[5] M. Li, T. Utigard and M. Barati, MMTB, 2014. 45(1): p. 221-228.

[6] J.J. WU, W.H. Ma, B.J. Jia, B. Yang, D.C. Liu and Y.N. Dai, J Non-Cryst Solids, 2012. 358(23): p. 3079-3083.

[7] C.H. Yin, B.F. Hu and X.M. Huang, Journal of Semiconductors, 2011. 32(9): p. 092003-1.

[8] L. Zhang, Y. Tan, F.M. Xu, H.Y. Wang and Z. Gu, Separ Sci Techno, 2013. 48(7): p. 1140-1144.

[9] H. Sasaki, E. Tokizaki, K. Terashima and S. Kimura, JJAP, 1994. 33(7R): p. 3803.

[10] T. Ozawa, B Chem Soc Jpn, 1965. 38(11): p. 1881-1886.

[11] SC. Hardy, J Cryst Growth, 1984. 69(2): p. 456-460.

[12] JD. Mackenzie, J Chem Phys, 1958. 29(3): p. 605-607.

[13] F.M. Najib and S. Othman, Talanta, 1992. 39(10): p. 1259-1267.

[14] Y. Wang. X.D. Ma and K. Morita, MMTB, 2014. 45(2): p. 334-337.

[15] X.D. Ma, doctoral dissertation, The University of Tokyo, 2013.

[16] L. Muhmood, and S. Seetharaman, MMTB, 2010. 41(4): p. 833-840.

[17] B. Kelly and P. Walker, Carbon, 1970. 8(2): p. 211-226.

[18] Q.Z. Huang, China Metallurgical Encyclopedia-Carbon Material. 2004: Metallurgical Industry Press.

[19] P.A. Premkumar, K. S. Nagaraja, R. Pankajavalli, C. Mallika and O. M. Sreedharan, Materials Letters, 2004. 58(3): p. 474-477.

[20] H. Bhadeshia, Thermal analyses techniques, University of Cambridge, Material Science and Metallurgy. 2004.

[21] L. Hillert, Acta Cgenuca Scandinavica. 1966. 20(290): p. 296.

[22] P.C. Robert and W.R. Frederick, Thermochimica acta, 1975. 12: p. 5.

[23] FACT salt databases.

[24] S.R. Robert, A.C. Mary and M. Deirdre, Phase Diagrams for Ceramists, Vol. I. 1984: American Ceramic Society. 237-238.

[25] S.R. Robert, A.C. Mary and M. Deirdre, Phase Diagrams for Ceramists, Vol. Ⅲ. 1984: American Ceramic Society.

[26] X.G. Huang, Principle of Ferrous Metallurgical 2005, Metallurgical Industry Press: Bei Jing.

CHAPTER FOUR

REACTION MECHANISM AND KINETICS OF BORON REMOVAL FROM MOLTEN SILICON BY CAO-SiO_2-$CaCl_2$ SLAG TREATMENT

4.1 Introduction

The availability of abundant and low-cost solar-grade Si (SOG-Si) feedstock is essential to support the widespread use of solar cells; and indeed, there has been great progress in reducing energy consumption in the modified Siemens and fluidized bed reactor processes of fabricating SOG-Si. However, the potential for cost reduction in these processes is limited by low productivity of Si and the amount of chemical energy required to convert metallurgical-grade Si (MG-Si) into gaseous compounds, not to mention the distillation, reduction, and deposition of these compounds as solid Si. A more cost-effective and energy-efficient alternative for the production of SOG-Si is to use a metallurgical process, which provides sustainability and a number of benefits in terms of productivity and process costs. Metallurgical methods such as directional solidification [1-3], alloy refining [4-6], oxidation with plasma melting [7, 8] , and vacuum melting [9, 10] have all been investigated; however, each has its own unique limitations that prevent the total removal of impurities. This is largely a result of the fact that the segregation coefficients of B and P are both close to 1 in molten Si, meaning that they are not easily removed from the melt. Thus, in order to meet the strong demand for Si that is free of B and P via a low-cost process, the use of slag treatment as a method for the removal of B and P has received increased attention owing to its low cost and high mass productivity.

In the slag treatment, ternary slags of CaO-SiO_2-$CaCl_2$ have been confirmed to be effective in removing B theoretically. After investigating the properties of the ternary slag, there is clearly a need for further research into the transportation kinetics of B from molten Si to molten slag, and its evaporation from slag to a gas phase. Thus, in the present chapter, a model for the mass transfer of B from molten Si through slag to the gas phase is

discussed. The diffusion coefficient of B in molten Si has been previously reported [11] ; however, its diffusion coefficient in molten $CaO-SiO_2-CaCl_2$ slag is still undefined. To address this, the diffusion coefficient of B in $CaO-SiO_2-CaCl_2$ slag was investigated by the tube-molten pool method at 1723 K. Finally, in order to investigate the rate controlling step and quantify the mass transfer of B from molten Si through slag to the gas phase, the mass transfer coefficients of B in the slag were also characterized.

4.2 Diffusion coefficient of B in the $CaO\text{-}SiO_2\text{-}CaCl_2$ slag

4.2.1 Experimental Procedure

To measure the diffusion coefficient of B in molten slag, a graphite tube (length = 20 mm, width = 15 mm, height = 12 mm) was prepared with some holes (diameter = 1.5 mm). Next, 20 g of various compositions of $CaO\text{-}SiO_2\text{-}CaCl_2$ slag system were mixed and put in a graphite crucible and pre-melted in an induction furnace under vacuum, into which the graphite tube was immersed for 10 min. A flow of Ar gas was then introduced to force the slag into the vacuum graphite tube, which was finally lifted up and furnace cooled to produce a slag-filled tube.

Diffusion coefficient experiments were carried out by melting 30 g of the same slag composition with 100 ppmw of B in a resistance furnace at 1723 K (1450 ℃) for 5 min, into which the slag-filled tube was immersed for 20 min. After the tube was removed, it was cut into portions (as shown in Fig. 4.1), and the slag was collected from the holes. B concentration (CB) of each portion (l = 2 mm) of the tubes was analyzed by inductively coupled plasma atomic emission spectrometry (ICP-AES).

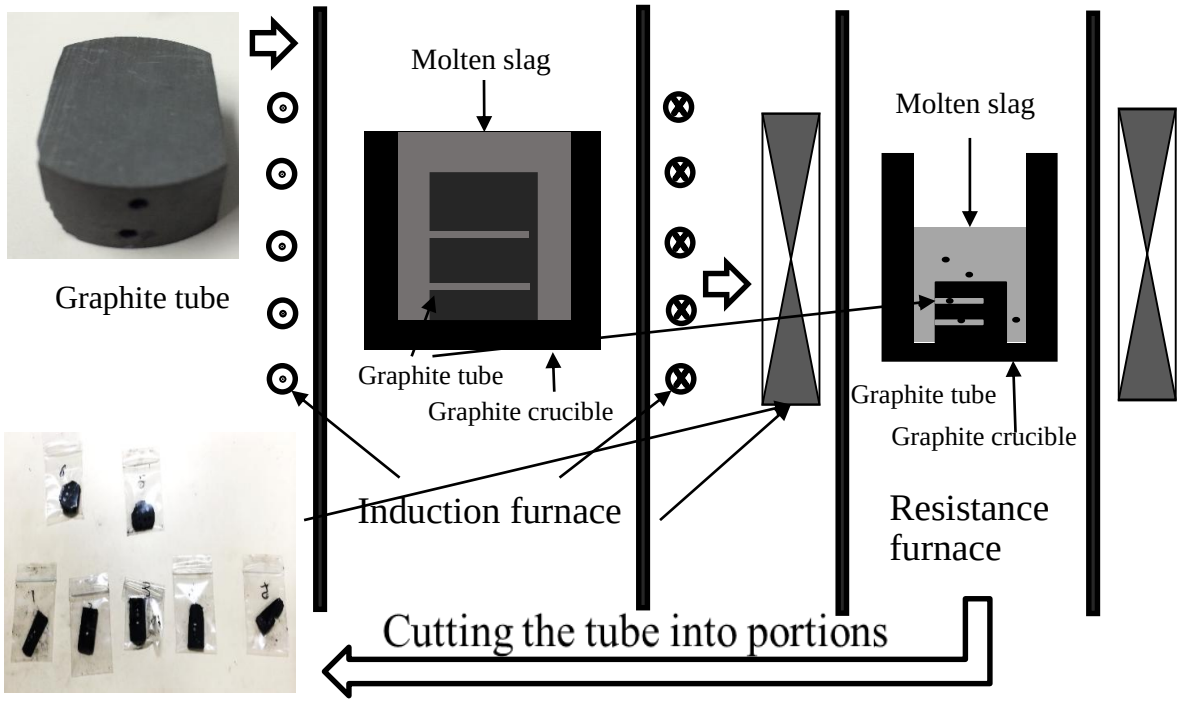

Figure 4.1. Schematic of the diffusion coefficient experiment

4.2.2 Sample analysis

B contents in the Slag

1) About 0.3 g~0.5g of slag sample was weighed and inserted in a 50ml Teflon beaker.
2) 2ml of H_2SO_4, 5ml of HNO_3 and 5ml of HF were added into the beaker.
3) The beaker was covered and kept for 1~2 days until the slag was fully dissolved.
4) The solution was filtered into a 50ml volumetric flask (Teflon) and completed to 5 ml with distilled water.
5) The concentrations of B in the solution were analyzed by ICP-AES. The standard solution of B were prepared in the range of 0.1~2 ppm (mg/L). The wavelengths of B was selected to be 249.77 nm.

4.2.3 Results and discussion

Fig. 4.2 and Table 4.2 show the B distributions that were obtained with four different slag compositions after 20 min at 1723 K, in which it can be clearly seen that the concentration of B (C_B) decreases from 100 to 0 ppmw with increasing distance from the end of the tube (x).

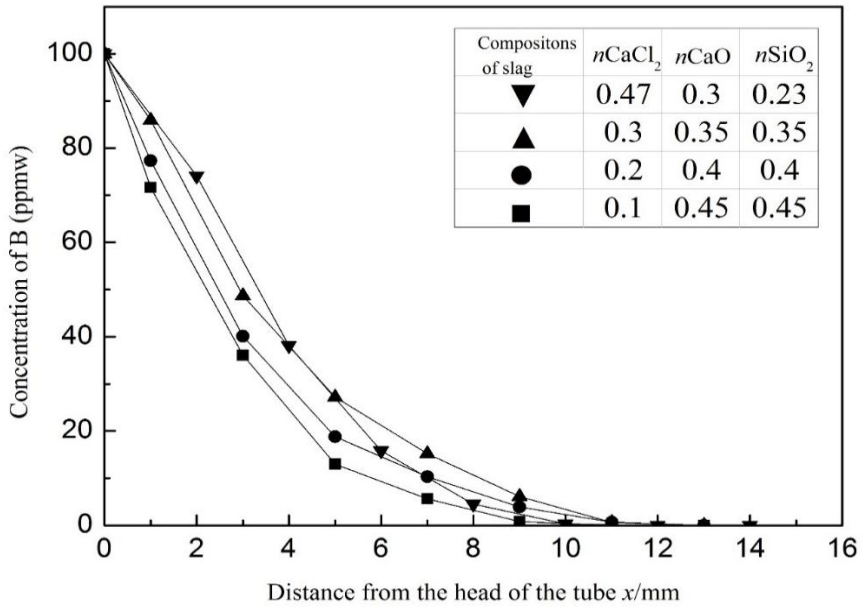

Figure 4.2. Relationship between slag composition and the C_B at various positions

If it is assumed that dimension along which diffusion is taking place in the slag is sufficiently long, then diffusion can be considered to begin at one edge of the slag, with the concentration remaining zero at the other end. This type of diffusion can be expressed using the semi-infinite one-dimensional model, wherein the range of the diffusion distance, x, is $(0, \infty)$. At time $t = 0$, it can be expressed as follows:

$$\frac{\partial C}{\partial t} = \frac{\partial}{\partial x}(D\frac{\partial C}{\partial x}) \quad (4\text{-}1)$$

$$C_B(x,t) = C_B^0 - \left(C_B^0 - C_0\right) erf\left(\frac{x}{2\sqrt{D_s t}}\right) \quad (4\text{-}2)$$

Initial condition $C(x, 0) = C_0 \quad (t = 0)$

Boundary condition $\begin{cases} C(0,t) = C_B^0 \\ C(\infty,t) = C_0 \end{cases} \quad (t > 0) \quad (4\text{-}3)$

Here, C_B represents the concentration of B in the slag at various positions, while C_B^0 is the initial concentration at the edge and is regarded as being equal to the concentration of the solute diffusion source (100 ppmw); C_0 is the initial concentration of slag in the tube, which is 0; D_s is the diffusion coefficient; and t is the diffusion time, t = 1200 s. Erf (y) is the error function, as shown in Table 4.1

Table 4.1 Error function table

x	0.000	0.010	0.020	0.030	0.040	0.050	0.060	0.070	0.080
erf(y)	0.000	0.011	0.023	0.034	0.045	0.056	0.068	0.079	0.090
x	0.090	0.100	0.110	0.120	0.130	0.140	0.150	0.160	0.170
erf(y)	0.101	0.112	0.124	0.135	0.146	0.157	0.168	0.179	0.190
x	0.180	0.190	0.200	0.210	0.220	0.230	0.240	0.250	0.260
erf(y)	0.201	0.212	0.223	0.234	0.244	0.255	0.266	0.276	0.287
x	0.270	0.280	0.290	0.300	0.310	0.320	0.330	0.340	0.350
erf(y)	0.297	0.308	0.318	0.329	0.339	0.349	0.359	0.369	0.379
x	0.360	0.370	0.380	0.420	0.430	0.440	0.450	0.460	0.470
erf(y)	0.389	0.399	0.409	0.447	0.457	0.466	0.475	0.485	0.494
x	0.480	0.490	0.500	0.510	0.520	0.530	0.540	0.550	0.560
erf(y)	0.503	0.512	0.521	0.529	0.538	0.546	0.555	0.563	0.572
x	0.570	0.580	0.590	0.600	0.610	0.620	0.630	0.640	0.650
erf(y)	0.580	0.588	0.596	0.604	0.612	0.619	0.627	0.635	0.642
x	0.660	0.670	0.680	0.690	0.700	0.710	0.720	0.730	0.740
erf(y)	0.649	0.657	0.664	0.671	0.678	0.685	0.691	0.698	0.705
x	0.750	0.760	0.770	0.780	0.790	0.800			
erf(y)	0.711	0.718	0.724	0.730	0.736	0.742			

After taking the definite integral, Eq. (4-1) can be expressed as

$$\frac{c_B - c_B^0}{c_0 - c_B^0} = \frac{2}{\sqrt{\pi}} \int_0^{x/(2\sqrt{D_s t})} e^{-\lambda^2} d\lambda \quad (4\text{-}4)$$

Right-hand side of Eq. (4-4) is the error function, which is erf(y) and $C_0 = 0$. Thus, Eq. (4-4) can be simplified as

$$C_B = C_B^0\left[1 - erf\left(\frac{x}{2\sqrt{D_s t}}\right)\right] \tag{4-5}$$

The value of D can therefore be calculated from C_B, C_B^0 and the table of error for erf(y).

The diffusion coefficients obtained using Eq. (4-5) are shown in Fig. 4.3, in which the slopes of x^2 and $4y^2t$ are the diffusion coefficients of the four different slag compositions. The accurate values of C_B and D_s are shown in Table 4.2.

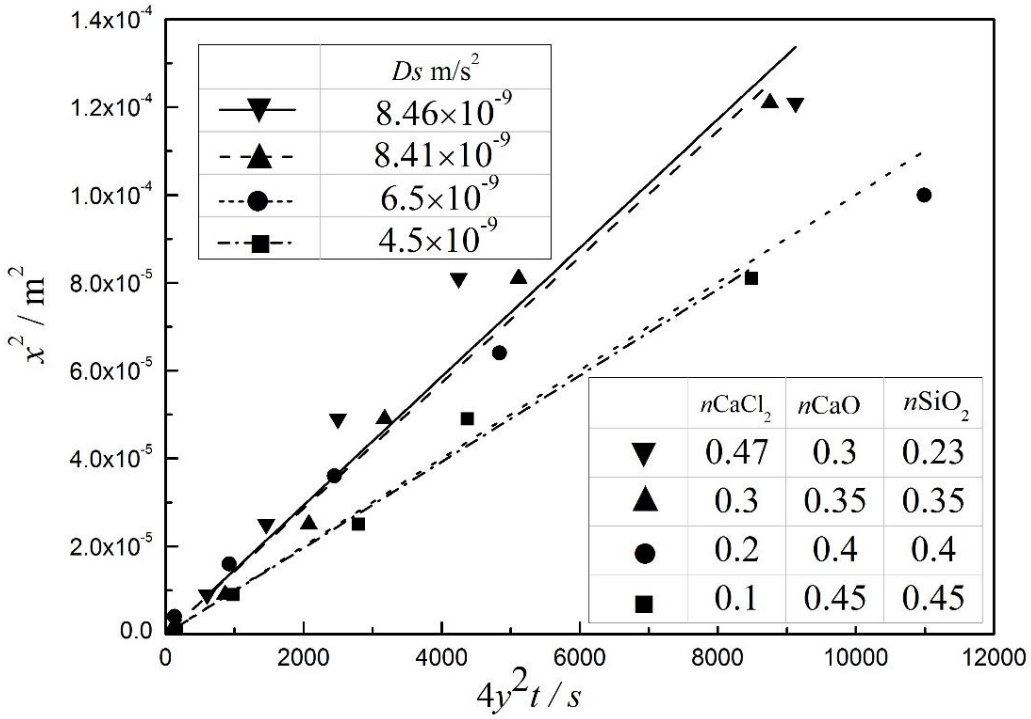

Figure 4.3. Diffusion coefficients of four different slags

Table 4.2. Diffusion coefficients and B concentrations

Distance from the head of the tube x / mm		2.0	4.0	6.0	8.0	10	12	14	D_s
Composition of slag	C_B (ppmw)	74.1	38.1	15.8	4.5	0.3	0	0	8.46 × 10^{-9} m^2s^{-1}
x_{CaCl2}:x_{CaO}:x_{SiO2}=47:30:23	D_B (10^{-8} m^2 s^{-1})	1.5	0.87	0.74	0.66	0.45	-	-	
Distance from the head of the tube x / mm		1.0	3.0	5.0	7.0	9.0	11	13	D_s
Composition of slag	C_B (ppmw)	85.9	48.7	27.2	15.2	6.1	0.6	0.0	8.41 × 10^{-9} m^2 s^{-1}
x_{CaCl2}:x_{CaO}:x_{Si}	D_B (10^{-8}	1.3	0.75	0.86	0.98	0.95	0.66	-	

$_{O2}$=30:35:35	m^2 s^{-1})								
Composition of slag	C_B (ppmw)	77.3	40.1	18.8	10.3	3.9	0.7	0.0	6.50 × 10^{-9} m^2 s^{-1}
x_{CaCl2}:x_{CaO}:x_{Si} $_{O2}$=20:40:40	D_B (10^{-8} m^2 s^{-1})	0.52	0.52	0.60	0.77	0.79	0.69	-	
Composition of slag	C_B (ppmw)	71.6	36.1	13.0	5.6	0.8	0.0	0.0	4.50 × 10^{-9} m^2 s^{-1}
x_{CaCl2}:x_{CaO}:x_{Si} $_{O2}$=10:45:45	D_B (10^{-8} m^2 s^{-1})	0.31	0.46	0.45	0.56	0	-	-	

The value of *Ds* was found to increase from 4.5 $\times 10^{-9}$ to 8.46 $\times 10^{-9}$ m/s^2 when $CaCl_2$ concentration was increased from 10 to 47 mol%, as shown in Fig. 4.4. Given that $CaCl_2$ can decrease the viscosity of the slag, the maximum value shows that the solubility of $CaCl_2$ in a $CaCl_2$-CaO-SiO_2 slag is approximately 50 %.

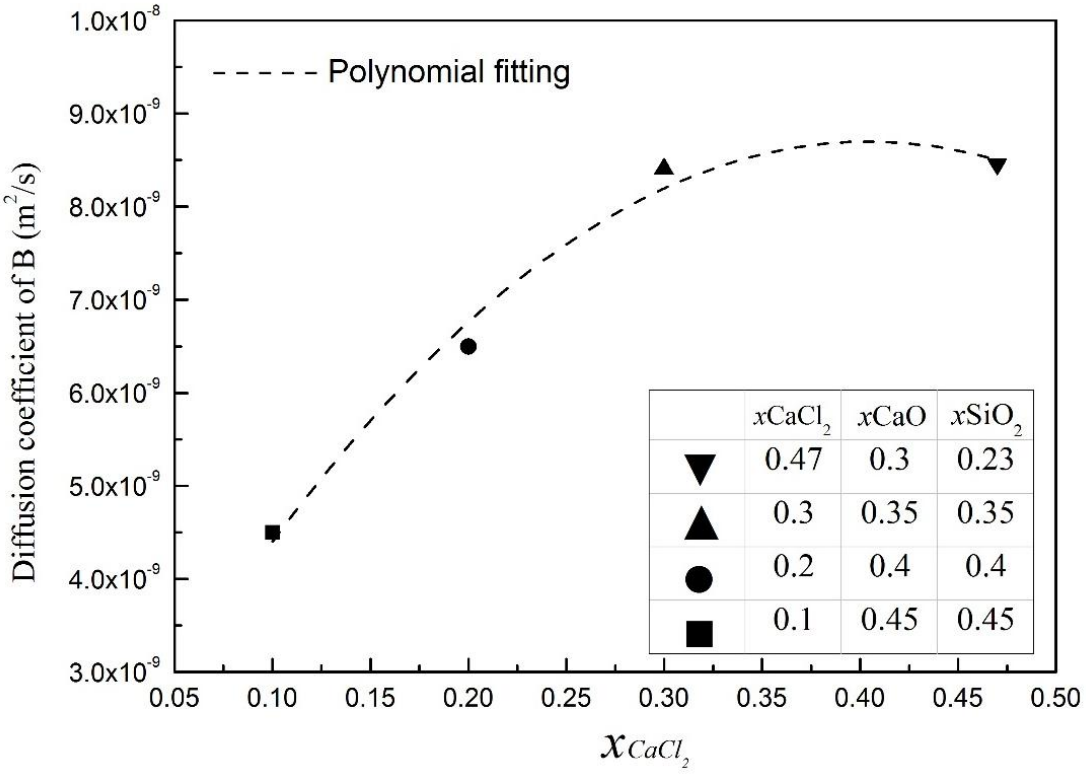

Figure 4.4. Change in the diffusion coefficient of B with slag composition

Table 4.3 compares the diffusion of different elements in various slag systems, revealing that the diffusion of B in a CaO-SiO_2-$CaCl_2$ slag is faster than the diffusion of S in the more viscous CaO-SiO_2-Al_2O_3 slag system. Moreover, the diffusion of B is faster in molten Si than in slag, suggesting that the rate-limiting step in the B removal process

may be controlled by the transportation of B in the slag. However, the diffusion of B in slag can be separated into two distinct steps depending on whether it occurs at interface or surface of the slag. To investigate the diffusion of B in bulk slag, its mass transfer coefficient in the slag needs to be considered.

Table 4.3. Diffusion coefficients of different series

Diffusant	**Material system (mass %)**	**D (m^2/s)**	**T (K)**
B	$CaO\text{-}SiO_2\text{-}CaCl_2$ (0.15-0.18-0.66)	8.46×10^{-9}	1723
S [12]	$CaO\text{-}SiO_2\text{-}Al_2O_3$ (0.52-0.39-0.96)	4.14×10^{-10}	1723
B [11]	Si	$(2.4 \pm 0.7) \times 10^{-8}$	Melt state
Al [11]	Si	$(7.0 \pm 3.1) \times 10^{-8}$	Melt state
P [11]	Si	$(5.1 \pm 1.7) \times 10^{-8}$	Melt state

4.3 Mass transfer coefficients of B in $CaO\text{-}SiO_2\text{-}CaCl_2$ slag

4.3.1 Experimental procedure

The mass transfer coefficient was measured using a vertical SiC resistance furnace (60 mm O.D., 53 mm I.D., 1000 mm length), the temperature of which was maintained at 1723 ±2 K using a PID controller (Fig. 4.5). In this experiment, 3 g of Si containing 300 ppmw of B was premelted at 1723 K, and then, 3, 6, or 9 g of 30mol%CaO-23mol%SiO_2-47 mol%$CaCl_2$ slag was added and held at 1723 K under an Ar atmosphere for various periods of time. NaOH solution was used to absorb any evaporated Cl-containing gas; and after the experiment, B concentration in the slag ($(B^{3+})_b$) and Si ($[B]_b$) was measured by ICP-AES.

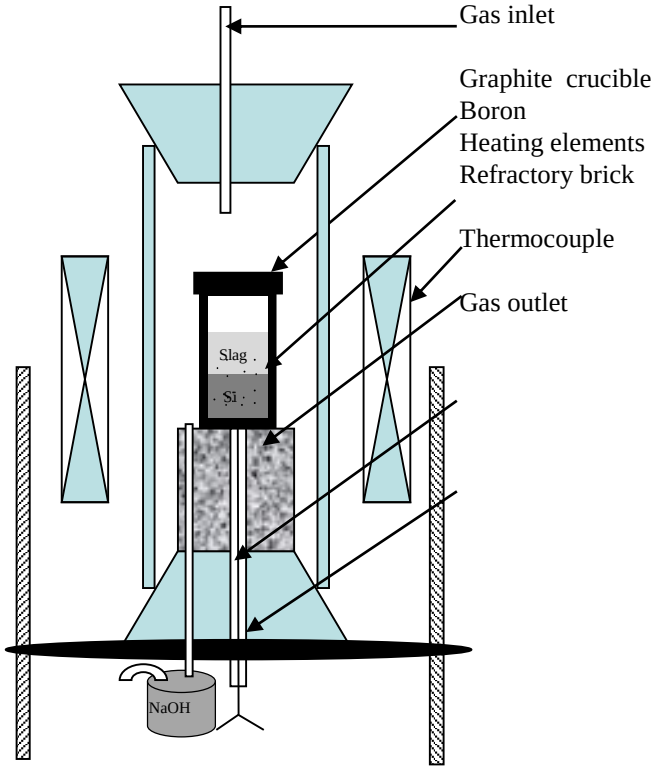

Figure 4.5 Experimental set up of the resistance furnace

4.3.2 Sample analysis

a) B contents in Si

1) The bulk Si was separated from the Si-slag mixture. The surface of bulk Si was removed by mechanical grinding and then cleaned ultrasonically in acetone.
2) The bulk Si was crushed into powder of the size less than 50 μm, followed by acid leaching to remove inclusions in 10 ml of HCl.

3) The powder was filtered, washed to neutrality by distilled water and dried.
4) About 0.3 g of Si powders was accurately weighed and placed into a 100 ml Teflon beaker.
5) 5 ml of HNO_3 and 2 ml of H_2SO_4 were added into the beaker, and then 5 ml of HF was added drop by drop until the sample was completely dissolved.
6) The solution was filtered into a 50 ml volumetric flask (Teflon) using a Teflon funnel and a filtered paper.
7) The volumetric flask was completed to 50 ml with distilled water.
8) The concentrations of B was analyzed by Seiko SPS7700 Inductive Coupled Plasma Atomic Emission Spectroscope instrument. The standard solutions of B was prepared in the range of 0.1~4 ppm, respectively. The acid matrix of standard solutions and blank were adjusted to be the same as the sample solutions. The wavelength of B was selected to be 249.77 nm.

b) B contents in Slag

The analysis method was the same as that in 4.2.2.

4.3.3 Results and discussion

The positions within the sample used for B analysis in slag and Si were, as shown in Table 4.4, at the top of the slag and the bottom of the Si, as the distribution of B in both was homogeneous. The mass transfer coefficient measurements are also shown in Table 4.4, where in the ratio of B removed to the gas phase was defined as $(300-c_{B\ in\ Si}-\mu \cdot c_{B\ in\ slag})/300$; μ being the mass ratio between slag and Si (μ=1, 2, 3). It is evident that 40-60 % of the B is evaporated as a gas phase. Moreover, from the mass ratio between Si and slag, we see that the B concentration in the molten Si decreased from 300 to approximately 30 ppmw, while the B concentration in slag increased from 0 to approximately 40 ppmw, after 3600 s at 1723 K. The mass transfer coefficient of B in slag boundary layer adjacent to Si (k_i) and the surface (k_s) will be discussed in next section.

Table 4.4. Experimental conditions and results for the $CaO\text{-}SiO_2\text{-}CaCl_2$ slag-silicon reaction at 1723 K

No.	*t* / ks	Weight of Si (g)	Weight of slag (g)	B content of Si (ppmw)	Change in B content of the slag (ppmw)	Ratio of B removed to the gas phase
I -1	0	3.0	3.0	300	0	0

I -2	0.3			233.5	20.7	15.3%
I -3	0.6			196.8	43	20.1%
I -4	0.9			136.4	51.8	37.3%
I -5	1.2			112.3	60.1	42.5%
I -6	1.5			85.7	54.5	53.3%
I -7	3.6			69.6	42.7	62.6%
I -8	7.2			68.1	40.3	63.9%
П-1	0	3.0	6.0	300	0	0
П-2	0.3			225.0	14.37	15.4%
П-3	0.6			173.0	20.56	28.6%
П-4	0.9			126.0	33.59	35.6%
П-5	1.2			109.0	39.31	37.5%
П-6	1.5			83.7	44.15	42.7%
П-7	3.6			76.2	57.33	36.4%
П-8	7.2			65.4	38.89	52.3%
П-9	9			40.4	30.07	66.5%
П-10	12			40.3	30.35	66.3%
Ш-1	0	3.0	9.0	300	0	0
Ш-2	0.3			217.6	24.5	3.0%
Ш-3	0.6			164.8	37.3	7.8%
Ш-4	0.9			122.7	40.7	18.4%
Ш-5	1.2			105.5	55.1	9.7%
Ш-6	1.5			70.3	57.2	19.4%
Ш-7	3.6			30.8	50.4	39.3%
Ш-8	7.2			31.6	49.2	40.3%

In order to investigate the mass transfer coefficient of B in $CaO-SiO_2-CaCl_2$ slag, kinetics of B removal in this system should be discussed firstly.

4.4 Kinetics of the B removal process using the $CaO\text{-}SiO_2\text{-}CaCl_2$ slag system

The process of removing B using $CaO\text{-}SiO_2\text{-}CaCl_2$ slag can be divided into six steps: (1) mass transport in Si, (2) chemical reaction at the interface between slag and Si, (3) mass transport in slag from the interface to bulk slag, (4) mass transport from bulk slag to the surface, (5) chemical reaction at the surface, and finally, (6) evaporation from surface to the gas phase.

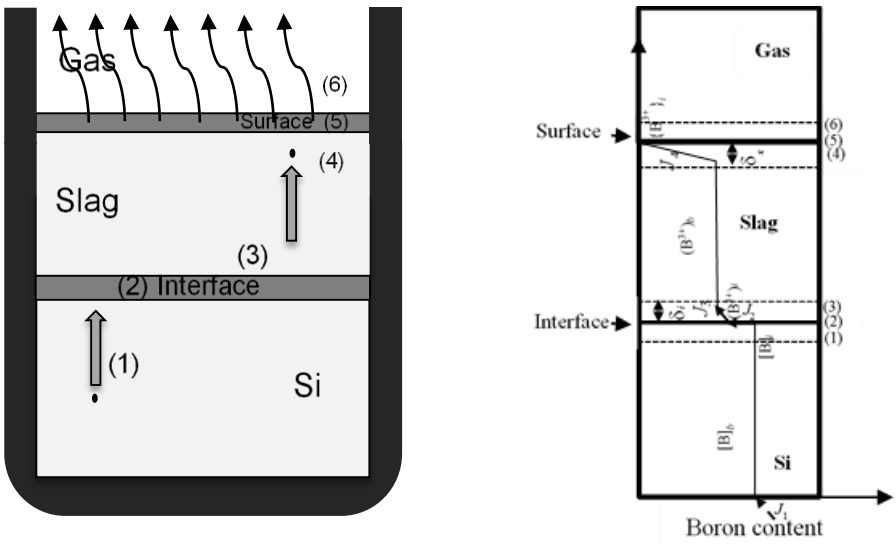

Figure 4.6. Profile of B transfer from molten Si to a gas phase

In Fig. 4.6, $[B]_i$, $[B]_b$, $(B^{3+})_i$, $(B^{3+})_b$, and $\{B^{3+}\}_s$ represent the weight concentration of B in: the molten Si interface, the bulk molten Si, the interface between Si and slag, the bulk molten slag, and the surface of molten slag. Variables $C_{B_i^{3+}}$ and $C_{B_b^{3+}}$ are mole concentrations of B in the interface and bulk slag phase, respectively, while J_i is the mass flux of B in step i (i = 1-6). Assuming that the concentration of B in bulk slag is homogeneous because of convection but changes over time in the boundary layer at the interface and surface, C_B can be considered a function of t in the boundary layers and the process can be simplified to unsteady-state diffusion.

In order to confirm the homogeneity of B in slag and Si phases, slag and Si of sample I-2 was analyzed at various points by ICP, as shown in Fig. 4.7. This revealed that B content of slag was approximately 20.7 ppmw at each location, whereas that of the Si was much higher at approximately 233.5 ppmw. As each value represents an average of three readings, this demonstrates that distribution of B in both phases was indeed homogeneous.

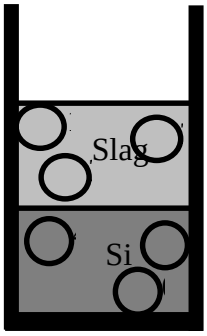

B content	B content
Part 1: 20.8 ppmw	Part 4: 232.9 ppmw
Part 2: 21.5 ppmw	Part 5: 233.5 ppmw
Part 3: 20.1 ppmw	Part 6: 234.1 ppmw

Figure 4.7. Distribution of B in the slag and Si phase of sample I-2

In step (1) of B removal process, if it is assumed that the mass transfer of B in molten Si is very fast and that the distribution of B in molten Si is homogenous, then the condition $[B]_i = [B]_b$ can be imposed. The diffusion coefficient of B in molten Si ($D_{B\text{-}Si}$) can therefore be calculated as $(2.4 \pm 0.7) \times 10^{-8}$ m/s^2

In step (2), the overall interfacial reaction of B removal can be represented by following reaction:

$$[B] + \frac{3}{4}(Si^{4+}) = (B^{3+}) + \frac{3}{4}Si \tag{4-6}$$

Assuming this reaction occurs at the interface between molten Si and slag, and is in an equilibrium state, the reaction rate can be regarded as very fast. This is predicated on the bases that the mass transfer of boron oxide is the limiting control step in Na_2SiO_3-CaO-SiO_2 slag refining, as Lei Zhang *et al*. [13] have reported. However, if we assume instead that the chemical reaction is the rate-limiting step, then B transfer in both Si and slag is faster than the chemical reaction in the boundary layer due to the fact that diffusion coefficients of B in both phases is of the same order. The distribution of B in Si and slag should therefore exhibit a linear relation with distance; this is clearly reflected in the curve obtained from experiment results. Thus, step (2) is not the rate-limiting step.

The process in step (3) is the transfer of B through slag boundary layer adjacent to Si, as shown in Fig. 4.6. This means that the mass transfer of B in slag, k_i, can be expressed as

$$J_3 = k_i\left(C_{B_i^{3+}} - C_{B_b^{3+}}\right) \tag{4-7}$$

In step (4), B is transferred through the slag boundary layer at the surface, and according to the definition of mass flux, mass transfer coefficient of this process (k_s) can be expressed as

$$J_4 = k_s\left(C_{B_s^{3+}} - C_{B_b^{3+}}\right) \tag{4-8}$$

The rate of change in C_B of bulk slag, ($d(B^{3+})_b/dt$) is related to (J_3 - J_4) as follows:

$$\frac{dC_{(B^{3+})_b}}{dt} = \frac{S}{V_{slag}}\left(J_3 - J_4\right) \tag{4-9}$$

Where S is the surface area and V_{slag} is the total volume of bulk slag. By changing C_B to weight percentage of B (B^{3+}), and substituting Eq. (4-8) and (4-9) into Eq. (4-10), we get

$$\frac{d(B^{3+})_b}{dt} = \frac{(J_3 - J_4)}{(V_{Slag}/S)\rho_{slag}} = \frac{Sk_i}{m_{slag}}\left((B^{3+})_i - (B^{3+})_b\right) - \frac{Sk_s}{m_{slag}}\left((B^{3+})_b - \{B^{3+}\}_s\right) \tag{4-10}$$

Where ρ_{slag} is the density, m_{slag} is the mass, and h is the height of the slag ($h = V_{slag}/S$). Considering the partition ratio $L_B = (B)_i/[B]i = (B)_e/[B]_e = 0.64$ [错误!未定义书签。4] and $[B]_i = [B]_b$ of the chemical process, evaporation can be assumed to be so fast that concentration of B at surface, $\{B^{3+}\}_s$, is zero. Thus, Eq. (4-10) can be simplified to

$$\frac{d(B^{3+})_b}{dt} = \frac{Sk_i}{m_{slag}}\left(L_B[B]_b - (B^{3+})_b\right) - \frac{Sk_s}{m_{slag}}(B^{3+})_b \tag{4-11}$$

In the same manner, J_1 can be assumed to be equal to the input flux of B into molten Si, which is zero. The value of J_2 is the flux of B in the interface between Si and slag phases, as shown in Fig. 4.6, and therefore, the change rate of in the C_B of molten Si ($d[B]_b/dt$) has following relationship with (J_1- J_2) :

$$\frac{dC_{[B]_b}}{dt} = \frac{S}{V_{slag}}\left(J_1 - J_2\right) \tag{4-12}$$

According to the principle of conservation of mass, B flux transferred from molten Si to the interface should be equal to the B flux transferred from the interface to bulk slag; which is to say, $J_2 = J_3$. Because $(B^{3+})_i = L_B[B]_b$ and $J_1 = 0$ in Eq. (4-12), we therefore get:

$$-\frac{d[B]_b}{dt} = \frac{J_3}{(V_{Si}/S)\rho_{Si}} = \frac{Sk_i}{m_{Si}}\left((B)_i - (B^{3+})_b\right) \Rightarrow -\frac{d[B]_b}{dt} = \frac{Sk_i}{m_{Si}}\left(L_B[B]_b - (B^{3+})_b\right) \tag{4-13}$$

Assuming $y = (B^{3+})_b$ and $x = [B]_b$, first-order ordinary differential equation system for the mass transfer of B within bulk melts can be obtained from Eq. (4-11) and (4-13) as:

$$\begin{cases} \dfrac{dy}{dt} = \dfrac{Sk_iL_B}{m_{slag}}x - \dfrac{S(k_i+k_s)}{m_{slag}}y \\ \dfrac{dx}{dt} = -\dfrac{SL_Bk_i}{m_{Si}}x + \dfrac{Sk_i}{m_{Si}}y \end{cases}, \text{ when } t = 0,\ x = x_0,\ y = 0 \qquad (4\text{-}14)$$

Solving Eq. (4-14) and assuming

$$\begin{cases} A=\left(-k_i-k_s-k_iL_B-\sqrt{-4k_ik_sL_B+(k_i+k_s+k_iL_B)^2}\right)\Big/2(m/S) \\ B=\left(-k_i-k_s-k_iL_B+\sqrt{-4k_ik_sL_B+(k_i+k_s+k_iL_B)^2}\right)\Big/2(m/S) \\ C=\sqrt{-4k_ik_sL_B+(k_i+k_s+k_iL_B)^2} \end{cases} \qquad (4\text{-}15)$$

We get a general solution for x and y as:

$$\begin{cases} x(t) = \dfrac{1}{2C}\left(-e^{At}k_i + e^{Bt}k_i - e^{At}k_s + e^{Bt}k_s + e^{At}k_iL_B - e^{Bt}k_iL_B + e^{At}C + e^{Bt}C\right)x_0 \\ y(t) = -\dfrac{1}{C}(e^{At} - e^{Bt})k_iL_Bx_0 \end{cases} \qquad (4\text{-}16)$$

Where $[B]_0$ = 300 ppmw, ρ_{slag} = 2.01 g/cm^3, ρ_{si} = 2.57 g/cm^3, S = 3.14 cm^2, and L_B = 0.64. Because the initial content of B in slag is 10.9 ppmw, change in B content of slag is the difference between actual content and 10.9 ppmw, as shown in Table 4.4. In Eq. (4-16), x and y are functions of the variable t, while k_i and k_s are the only unknown constants. Thus, k_i and k_s were obtained from three sets of data displayed in Table 4.4 via nonlinear regression analysis method using *1stOpt* software. These results are shown in Fig. 4.8.

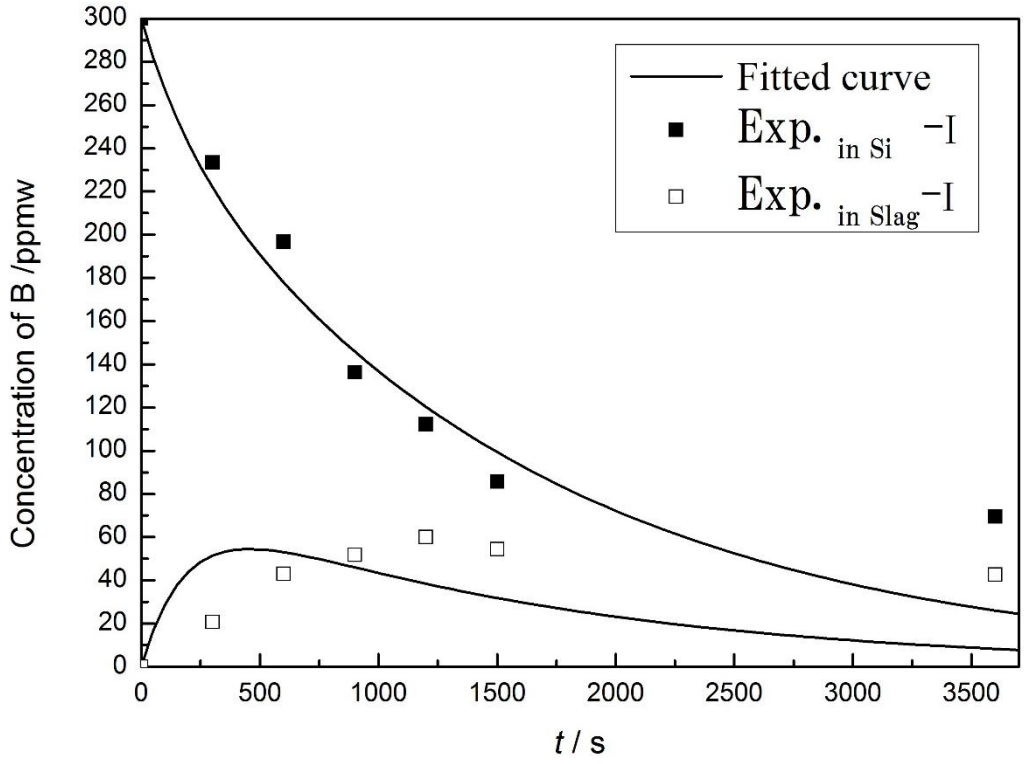

Sample I series

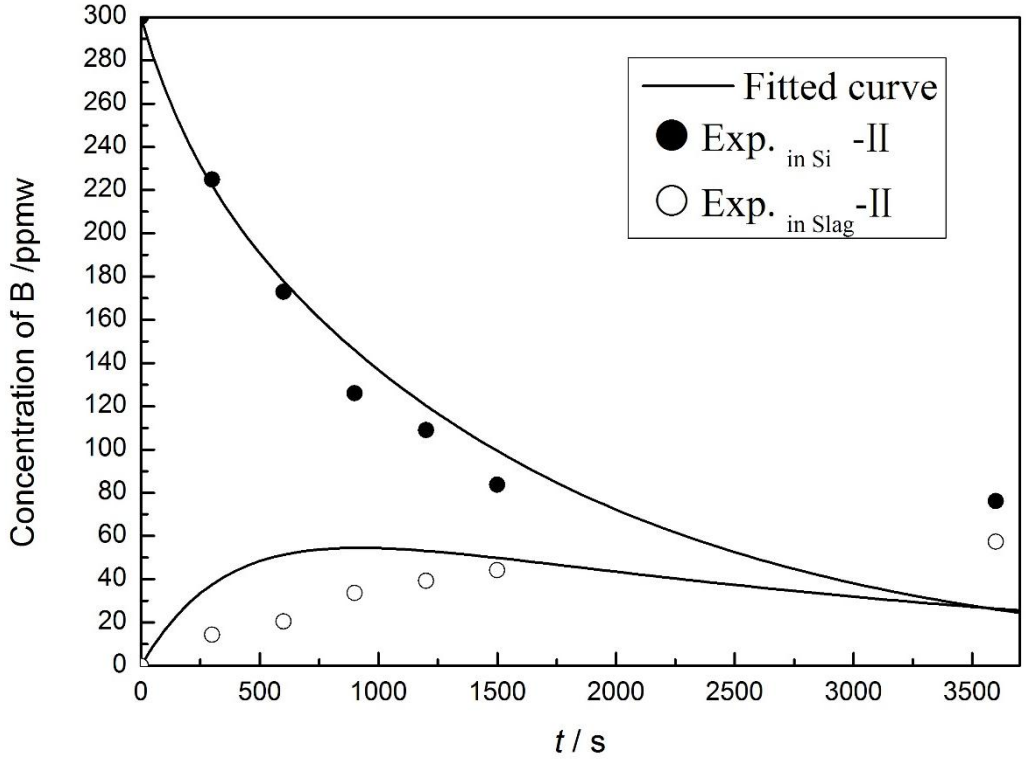

Sample II series

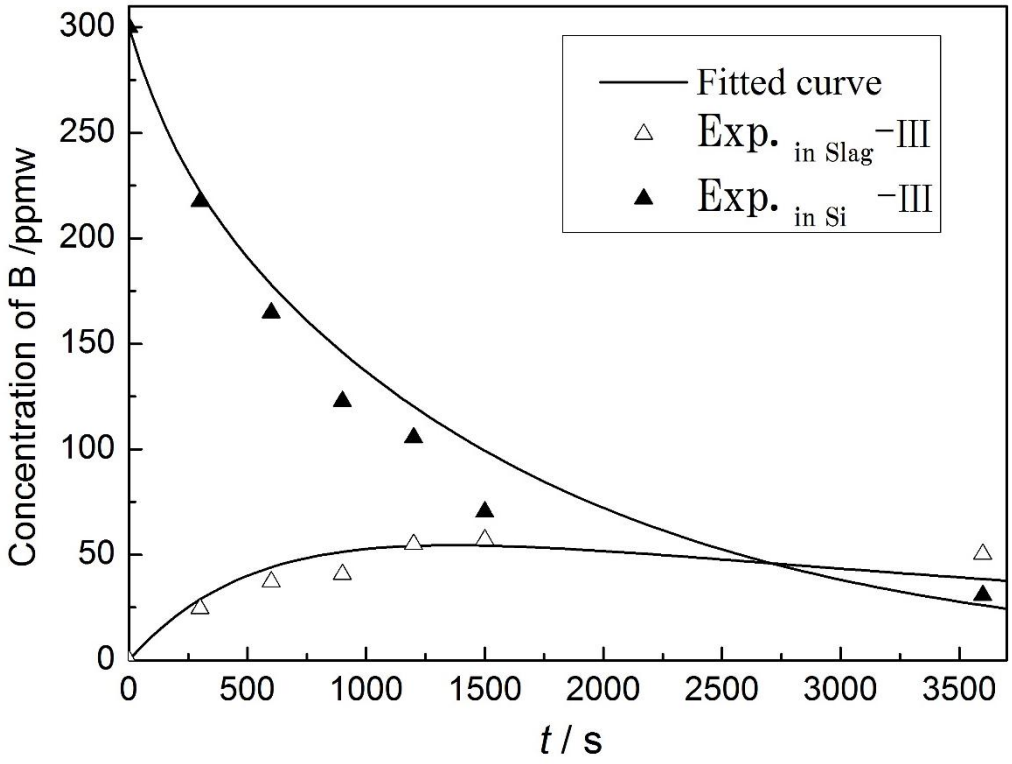

Sample III series

Figure 4.8. Change in $(B^{3+})_b$ and $[B]_b$ with time

Fig. 4.8 shows that the fitted values from the model for k_i (1.91×10^{-5} m/s) and k_s (2.50×10^{-5} m/s) are reasonable and agree with all three series results in molten Si and slag, as shown in Table 4.5.

In step (5), the reaction between slag and gas phase is assumed to occur at the surface in accordance with following reaction [14, 15]:

$$BO_{1.5(l)} + \frac{1}{2}CaCl_{2(l)} = BOCl_{(g)} + \frac{1}{2}CaO_{(s)} \qquad (4\text{-}17)$$

As the rate of this reaction is very rapid at high temperatures, step (5) is not the rate-limiting step. In the case of step (6), diffusion of BOCl gas in an Ar atmosphere is likely to be very fast, and therefore, step (6) also cannot be the rate-limiting step.

The thickness of the boundary layers of slag adjacent to Si (δ_i) and at the surface (δ_s) can be obtained from:

$$\delta_i = D_s / k_3 \qquad \delta_s = D_s / k_4 \qquad (4\text{-}18)$$

Using Eq. (4-18), different values of δ_i and δ_s for different mass ratios of slag and Si were calculated. As shown in Table 4.5, it was found that the value of k_i (1.91×10^{-5} m/s) is slightly lower than that of k_s (2.50×10^{-5} m/s), which means that the rate-limiting step

is controlled by both the boundary layers adjacent to Si and at the surface. However, it is former that has the greatest influence, because the thickness of the boundary layer of slag in the Si/slag interface (0.44 mm) is thicker than that at the surface (0.34 mm).

Table 4.5 k_i, k_s, δ_i, and δ_s with different mass ratios of slag and molten Si

D_s (m^2/s)	k_i (m/s)	k_s (m/s)	δ_i (mm)	δ_s (mm)	Correlation coefficient
8.46×10^{-9}	1.91×10^{-5}	2.50×10^{-5}	0.44	0.34	0.97

4.5 Summary

To investigate the kinetics of B removal by evaporation using different compositions of CaO-SiO_2-$CaCl_2$ slag, a model for the transfer of B from Si to molten slag by diffusion and its evaporation as a gas phase was established. The mass transfer and diffusion coefficients of B in the slag were measured at 1723 K for different times and different mass ratios between slag and Si. In addition, the rate controlling step was also investigated based on the kinetics model and calculated values of k_s and D_s. Thus, from this study, following conclusions have been drawn:

1) The diffusion coefficient of B in slag (D_s) is 8.46×10^{-9} m/s^2, which means the rate of step (3) is slower than that of B diffusion in Si ($(2.4 \pm 0.7) \times 10^{-8}$ m/s^2). Thus, unlike other elements such as Al, Ca, Mg, and P, the rate-limiting step of B diffusion in CaO-SiO_2-$CaCl_2$ slag refining is controlled by B transfer in the slag.

2) Regarding the reaction rate, B oxidation (step 2), B oxychlorination (step 5), and the evaporation of BOCl from the surface (step 6) all occur very quickly, and therefore, they cannot be considered rate-limiting steps. The mass transfer coefficient of B in slag was measured and found to be 1.91×10^{-5} m/s for the transfer from slag interface to bulk slag, and 2.50×10^{-5} m/s for the transfer from bulk slag to the surface.

3) The rate-limiting step in the removal of B from Si by slag refining is the transfer of B at both the boundary layer adjacent to Si and at the surface of slag. However, the former of these has a greater influence, because the thickness of Si/slag interface (0.44 mm) is greater than the boundary at the surface (0.34 mm).

References

[1] X.D. Ma, T. Yoshikawa and K. Morita, MMTB, 2013, 443: p. 528-533.

[2] X.D. Ma, T. Yoshikawa and K. Morita, J. Cryst. Growth, 2013, 377: p. 192-196.

[3] N. Yuge, K. Hanazawa and Y. Kato, MMTB, 2004, 453: p. 850-857.

[4] M. Martorano, J.F. Neto, T. Oliveira and T. Tsubaki, MMTA, 2011, 427: p. 1870-1886.

[5] X.D. Ma, T. Yoshikawa and K. Morita, J Alloy Compd, 2012, 529: p. 12-16.

[6] K. Morita and T. Miki, Intermetallics, 2003, 1111: p. 1111-1117.

[7] K. Suzuki, T. Kumagai and N. Sano, ISIJ Int, 1992, 325: p. 630-634.

[8] H. Nishimoto and K. Morita, Supplemental Proceedings: Materials Processing and Energy Materials, 2011(1): p. 701-708.

[9] T. Ikeda and M. Maeda, ISIJ Int, 1992, 325: p. 635-642.

[10] S. Zheng, T.A. Engh, M. Tangstad and X.-T. Luo, MMTA, 2011, 428: p. 2214-2225.

[11] H. Kodera, Jap. J. Appl. Phys, 1963, 24: p. 212.

[12] L.M.N.N. Viswanathan and S. Seetharaman, 9th International Conference on Molten Slags, Fluxes and Salts, 2012: p. 11.

[13] L. Zhang, Y. Tan, J. Li, Y. Liu, D. Wang, Mater Sci Semicond Process 2013, 16(6): p. 1645-1649.

[14] Y. Wang, X.D. Ma, K. Morita, MMTB, 2014, 45: p.334-337.

[15] B. Helene, doctoral dissertation, NTNU, 2012.

CHAPTER FIVE

MG-SI PURIFICATION TREATMENT AND ITS PRACTICAL APPLICATION

5.1 Introduction

According to the thermodynamic calculation, partial pressure analysis, confirm experiment, phase diagram study of $CaO\text{-}SiO_2$ and $CaO\text{-}SiO_2\text{-}CaCl_2$, mass transfer coefficient and diffusion coefficient of B transferred from molten Si to the gas phase through molten slag, the B removal from molten Si using $CaO\text{-}SiO_2\text{-}CaCl_2$ slag system has proved to be effective theoretically. Therefore B removal experiments performed in the study consisted of following two parts.

On the one hand, B removal from Si was carried out using $CaO\text{-}SiO_2\text{-}CaCl_2$ slag. Pure Si (10 N) containing B and $CaO\text{-}CaCl_2$, $SiO_2\text{-}CaCl_2$, or $CaO\text{-}SiO_2\text{-}CaCl_2$ slag were pre-melted in an induction furnace; 5 g of pure Si doped with 0.5 mg of B and 10 g of slag were placed in a graphite crucible and kept at 1723 K in a SiC resistance furnace in an Ar atmosphere for 12 h; c_B in slag and Si was measured using ICP. The c_{SiO2} and c_{Cl^-} were measured using the gravimetric method [1] and ion-selective electrode method [2] , respectively.

On the other hand, in order to ascertain whether this performance would hold true at various scales of production, more practically-orientated production tests were carried out using large-scale equipment. Real metallurgical-grade ($c_{B\ initial}$ =20 ppmw) Si was used instead of doped pure Si. Si (2N) and mixed $CaO\text{-}SiO_2\text{-}CaCl_2$ (x_{CaO}: x_{SiO2}: x_{CaCl2} = 0.3:0.23:0.47) slag were first pre-melted at 1723K. Then, different quantities of this sample were refined in either an induction furnace or vacuum resistance furnace for 1, 1.5, or 2 hours at 1723K. Finally, these samples were linearly sectioned and analyzed by ICP-AES.

5.2 B removal experiment at lab scale

5.2.1 Experimental procedure

a) Experimental chemicals

The chemicals used in the experiments are shown in Table 5.1

Table 5.1 Species and types of chemicals

Name	Chemical formula	Producer	Purity
Calcium carbonate	$CaCO_3$	Wako pure Chemical industries, Ltd.	99.5%
Silicon oxide	SiO_2	Kanto Chemcial Co., INC.	99.5%
Calcium chloride	$CaCl_2$	Wako pure Chemical industries, Ltd.	95.0%
Silicon	Si		99.9999%
Boron	B	Soekawa Chemicals , Ltd.	99%

b) Experimental Setup

The pure bulk Si along with B and various compositions of CaO-SiO_2-$CaCl_2$ slag were pre-melted in a graphite crucible (99.999% purity, Thickness: 5 mm, Inner diameter: 23 mm, Height: 60 mm, Bottom thickness: 10 mm) using induction furnace in an Ar gas atmosphere. The schematic diagram of premelting using inductive furnace is shown in Fig. 5.1. The high-purity of Ar gas was purified using silica gel and Na_2O+$Mg(ClO_4)_2$ agent to remove steam and oxygen. During the experiment, surface temperature of the sample was monitored by a dual wavelength infrared pyrometer through the prism.

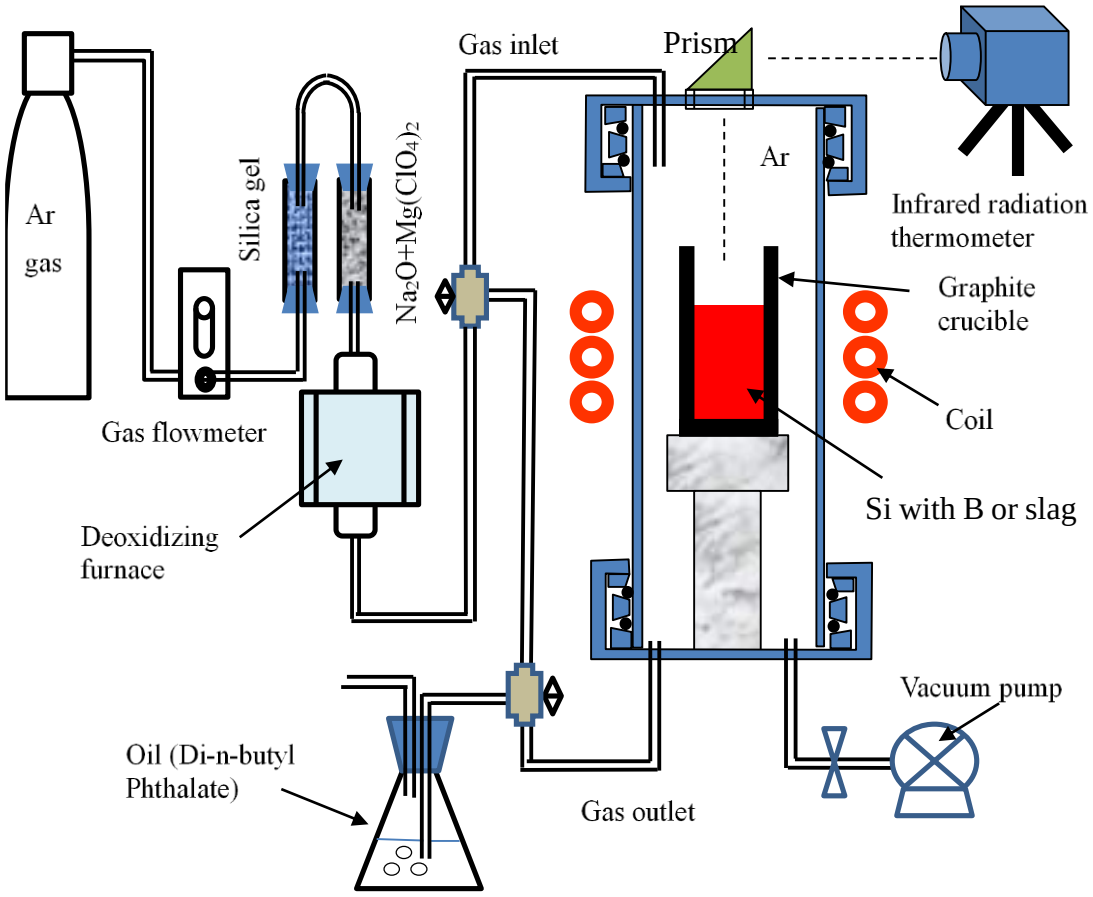

Figure 5.1 Schematic diagram of premelting molten Si and slag using inductive furnace.

A SiC electric resistance furnace was used to carry out the experiments, as shown in Fig. 5.2. The pre-melted sample was placed into a closed-end mullite reaction tube, which was inserted into the furnace. The sample in mullite tube was maintained above the liquidus temperature of alloys for 30 min in an Ar atmosphere so that the sample melted uniformly. The moisture, CO_2 and oxygen in the Ar gas were removed by passing successively through silica gel, soda lime, magnesium perchlorate and magnesium turnings heated at 823 K. The experiments were carried out at 1723 K for 2 hours. After experiment, the sample was withdrawn from mullite tube and cooled to room temperature by Ar gas cooling. The sample was cut parallel to the growth direction and polished for observation, the setup is shown in Fig. 5.2.

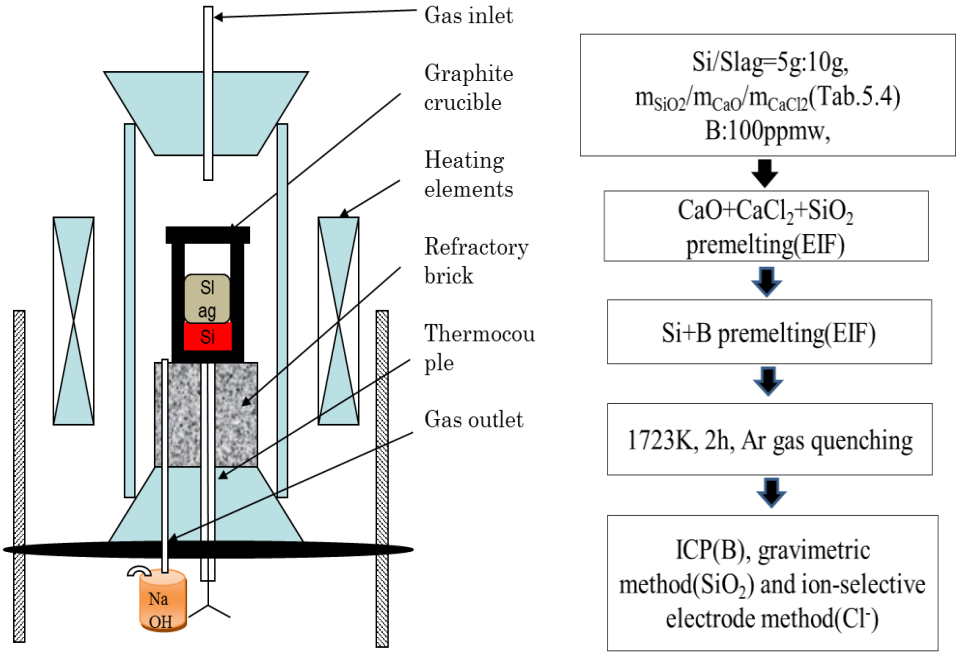

Figure 5.2 Experimental procedure of B removal

5.2.2 Sample analysis

a) B contents in the Si

The analysis method was the same as that in 4.3.3.

b) Ca contents in slag

1) About 0.3 g~0.5g of slag sample was weighed and inserted in a 50ml Teflon beaker.
2) 15ml of HNO_3 and 5ml of HCl were added into the beaker.
3) The beaker was covered and kept for 1~2 days until the sample was fully dissolved.
4) The solution was filtered into a 50ml volumetric flask (Teflon) and completed to 5 ml with distilled water.
5) The concentrations of Ca in the solution were analyzed by ICP-AES. The standard solution of Ca was prepared in the range of 50~300 ppm (mg/L), respectively. The wavelengths of Ca was selected to be 393.37 nm.

c) SiO_2 content in slag

1) 0.5 g slag of sample (W_{slag}), 0.5 g of Na_2CO_3 and 0.5 g of $Na_2B_4O_7$ were weighed and inserted in a Pt crucible after mixing thoroughly.
2) The Pt crucible was heated on a Bunsen burner for about 20 minutes until a homogeneous melt was obtained.
3) The Pt crucible was quenched by rinsing the outside of it with distilled water to avoid any external contamination.

4) The Pt crucible was inserted in a 500 ml beaker and then 300 ml acid solution (H_2O:HCl=2:1) were added.
5) The Pt crucible was taken out and washed after the alkaline fused sample in the crucible was totally dissolved.
6) 10 ml of $HClO_4$ acid was added into the beaker. The solution was heated at 523 K until approximately total drying for residue.
7) 30 ml of 1:4 HCl:H_2O solution was added to dissolve salt of the residue.
8) The solution was filtered into a 250 ml volumetric flask. All residue was taken from the beaker using a PE rod.
9) The residue was washed several times with hot 1:10 HCl:H_2O solution and 1:10 H_2SO_4:H_2O solution, finally with hot distilled water.
10) The filter paper and residue were placed into a Pt crucible and burned on a Bunsen burner.
11) The Pt crucible was cooled to room temperature in a desiccator.
12) The Pt crucible with the residue was weighed accurately (W_1).
13) For the vaporization of the SiO_2, 5 ml of HF and 3~4 drops of 1:1 H_2SO_4:H_2O solution were added into the Pt crucible.
14) The Pt crucible was heated slowly to let the SiO_2 react with the HF to evaporate as gaseous.
15) The Pt crucible was reweighed after total evaporation (W_2).
16) The content of SiO_2 in slag was determined as follows.

$$\text{Wt.pct.of } SiO_2 = \frac{W_1 - W_2}{W_{slag}}$$

<u>d) $CaCl_2$ content in slag</u>

1) 0.5 g of CaO-SiO_2-$CaCl_2$ slag sample, 0.5 g of Na_2CO_3, 0.5 g of K_2CO_3 and 0.25 g of SiO_2 were weighed and inserted in a Pt crucible after mixing thoroughly.
2) The Pt crucible was heated on a Bunsen burner for about 20 minutes until a homogeneous melt was obtained.
3) The Pt crucible was quenched by rinsing the outside of it with distilled water to avoid any external contamination.
4) The Pt crucible was inserted in a 500 ml Teflon beaker and then 200 ml distilled water were added.

5) The Pt crucible was taken out and washed after the alkaline fused sample was totally dissolved.
6) The solution was stirred by a magnetic stirrer for 2 hours (the beaker should be covered).
7) The solution was filtered in a 500 ml volumetric flask and completed to the volume of 500ml with distilled water.
8) 20ml of solution was transferred to a 100ml Teflon beaker by a 20ml pipette. 20ml of TISAB (Total Ionic Strength Adjustment Buffer) solution (1mol/L NH_4NO_3-0.06mol/L HNO_3) was added in the beaker.
9) The PH of solution was adjusted to about 5.5 with HNO_3 acid by using HIROBA Cl-23 pH/Ion meter instrument.
10) The solution was transferred in a 100ml volumetric flask and completed to the volume of 100ml with distilled water.
11) The Cl^- standard solutions were prepared in the range of 10~50 ppm from the 1000ppm Cl^- standard solution. The matrix of standard solutions and blank were adjusted to be the same as the sample solutions.
12) The Cl^- concentration in the solution was measured by using HIROBA F-23 pH/Ion meter instrument.
13) The $CaCl_2$ content of slag was calculated according to the Cl content of slag, assuming the existence of Cl in slag in the form of $CaCl_2$.

5.2.3 Results and discussion

By melting various slags with B-containing Si, the B removal efficiency was evaluated as 1- $c_{\text{B final in Si}}$ / $c_{\text{B initial}}$, and because the ratio between slag and Si is 2, the evaporative efficiency of B was estimated as 1-($c_{\text{B final in Si}}$ + 2$c_{\text{B final in slag}}$) / $c_{\text{B initial}}$. The basicity of each slag was defined as the weight ratio of CaO and SiO_2 (w_{CaO}/w_{SiO2}).

The removal efficiency (R.E.) and evaporative efficiency (E.E) of slags with different compositions listed in Table 5.2. The C_B decreased from 150 to around 30 ppmw, and the B removal efficiencies were between 50% and 86%. It is clear that B can be evaporated from Cl-containing slags with evaporative efficiencies between 7% and 66%. The L_B values were between 0.33 and 2.4.

In the three binary slag systems, the CaO-SiO_2 slag showed the lowest removal efficiency (51%) and almost negligible evaporative efficiency (2%) because there was

no Cl^- in this slag for gas evaporation. In comparison to the CaO-$CaCl_2$ slag, the SiO_2-$CaCl_2$ slag showed slightly higher B removal and evaporative efficiencies. Because p_{O2} increases with increasing activity of SiO_2, Eq. (5-1) will proceed to the right-hand side.

When the x_{CaO} / x_{SiO2} was 0.45 and x_{CaCl2} decreased, the removal efficiency increased from 0.67 to 0.82, indicating that not only [Cl] but also [O] affected B removal. Among the three slag systems, the ternary system (x_{CaO} / x_{SiO2} / x_{CaCl2} = 4.7 / 2.3 / 3) showed the best potential to achieve good B removal (86%) efficiency; this might be attributed to the appropriate activity ratio of [O] and [Cl] that can oxidize and chloridize B adequately.

Table 5.2. Mole fraction (x_i) of slag after experiments and L_B, evaporative efficiency (E.E), removal efficiency (R.E.)

x_{SiO2}	x_{CaO}	x_{CaCl2}	$c_{B\ final\ in\ Si}$ (ppmw)	$c_{B\ final\ in\ Slag}$(ppmw)	*R.E.*	L_B	*E.E.*	*Basicity*
0.175	0.125	0.7	35	14	0.65	0.4	0.37	0.48
0.3	0.2	0.5	23	20	0.77	0.9	0.37	0.44
0.4	0.25	0.35	15	24	0.85	1.6	0.37	0.42
0.4	0.3	0.3	19	27	0.81	1.4	0.27	0.50
0.475	0.325	0.2	18	30	0.82	1.7	0.22	0.46
0.55	0.35	0.1	21	36	0.79	1.7	0.07	0.42
0.1	0.35	0.55	12	21	0.88	1.8	0.46	2.33
0.325	0.3	0.375	15	26	0.85	1.7	0.33	0.62
0.275	0.425	0.3	20	34	0.8	1.7	0.12	1.03
0.125	0.4	0.475	12	26	0.88	2.2	0.36	2.13
0.1	0.525	0.375	29	27	0.71	0.9	0.17	3.50
0.4	0.125	0.475	27	24	0.73	0.9	0.25	0.21
0.525	0.1	0.375	26	22	0.74	0.8	0.3	0.13
0.6	0.15	0.25	27	19	0.73	0.7	0.35	0.17

Fig. 5.3 shows the relationship between L_B and R. E. With the increasing of partition ratio between slag and molten from 0.25 to 2.5, the remove efficiency increased from 57% to 86%. Because higher value of L_B means more B was oxidized and transferred from molten Si to the slag, as shown in Eq. (5-1):

$$B_{(l)} + \frac{3}{4}SiO_{2(l)} = BO_{1.5(l)} + \frac{3}{4}Si_{(l)} \quad (5\text{-}1)$$

Fig. 5.4 shows the relationship between remove efficiency and evaporative efficiency.

This indicates that with an increase in the evaporative efficiency of B, the remove efficiency value is increased until 30% and decreased. Because if the evaporative efficiency is higher than 30%, slag composition contained too much $CaCl_2$ and less CaO and SiO_2, which means oxidation reaction as shown in Eq. (5-1) is not enough. Therefore, it demonstrated that a suitable activity ratio of [O] and [Cl] for the simultaneous oxidation and chlorination of B is necessary.

Fig. 5.5 shows the relationship between L_B and the basicity (w_{CaO}/w_{SiO2}) of a CaO-SiO_2-$CaCl_2$ slag, with the results of other slag systems shown for comparison. This indicates that with an increase in the basicity value of a CaO-SiO_2-$CaCl_2$ slag, the L_B value is also increased. Furthermore, the L_B values of a CaO-SiO_2-$CaCl_2$ slag are higher than those of a CaO-SiO_2-CaF_2 slag. Given that B can be removed as a gas phase in the case of the former, it is evident that the former slag is superior to a CaF_2-containing slag.

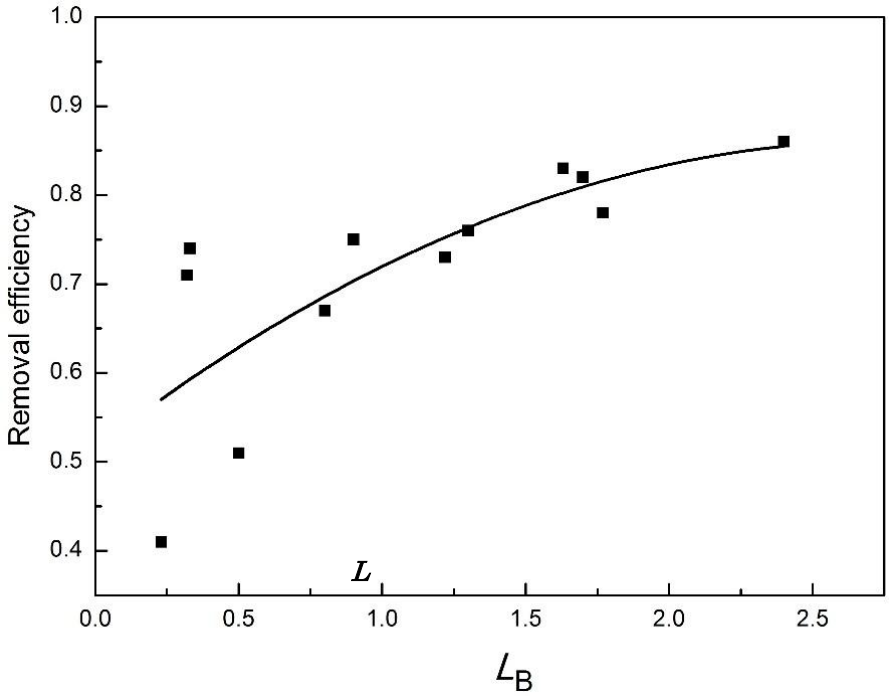

Figure 5.3 Relationship between L_B and R. E.

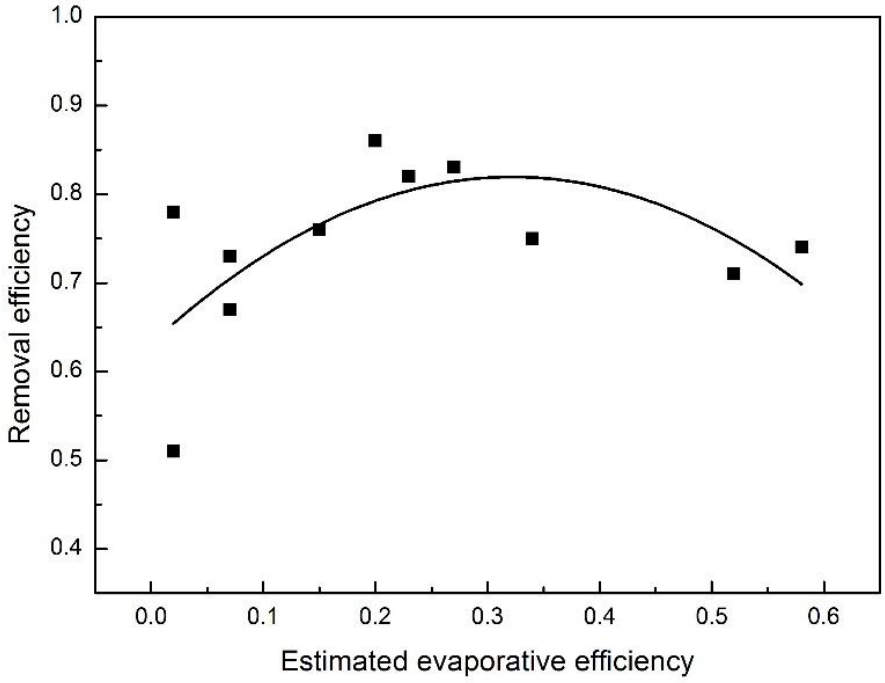

Figure 5.4 Relationship between E. E. and R. E.

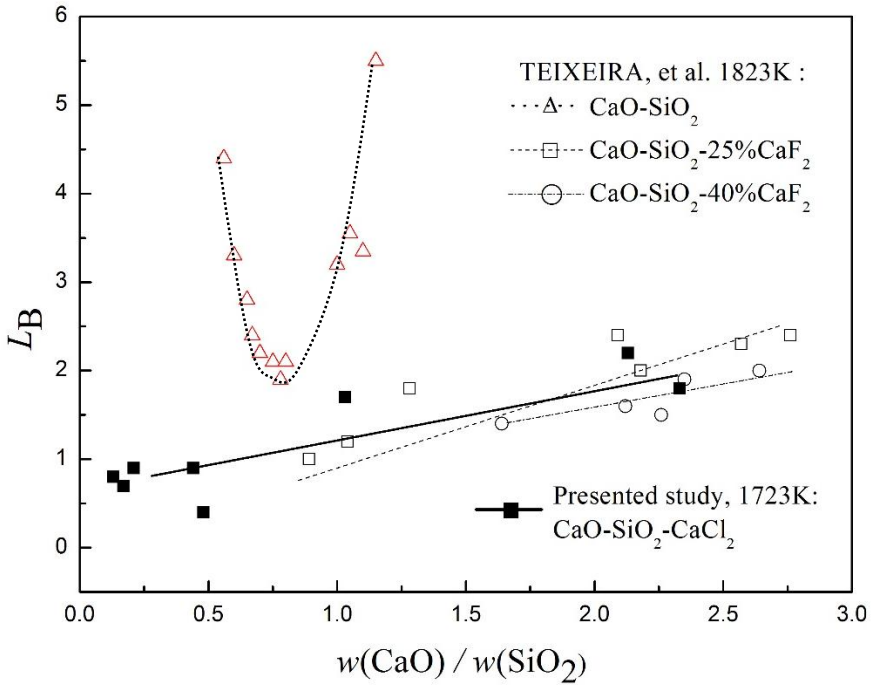

Figure 5.5 Relationship between L_B and basicity (w_{CaO}/w_{SiO2})

Fig. 5.6 shows the relationship between compositions and removal efficiency. It indicates that the removal efficiencies of B increased from 71% to 90% when the compositions of slag are all in the liquid area. Theoretically, more B will be evaporated

when the compositions of slag moving to the $CaCl_2$-riched area due to the lower melting point, viscosity and higher evaporation rate. However, experiments (Fig. 5.6) shows that the removal efficiency increased from 75% to 90% when the compositions of ternary slag moved from the boundary of liquidus until the middle $CaCl_2$-riched area. Because when oxidizing slag is added onto the surface of molten Si, B in molten Si is partly oxidized and transferred to the slag as $BO_{1.5}$:

$$B_{(l)} + \frac{3}{4} O_{2(g)} = BO_{1.5} \tag{5-2}$$

Then, $BO_{1.5}$ in molten slag is chlorinated by $CaCl_2$ according to the principle of selective chlorination, which can be represented as

$$BO_{1.5(l)} + \frac{1}{2} CaCl_{2(l)} = BOCl_{(g)} + \frac{1}{2} CaO_{(s)} \tag{5-3}$$

Finally, B oxychlorides with high vapor pressure, such as BOCl, evaporate from the molten slag. Thus, B in molten Si is removed by this oxidized chlorination and evaporation process.

Therefore, both of the results of liquid area of the ternary slag at 1723K and the results of removal efficiency demonstrate that B could not be removed effectively unless [Cl] and [O] oxidize and chloridize [B] in the meanwhile. When the compositions of slag moved to the $CaCl_2$-riched area, there is not enough [O] to oxdize [B] to generate $BO_{1.5}$.

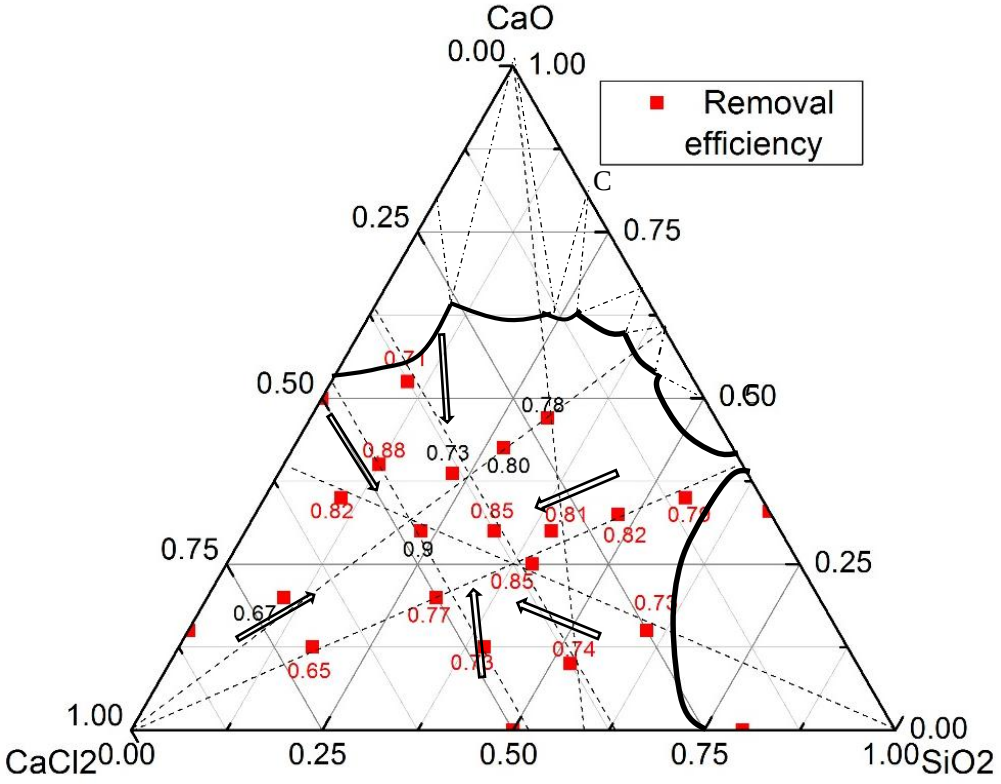

Figure 5.6 Relationship between compositions and removal efficiency

5.3 Large scale experiments

Having confirmed that a CaO-SiO_2-$CaCl_2$ slag system offers the best potential to achieve good B-removal (86 %), it was explored further to ascertain whether this performance held true at various scales of production for times of 1, 1.5, and 2 h at 1723 K.

5.3.1 Experimental procedure

a) Experimental chemicals

The impurity element content of metallurgical grade silicon and species of used chemicals are shown in Table 5.3 and Table 5.4

Table 5.3 Impurity element content of metallurgical grade silicon (ppmw)

Element	Si	**B**	Fe	Al	Ca	Ti	Cu	V
Content	99.8%	**20**	1220	1120	85	120	18	94

Table 5.4 Species and types of chemicals

Name	**Chemical formula**	**Producer**	**Purity**
Silicon oxide	SiO_2	Sinopharm Chemical Reagent Co.,Ltd	99.7%
Calcium chloride	$CaCl_2$	Tianjin Shengao Chemical Reagent Co., Ltd	95.0%
Calcium oxide	CaO	Tianjin Fengchuan Chemical Reagent Co., Ltd	99.7%
Ar gas	Ar	Messer Co., Ltd	≥99.99%

b) Experimental Setup

The schematic illustration of induction furnace (IF) is shown in Fig. 5.7. The photograph of vacuum resistance furnace (VRF) and its capacity are shown in Fig. 5.8 and Table 5.5. The profile map of large graphite crucible is shown in Fig. 5.9.

The real metallurgical-grade (C_B initial =20 ppmw) Si was used instead of doped pure Si. Si (2N) and CaO-SiO_2-$CaCl_2$ (x_{CaO}: x_{SiO2}: x_{CaCl2} = 0.3:0.23:0.47) mixed slag were first pre-melted at 1723K. Then, different quantities of sample (Table 5.7) were refined in either an induction furnace or vacuum resistance furnace for 1, 1.5, or 2 hours at 1723K. Finally, the samples were linearly sectioned and analyzed by ICP-AES.

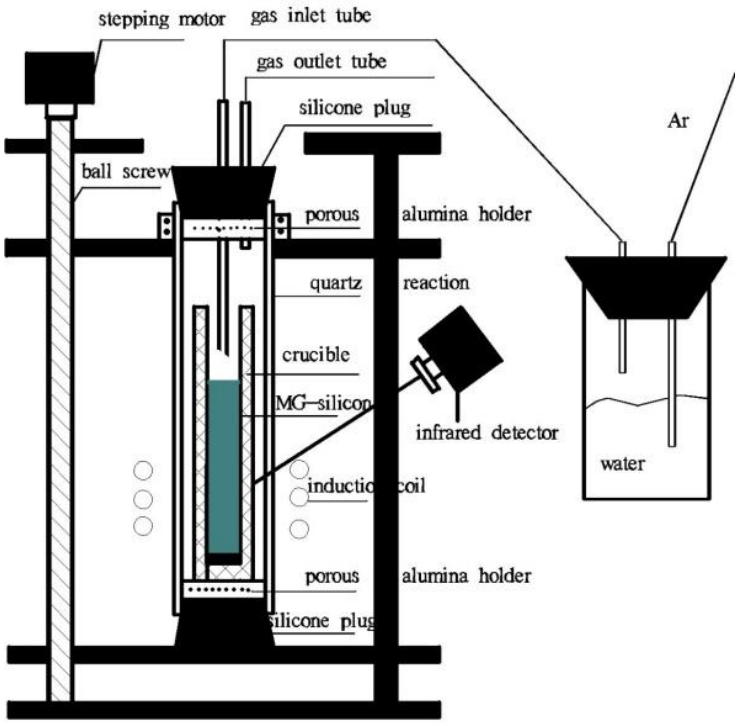

Figure 5.7 Schematic illustration of induction furnace (IF)

Figure 5.8 Photo of vacuum resistance furnace (VRF)

Table 5.5 The list of capacity of VRF

Output capacity	**Frequency**	**Input voltage**	**Max input current**	**Load Voltage**	**Max load current**
34KV·A	50HZ	380V	89A	35V	971A

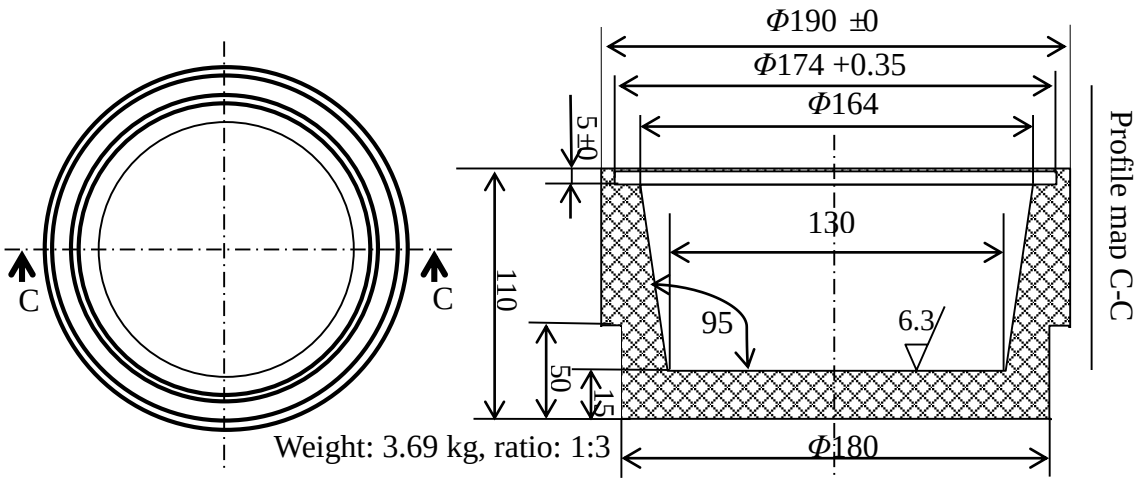

Figure 5.9 The profile map of large graphite crucible

After refining, the Si bulk was cut into pieces by wire cutting machine, as shown in Fig. 5.10.

Figure 5.10 Cut of Silicon using wire cutting machine

5.3.2 Results and discussion

The Si ratios and slag compositions of samples heated for different times in either a medium-frequency induction furnace (IF) or vacuum resistance furnace (VRF) are shown in Table 5.6. Photographs of the samples are shown in Fig. 5.11.

Table 5.6 Si ratio and slag composition

No.	Si	CaO (g)	SiO_2 (g)	$CaCl_2$ (g)	Hours (h)	Furnace
1	25g	10.1	8.5	31.4	2	I. F.
2-4	50.g	20.3	16.9	62.7	1, 1.5, 2	I. F.
5-7	100g	40.7	33.9	125.4	1,1.5, 2	I. F.

8-9	500g	154.2	179.9	665.8	1.5, 2	V. R. F

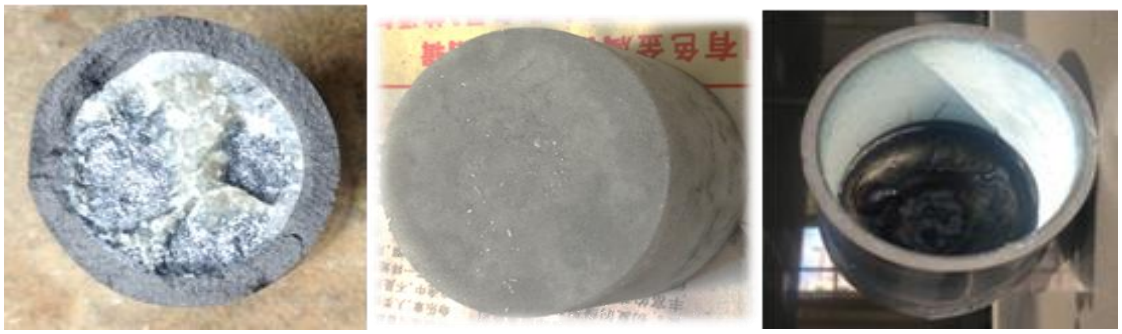

25 g Si after slag refining　　50 g slag after pre-melting　　100 g Si after pre-melting

Figure 5.11 Photos of samples

According to the experimental results shown in Table 5.7, the C_B decreased from 20 to around 3 ppmw, and the B removal efficiencies were between 78 % and 90 %. Thus, it is clear that B can be evaporated from Cl-containing slags with evaporative efficiencies between 62 % and 78 %.

With an increase in time, the evaporation efficiency and removal efficiency are increased slightly. A larger-scale experiment using V. R. F. also demonstrated an improvement in the B removal efficiency, as this method not only allowed for a more accurate control over temperature accurately, but also provides a negative pressure environment that is beneficial to the evaporation of BOCl gas.

Table 5.7 B content following different scale experiments

No.	**Weight of Si / slag**	**$C_{B\ in\ Si}$ (ppmw)**	**$C_{B\ in\ slag}$ (ppmw)**	**L_B**	**Holding time (h)**	**E. E.**	**R. E.**
1	25g / 50g	3.3	1.2	0.4	2.0	**0. 78**	0.84
2	50g / 100g	3.7	4.0	1.1	1.0	0.62	0.81
3	50g / 100g	3.3	2.8	0.8	1.5	0.70	0.84
4	50g / 100g	2.8	3.3	1.2	2.0	0.70	0.86
5	100g / 200g	3.5	3.7	1.1	1.0	0.64	0.82
6	100g / 200g	3.1	4.2	1.4	1.5	0.64	0.85
7	100g / 200g	2.3	3.2	1.4	2.0	0.73	0.88
8	500g / 1Kg	3.6	3.9	1.1	1.5	0.63	0.82
9	500g / 1Kg	2.1	3.2	**1.5**	2.0	0.74	**0.90**

Fig. 5.12 and Fig. 5.13 show the relationship between L_B, removal efficiency (*R.E.)*

and evaporation efficiency (*E.E).* It indicates that, as the L_B value of a CaO-SiO_2-$CaCl_2$ slag increases, the *R.E.* also increases. Furthermore, in the L_B values, the R.E. in the larger scale is larger than that in the Lab scale due to convection and stirring in the induction furnace. In the same partial pressure (10^5Pa), the E.E. of large scale is larger than that of in the Lab scale due to large surface area. These two figures also show that at 10^3 Pa, the E.E of large scale is higher than at 10^5 Pa, as it is easier vaporize BOCl gas.

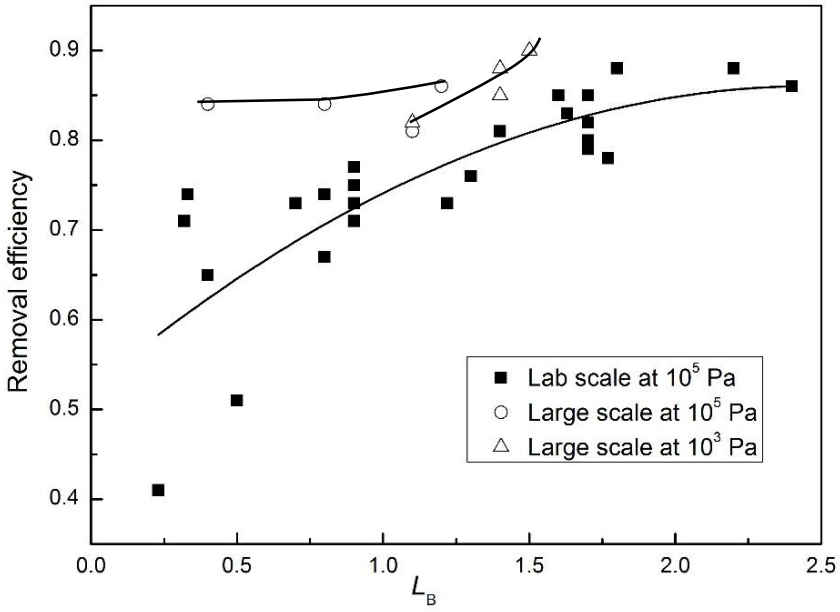

Figure 5.12 Relationship between L_B and basicity (w_{CaO}/w_{SiO2})

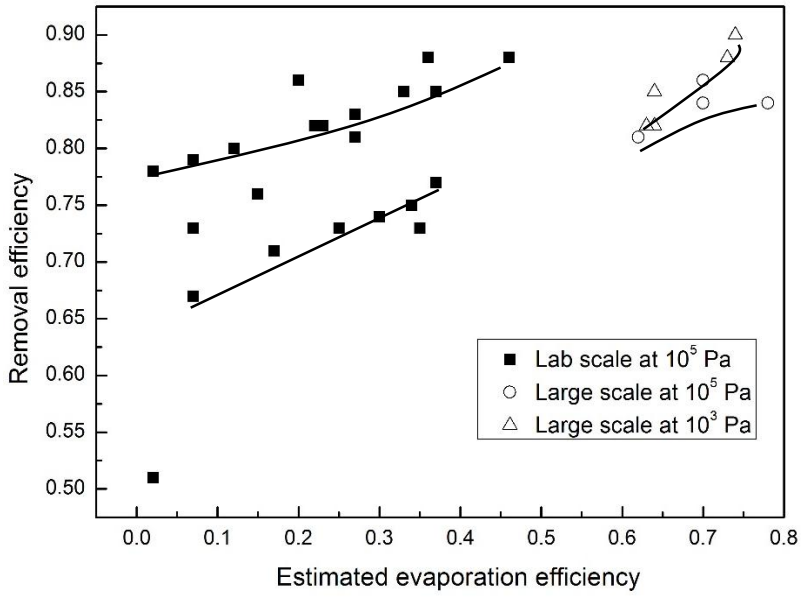

Figure 5.13 Relationship between Relationship between E. E. and R. E.

All in all, R.E. increases from the boundary of ternary phases diagram to $CaCl_2$-richarea in the middle which is between from 30% to 50%; also R.E increases with increasing L_B.

In the large-scale experiment, the distribution of B in the Si bulk was determined by ICP-AES, the results of which are shown in Fig. 5.14 and Table 5.8.

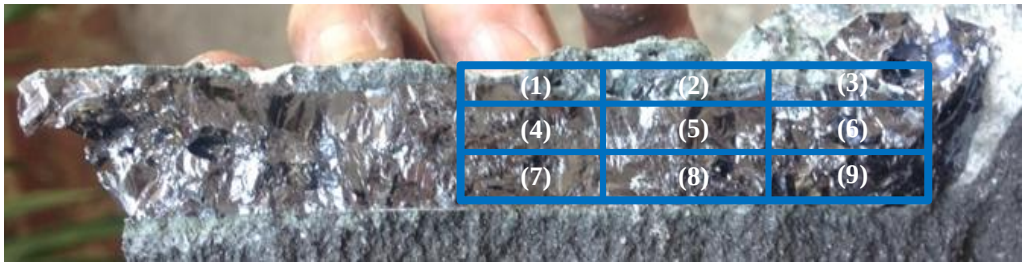

Figure 5.14 Photograph of sample 8

Table 5.8 Variation in B content with position

Position	(1)	(2)	(3)	(4)	(5)	(6)	(7)	(8)	(9)
Boron Content (ppmw)	3.5	4.8	5.9	0.5	0.6	3.3	1.1	1.6	2.5

According to the results shown in Table 5.9, the concentration of B increases in the order of middle (4-7) < bottom (7-9) < top (1-3), and inside (1, 4, 7) < middle (2, 5, 8) < outside (3, 6, 9). The reason for the lower B content in the middle than in the bottom can be attributed to segregation during cooling. Top of the bulk sample has a higher B content due to the mass transfer from Si to the Si / bulk interface.

For the large-scale Si refining using CaO-SiO_2-$CaCl_2$ slag in a vacuum resistance furnace, the energy consumption was determined as 9.45 kWh / kg, as shown in Table 5.9.

Table 5.9 Energy consumption of slag refining

U(v)	**I(A)**	**P(w)**	**T(h)**	**W(kW ħ/kg)**
15	420	6300	1.5	9.45

5.4 Summary

A new method for the removal of B from molten Si was proposed, based on the principle of oxidized chlorination and evaporation. After confirming that CaO-SiO_2-$CaCl_2$ slag system has the best B-removal efficiency, it was investigated further to determine whether this holds true in a scaled up industrial environment. From this, the following conclusions were drawn:

1) Compared with a binary slag system, such as CaO-SiO_2, CaO-$CaCl_2$, or SiO_2-$CaCl_2$, the ternary CaO-SiO_2-$CaCl_2$ slag system demonstrates good potential for B removal due to the dual action of O and Cl.
2) Large-scale experimentation confirmed that an improvement in B removal (90 %) can be achieved with CaO-SiO_2-$CaCl_2$ slag at 1723K in vacuum resistance furnace after 2.0 hours.
3) An increase in L_B and estimated evaporative efficiency causes the removal efficiency to increase accordingly. Furthermore, an increase in the basicity of the slag causes L_B to first decrease, and then increase.

Reference

[1] X.D. Ma, doctoral dissertation, The University of Tokyo, 2013.

[2] V. Gadzekpo and G. Christian, Analytica Chimica Acta, 1984. 164: p. 279-282.

CHAPTER SIX

CONCLUSIONS

In order to explore a novel B remove process for SOG-Si production with low cost, in this study, the physical chemistry of boron removal by evaporation in molten silicon using reactive fluxes was investigated.

In chapter 1, we discussed that in many kinds of renewable energy sources, photovoltaic industry has been under rapid development in this decade due to the global policies supporting the clean energy and reduction of CO_2 emission. While solar grade silicon (SOG-Si), as the raw material for producing solar cells, is mainly from the offcut of electronic grade silicon (SEG-Si) which was prepared from metallurgical grade silicon (MG-Si) using a modified Siemens process and a fluidized bed reactor process. Another method, named metallurgical method offers benefits both in mass productivity and low cost. As one of metallurgical methods, the slag and gas process offers the possibility of cost reduction due to its high purification efficiency and low cost. The objective of this study is to clarify the possibility of SOG-Si refining using reactive fluxes with the aim of developing a new Si refining process.

In chapter 2, Thermodynamics of reactions involved was investigated in order to determine the possibility of B evaporation from $CaO\text{-}SiO_2\text{-}CaCl_2$ slag system and the estimated relationships between the partial pressures of BOCl, BCl_x, $SiCl_x$, and $CaCl_2$ were investigated and the mole fraction of CaO in the $CaO\text{-}CaCl_2$ slag was also studied. Both of standard Gibbs free energy and partial pressure of reactions between B, Si with chlorine demonstrate that BOCl gas should be generated at 1723K theoretically, because the ratio of P_{BOCl} and P_{SiCl2} (1/500) is larger than that of x_B and x_{Si} (1/8000). The overall reaction associated with B removal by slag treatment can be represented:

$$B_{(l)} + 0.75O_2 + 0.5CaCl_{2(l)} = BOCl_{(g)} + 0.5CaO_{(s)}$$

$$\Delta G^0 = -92.5 + 0.01T \text{ kJ/mol.}$$

In chapter 3, Phase diagrams of $SiO_2\text{-}CaCl_2$ and $CaO\text{-}SiO_2\text{-}CaCl_2$ were investigated

using the Archimedean method and thermo gravimetric differential thermal analysis (TG-DTA), for the purpose of identifying the physical properties and the density of CaO-SiO_2-$CaCl_2$ slag system.

During the density measurement of various compositions of CaO-SiO_2-$CaCl_2$ slag, it was observed that with an increase in the mole fraction of CaO from 0.1 to 0.4, the density of the slag increases from 2.00 to 2.63 g/cm^3 from 1073K to 1723K. It was also found that the density of all the slags decreased slightly when the temperature was increased, as this causes increase in both, thermal motion of molecules and the volume. Because 30mol%CaO-23mol%SiO_2-47mol%$CaCl_2$ system shows the best B removal potential, value of density would be 2.01g/cm^3 after linear fitting of the points between 1073 and 1373K. The molar volume of various compositions of slag could also be calculated, which can be expressed as follows:

$$V_{m\mathrm{I}} = 88.6/\left(2.39 - 3\times10^{-4}T\right)$$

$$V_{m\mathrm{II}} = 78.0/\left(2.79 - 4.5\times10^{-4}T\right)$$

$$V_{m\mathrm{III}} = 72.4/\left(3.04 - 3.5\times10^{-4}T\right)$$

As for the binary phase diagram measurement of SiO_2-$CaCl_2$, two eutectics in the SiO_2-$CaCl_2$ binary system were located at 27 mole% SiO_2 (m.p. 1018K) and 60 mole% SiO_2 (m.p.1047K), and intermediate compound SiO_2·$CaCl_2$ melting congruently at (m.p. 1071 K) was found by TG-DTA and XRD. The binary phase diagram is shown below:

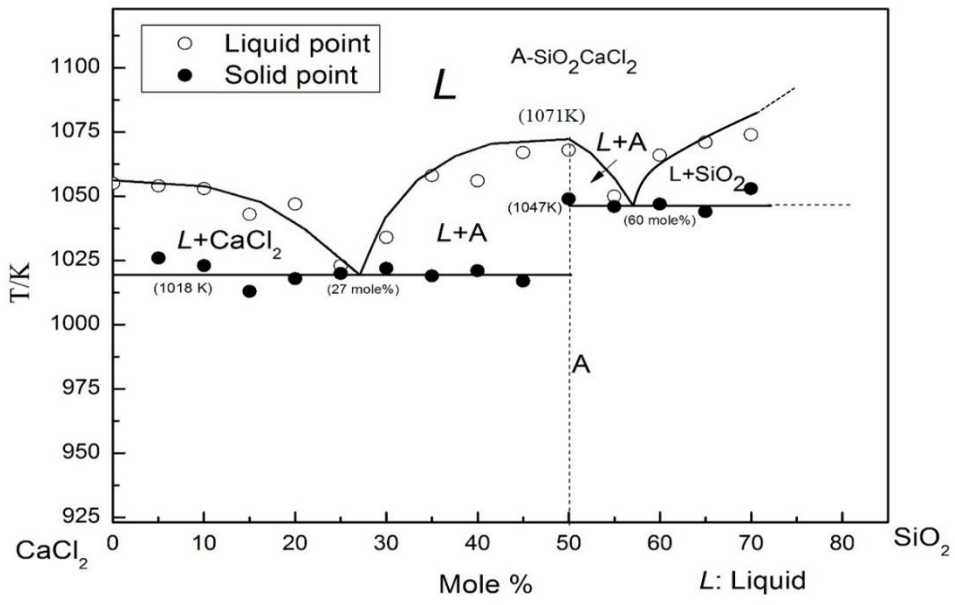

Figure 6.1. $CaCl_2$-SiO_2 phase diagram

The low activation energy value of vaporization shows that the evaporation could occur easily. The negative values of interaction coefficients such as $\varepsilon_{CaCl_2}^{CaCl_2}$, $\varepsilon_{CaCl_2}^{CaO}$, $\varepsilon_{CaCl_2}^{SiO_2}$ show that the CaO and SiO_2 can decrease the activity of $CaCl_2$.

The Liquidus of CaO-SiO_2-$CaCl_2$ ternary system at 1723K was detected as shown in Fig. 6.2. It was found that the ternary eutectic involving the compounds SiO_2, CaO·SiO_2 and $CaCl_2$·SiO_2 was in equilibrium at 1093K in the SiO_2-rich region.

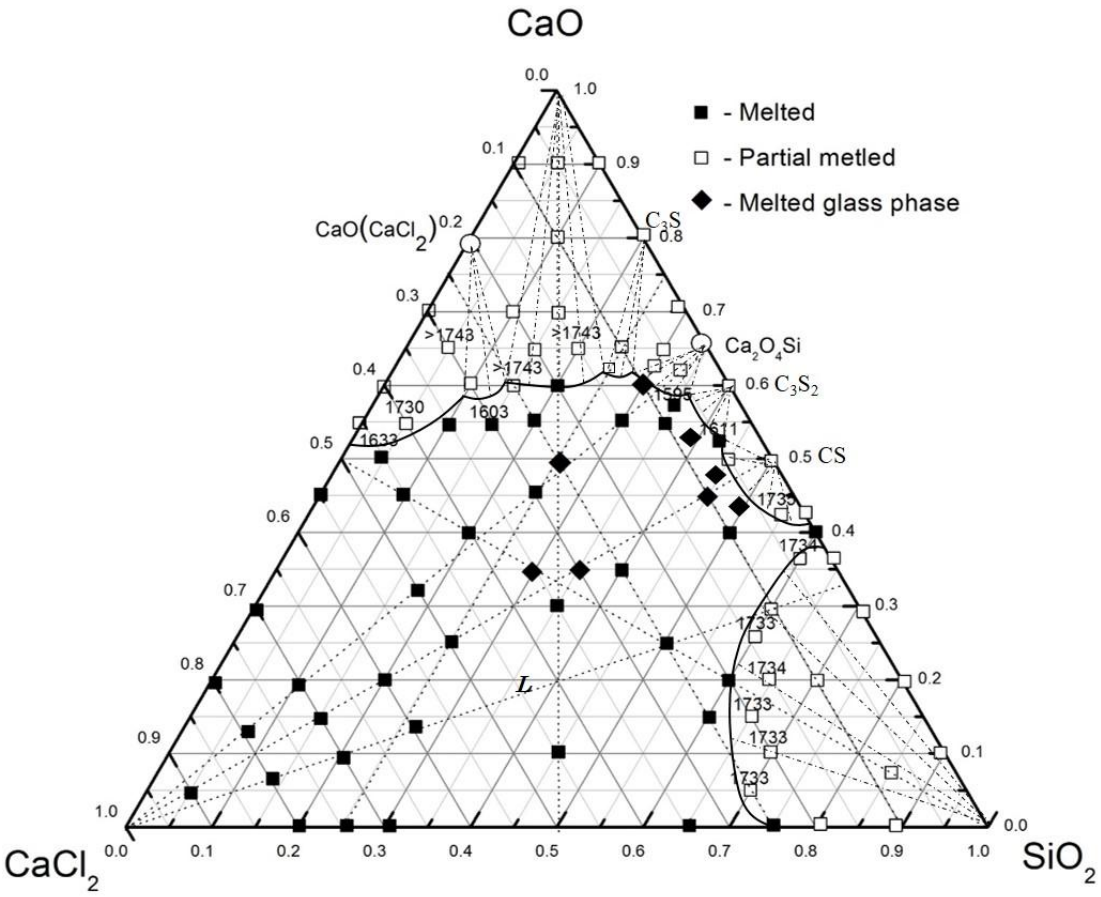

Figure 6.2. The Liquidus of CaO-SiO_2-$CaCl_2$ slag at 1723K

In chapter 4, A model for the transfer of B from Si to molten slag by diffusion and its evaporation as a gas phase was established in order to understand the kinetics of B removal process from molten Si using CaO-SiO_2-$CaCl_2$ slag,. The mass transfer and diffusion coefficients of B in the slag were measured at 1723 K for different times and different mass ratios between the slag and Si. In addition, the rate controlling steps were also investigated based on the kinetics model and calculated values of k_s and D_s. Thus,

from this study, the following conclusions have been drawn:

The diffusion coefficient of B in slag (D_s) is 8.46×10^{-9} m/s^2, which means the rate of B diffusion in slag (step 3) is slower than that of B diffusion in Si ($(2.4 \pm 0.7) \times 10^{-8}$ m/s^2). Thus, unlike other elements such as Al, Ca, Mg, and P, the rate-limiting step of B diffusion in CaO-SiO_2-$CaCl_2$ slag refining is controlled by the transfer of B in the slag.

With regards to the reaction rate, B oxidation (step 2), B oxychlorination (step 5), and the evaporation of BOCl from the surface (step 6) all occur very quickly, and therefore, they cannot be considered rate-limiting steps. The mass transfer coefficient of B in slag was therefore measured and found to be 1.91×10^{-5} m/s for the transfer from the slag interface to the bulk slag, and 2.50×10^{-5} m/s for the transfer from the bulk slag to the surface.

The rate-limiting step in the removal of B from Si by slag refining is the transfer of B at both the boundary layer adjacent to Si and at the surface of the slag. However, the former of these has a greater influence, because the thickness of the Si/slag interface (0.44 mm) is greater than the boundary at the surface (0.34 mm).

In chapter 5, Based on the thermodynamic and kinetics analysis in the B removal process using CaO-SiO_2-$CaCl_2$ slag system, B removal experiments were carried out using CaO-SiO_2-$CaCl_2$ slag system at different scale after confirming that B can be evaporated as gas phases using B_2O_3-$CaCl_2$.

Compared with a binary slag system, such as CaO-SiO_2, CaO-$CaCl_2$, or SiO_2-$CaCl_2$, the ternary CaO-SiO_2-$CaCl_2$ slag system demonstrates good potential for B removal due to the dual action of O and Cl. Among the ternary slag systems tested, 30mol%CaO-23mol%SiO_2-47mol%$CaCl_2$ system shows the best potential to achieve B-removal (86 %) efficiency.

Large-scale experimentation also confirmed that an improvement in B removal (90 %) can be achieved with a CaO-SiO_2-$CaCl_2$ slag at 1723K in a vacuum resistance furnace after 2.0 hours.

An increase in partition ratio of B between Si and slag (L_B) and estimated evaporative efficiency causes the removal efficiency to increase accordingly. Furthermore, an increase in the basicity of the slag causes L_B to first decrease, and then increase. The L_B values in the large scale experiments are greater than the values in Lab scale experiments due to convection and stirring in the induction furnace. At same partial pressure (10^5Pa), these

values in large scale experiments are bigger than the values in Lab scale due to large surface area. Evaporated efficiency (E.E.) for The large scale at 10^3 Pa is higher than that at 10^5 Pa due to BOCl gas is easier evaporation.

Eventually, based on the findings throughout this research, physical chemistry of B removal by evaporation in molten silicon using reactive fluxes was clarified. 90% B could be removed using 30mol%CaO-23mol%SiO_2-47mol%$CaCl_2$ slag system at 1723K for 2hours. Comprising of slag and solidification refining, acid leaching, vacuum melting and directional solidification steps, B oxychlorination and the evaporation of BOCl gas process for producing SOG-Si from MG-Si was proposed, which has been applied to practical process.

ACKNOWLEDGEMENTS

I would like to express my gratitude to all those who helped me during the writing of this thesis. Foremost, I would like to express my sincerest gratitude to my supervisor Prof. Kazuki Morita, for the continuous support of my Ph.D. study and research, for their patience, motivation, enthusiasm and immense knowledge. In the preparation of the thesis and papers, he had spent much time reading through each draft and provided me with inspiring advice. Without her patient instruction, insightful criticism and expert guidance, the completion of this achievements would not have been possible.

I would like to thank my thesis committee: Prof. Toru H. Okabe, Prof. Fumitaka Tsukihashi and Asis. Prof. Takeshi Yoshikawa, for their constructive critics and insightful comments.

I am greatly indebted to the Ministry of Education, Science, Sports, and Culture, Government of Japan (Monbukagakusho), for the financial support as the scholarship that gave me the great opportunity to pursue my studies in Japan.

I also wish to acknowledge the numerous assistances of Mr. Yutaka Yanaba and Mrs. Naomi Nakaya on the daily routine in the lab.

Thanks to all members of the Morita Lab with whom I spent memorable time during three years. They are Dr. Sakamoto, Dr. Ma, Dr. Lei, Dr. Nok, Dr. Chen, Dr. Kim, Dr, Li, Dr. Ueda, Mr. Kawamura, Mr. Suzuki, Mr. Kawamura, Mr. Matsunaga, Miss. Wang, Mr. GT and Mr. Kitano. Special thanks for their warm friendship, knowledge exchange, valuable discussion and the help throughout the life in Japan.

Last but not the least, I would like to thank to my parents for their always encouragements. Thanks my whole family and kind friends for giving me endless understanding and supports.

Ye WANG

June 2015